MICROCOPY RESOLUTION TEST CHART
NATIONAL BUREAU OF STANDARDS-1963-A

AFOSR-TR- 86-0837

NONLINEAR OPTICAL PROPERTIES AND SUBPICOSECOND DYNAMICS OF EXCITONS AND ELECTRON-HOLE PLASMAS IN MULTIPLE QUANTUM WELL STRUCTURES

AD-A173 370

A.L. Smirl, R.A. McFarlane, and J.F. Lam

Hughes Research Laboratories
3011 Malibu Canyon Road
Malibu, CA 90265

August 1986

F49620-84-C-0083
Annual Report
July 1984 through July 1986

DTIC
ELECTE
OCT 2 0 1986
S
D
D

Air Force Office of Scientific Research
Department of the Air Force
Bolling AFB, Washington, DC 20332-6448

DTIC FILE COPY

86 10 16 031

SECURITY CLASSIFICATION OF THIS PAGE

ADA173370

REPORT DOCUMENTATION PAGE

1a. REPORT SECURITY CLASSIFICATION	1b. RESTRICTIVE MARKINGS
Unclassified	

2a. SECURITY CLASSIFICATION AUTHORITY	3. DISTRIBUTION/AVAILABILITY OF REPORT
	Approved for public release;
2b. DECLASSIFICATION/DOWNGRADING SCHEDULE	distribution unlimited.

4. PERFORMING ORGANIZATION REPORT NUMBER(S)	5. MONITORING ORGANIZATION REPORT NUMBER(S)
	AFOSR·TR· 86-0837

6a. NAME OF PERFORMING ORGANIZATION	6b. OFFICE SYMBOL (If applicable)	7a. NAME OF MONITORING ORGANIZATION
Hughes Research Laboratories		Air Force Office of Scientific Research

6c. ADDRESS (City, State and ZIP Code)	7b. ADDRESS (City, State and ZIP Code)
3011 Malibu Canyon Road	Department of the Air Force
Malibu, CA 90265	Bolling Air Force Base,
	DC 20332-6448

8a. NAME OF FUNDING SPONSORING ORGANIZATION	8b. OFFICE SYMBOL (If applicable)	9. PROCUREMENT INSTRUMENT IDENTIFICATION NUMBER
AFOSR	NE	F49620-84-C-0083

8c. ADDRESS (City, State and ZIP Code)	10. SOURCE OF FUNDING NOS.			
Blg 410	PROGRAM ELEMENT NO.	PROJECT NO.	TASK NO.	WORK UNIT NO.
BAFB DC 20332	61102F	2305	B4	

11. TITLE (Include Security Classification) Nonlinear Optical Properties and Subpicosecond Dynamics of Electrons and Electron-Hole Plasmas in Multiple Quantum Well Structures

12. PERSONAL AUTHOR(S) AL Smirl, RA McFarlane, and JF Lam

13a. TYPE OF REPORT	13b. TIME COVERED	14. DATE OF REPORT (Yr., Mo., Day)	15. PAGE COUNT
Annual	FROM July 84 TO July 86	21 August 1986	

16. SUPPLEMENTARY NOTATION

17.	COSATI CODES		18. SUBJECT TERMS (Continue on reverse if necessary and identify by block number)
FIELD	GROUP	SUB GR	Nonlinear Optics; Optical Devices; Ultrafast Phenomena;
			Multiple Quantum Wells

19. ABSTRACT (Continue on reverse if necessary and identify by block number)

Here we report our progress in measuring the nonlinear optical properties and picosecond dynamics of carriers in multiple quantum wells and other bulk and MBE-grown structures. Discussions of our progress are divided into six parts: (1) fabrication and characterization, (2) picosecond time-resolved transient absorption, (3) picosecond time-resolved photoluminescence, (4) theory of dressed excitons, (5) picosecond photorefractive effects, and (6) picosecond and femtosecond laser development.

20. DISTRIBUTION/AVAILABILITY OF ABSTRACT	21. ABSTRACT SECURITY CLASSIFICATION
UNCLASSIFIED/UNLIMITED ☐ SAME AS RPT ☐ DTIC USERS ☐	Unclassified

22a. NAME OF RESPONSIBLE INDIVIDUAL	22b. TELEPHONE NUMBER (Include Area Code)	22c. OFFICE SYMBOL
		NE

DD FORM 1473, 83 APR EDITION OF 1 JAN 73 IS OBSOLETE. Unclassified

SECURITY CLASSIFICATION OF THIS PAGE

DISCLAIMER NOTICE

**THIS DOCUMENT IS BEST QUALITY
PRACTICABLE. THE COPY FURNISHED
TO DTIC CONTAINED A SIGNIFICANT
NUMBER OF PAGES WHICH DO NOT
REPRODUCE LEGIBLY.**

TABLE OF CONTENTS

INTRODUCTION

In this document, we report our progress on the AFOSR contract entitled "Nonlinear Optical Properties and Picosecond Dynamics of Excitons and Electron-Hole Plasmas in Multiple Quantum Well Structures," and on internal IRD projects on which we have agreed to provide AFOSR unrestricted access. For purposes of this report, discussions of our progress are divided into six parts: (i) fabrication and characterization, (ii) ps time-resolved transient absorption, (iii) ps time-resolved photoluminescence, (iv) theory, (v) ps photorefractive effects and (vi) ps and fs laser development. A section of this report is devoted to a discussion of our progress in each of these areas. This work has resulted in 14 technical presentations and 12 publications during the last 16 months.

TASK 1: FABRICATION AND CHARACTERIZATION

The primary objectives of this task were to grow multiple quantum well (MQW) structures by molecular beam epitaxy (MBE) for subsequent use in nonlinear optical studies; to characterize these structures as to composition, layer thickness, and spatial uniformity by linear optical techniques; and, finally, to develop selective etching techniques to remove the substrate from the multiple quantum well structure to provide semitransparent samples for use in many of the nonlinear optical experiments. We now discuss our progress in meeting the stated objectives.

MBE Fabrication. During the initial phases of this program, we have obtained MQW materials and other heterostructures from multiple sources: (i) several separate MQW structures were grown in house at HRL for use in this program, (ii) three were fabricated by P.K. Bhattacharya (of the University of Michigan) for a fee, and (iii) six were grown by Phi Corporation, also for a fee. In addition, four heterostructures (to be described later) and two modulation-doped (NIPI) superlattices were produced. We wish to emphasize that all of the initial sample growth was supported by Internal Research and Development funds at HRL and the samples made available for contract research.

Once they were fabricated, the as-grown materials were thoroughly characterized for dimensionality, stoichiometry, uniformity and reproducibility by using linear diagnostic procedures such as photoluminescence, photoreflectance and transmission spectroscopy. Such a characterization was deemed prudent before embarking on tedious and time consuming nonlinear optical studies.

Photoluminescence. The ideal linear diagnostic procedure would be one that is nondestructive and noncontacting. Photoluminescence satisfies these basic requirements.

5

Consequently, conventional steady-state photoluminescence spectra were recorded for all of our samples. In the low-temperature photoluminescence spectra of the MQW structures, the feature corresponding to the heavy-hole-to-conduction $n=1$ exciton transition was always visible. The width of this feature gave an initial indication of the variation in well width. Features corresponding to the GaAs substrate and the light-hole-to-conduction $n=1$ exciton transition were also usually visible, but were hundreds of times weaker than the heavy-hole excitonic feature. Higher order transitions ($n>1$) were not visible. This technique has two major disadvantages: First, only low order transitions ($n=1$) are observable. These are sensitive to well-width, but insensitive to well depth (i.e., composition). Second, the measurements usually must be performed at low temperatures.

Photoreflectance. By contrast, photoreflectance is a contactless form of modulation spectroscopy that suffers from none of the aforementioned problems. In this technique, the periodic optical generation of electron-hole pairs modulates the optical constants of the sample, producing a repetitive change in the reflectivity. In our experimental arrangement, the chopped light from a low powered He-Ne laser is gently focused onto the sample surface to produce the electron-hole pairs. The periodic reflection change induced in the MQW by the laser is interrogated by weak tunable light from a white light/monochromator combination that is focused onto the center of the laser-irradiated region. The reflected signal is measured by a p-i-n photodiode. A lock-in amplifier that is phase locked to the reference frequency of the laser chopper is then used to discriminate the small periodic reflectivity changes from the large background reflected signal. Finally, the lock-in signal is recorded on a strip chart recorder that is slaved to the wavelength servo drive of the monochromator.

As a modulation technique, photoreflectance has the advantage of measuring changes in the sample spectra rather than

the absolute spectra. This together with the phase sensitive detection, allows the measurement of very weak changes in reflectivity (1 part in 10^5). Finally, it suppresses strong background reflected signals and emphasizes local features by converting weak reflectivity changes into strong "derivative-like" features in the spectra. In fact, this technique produces such sharp spectra that even at room temperature all the interband quantum transitions can be observed in a MQW. The modulation spectra of these MQW and superlattice structures can be fit by a derivative functional form, thus making it possible to quantitatively determine the quantum energies and linewidths of the allowed transitions. From these, for example, one can then accurately determine the well width and barrier neight for compositional MQW structures.

Initially, measurements using this technique were performed on a photoreflectance apparatus assembled at HRL. Extensive spectra obtained in these early measurements provided qualitative information, but no satisfactory nonlinear-least-squares fit routine existed to provide a quantitative fit to spectral lineshapes. Subsequently, a collaboration was established with Prof. F.H. Pollak and his students at Brooklyn College of the City University of New York, whereby they performed additional measurements and quantitative analyses of selected MQW and NIPI structures. Concurrently, we have developed our own nonlinear-least-squares linefit code at HRL and have assembled a state-of-the-art photoreflectance apparatus at NTSU. We now routinely acquire and fit photoreflectance spectra of MQW and heterostructures at NTSU. We wish to emphasize, however, that Prof. Pollak continues to collaborate on studies both at CUNY and NTSU/HRL.

One of the most studied samples consisted of 100 periods of 100 Å-thick layers of GaAs alternating with 150 Å-thick layers of $Al_{0.17}Ga_{0.83}As$. All measurements and analyses were performed in collaboration with Dr. Fred Pollak and his students at Brooklyn College of the City University of New York. The entire room temperature photoreflectance spectra from this MQW was

successfully fit by a derivative functional form lineshape
expression. All allowed quantum transitions were clearly
identified. In addition, we observed, for the first time at room
temperature, three features corresponding to forbidden
transitions. This derivative line fit has allowed us to
accurately determine the energies and broadening parameters of
all transitions. These measured energies are in excellent
agreement with those calculated by Joel Schulman using a two-
band, tight-binding model. Finally, there are three features
that we speculate may be related to transitions involving
unconfined states. Initial results were presented at the
American Physical Society meeting in Las Vegas (31 March–4 April
1986) and further results were presented at the International
Conference on the Physics of Semiconductors in Sweden in August
1986. A manuscript has been accepted by Solid State
Communications. Details of this work are provided in Appendix A
and Appendix B in the form of preprints of the Solid State
Communications manuscript and the proceedings of the
International Conference on the Physics of Semiconductors,
respectively.

Also, (again working with Fred Pollak and his students), we
have performed photoreflectance studies of doping superlattices.
The experiments were performed at room temperature on two GaAs
superlattices having considerably different built-in potentials.
The first sample (NIPI 497) was grown in-house and consists of 21
layers of n ($n_d = 7 \times 10^{17} cm^{-3}$) and p ($n_a = 5 \times 10^{17} cm^{-3}$) doped GaAs
layers each having a thickness of 233A. The second sample, NIPI
498, has nominal dopings of $6.5 \times 10^{17} cm^{-3}$ for the n-type layers
and of $2.5 \times 10^{17} cm^{-3}$ for the p-type layers. The n and p layer
thicknesses for the latter sample were 800A and 1400A,
respectively. The built potential for NIPI 497 (498) is
estimated to be ~ 85 meV (~ 1200 meV). For the sample with the
small built in potential (NIPI 497), the spectral features can be
fit by a derivative functional form, and we have tentatively
identified a number of these features. The spectra from the
sample with large built-in potential (NIPI 498), however, cannot

8

be fit with this derivative functional form. Instead, it exhibits Franz-Keldysh oscillations. The period of these oscillations can be directly related to the built-in dc electric field. Consequently, this technique provides, for the first time, a method for measuring these built-in fields. Finally, by measuring the strength of the photoreflectance signal as the chopping frequency of the pump laser was varied, we were able to extract the carrier recombination lifetime. Our assignment of energy levels to specific spectral features is still somewhat tentative for the NIPI structures, and work in this area will continue. Toward this end, two additional NIPI structures with small built-in fields and with different doping densities have been recently grown in-house. During the coming months, we will thoroughly characterize these by photoreflectance. The information obtained from these samples should allow us to corroborate our initial spectral assignments. Nevertheless, we have made sufficient progress to report our initial findings at the American Physical Society meeting in Las Vegas (31 March-4 April) and at the International Conference on Superlattices and Microstructures (a Satellite of the International Conference on the Physics of Semiconductors) in Sweden in August 1986. A preprint of the proceedings of this conference is included as Appendix C.

Additionally, we have recently received a number of new simple compositional MQW structures from both in-house and external sources. We are currently characterizing these as to quality, dimensionality, and composition by both photoreflective and photoluminescence techniques. The best of these will be selected for detailed nonlinear optical measurements.

Selective Etching. Before a sample can be used in nonlinear optical experiments, it often must be rendered transparent in the spectral region near the lower lying quantum-confined energy levels. This requires that the GaAs substrate be removed from the MQW by etching. Initial attempts (both in-house and with collaborators at the University of Michigan) failed to produce a

satisfactory etching procedure for this purpose. Recently, however, Dr. C.A. Lee of Cornell University and his student K. Rauschenbach have worked with us to develop such a procedure. Their procedure was then used to successfully etch several well-defined "windows" in selected high-quality MQW structures grown by Perkin Elmer.

Transmission Spectroscopy. Absorption techniques provide a simple, direct, nondestructive, contactless alternative to photoreflectance that can be easily implemented at room temperature. Absorption measurements require a partially transmitting sample at the wavelengths of interest. Consequently, when transmitting MQW samples became available, we used transmission spectra to supplement the information obtained from photoluminescence and photoreflectance. Specifically, we measured the room temperature transmission spectra of the "transparent" regions of the samples - both at HRL and at North Texas State University. The excitonic features corresponding to all allowed optical transitions were sharp, well-defined, and clearly visible in the measured spectra. An example of such spectra are shown in Fig. 1 for an MQW consisting of 150Å barriers of $Al_{0.3}Ga_{0.7}As$ alternating with 100Å GaAs wells.
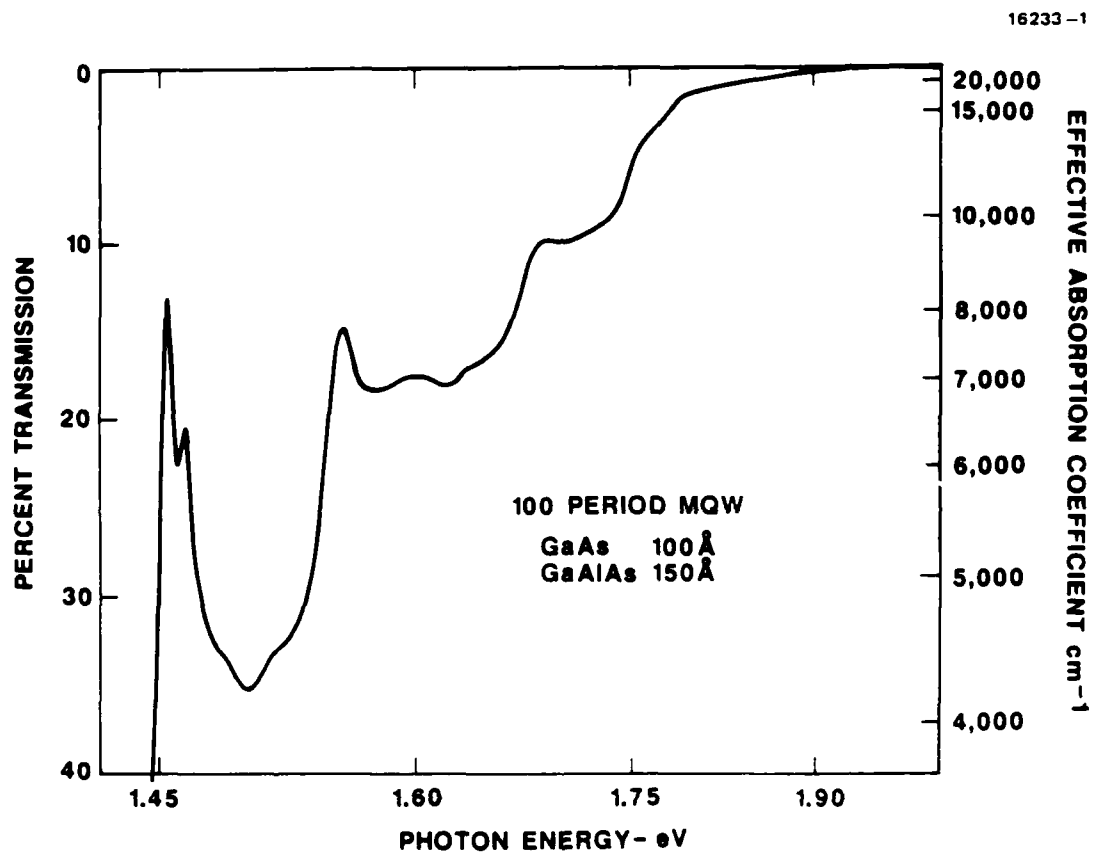
16233-1

Figure 1: Transmission spectrum of a compositional
multiple quantum well consisting of 100Å
layers of GaAs alternating with 150Å layers
of AlGaAs with x=0.3.

11

TASK 2:   PICOSECOND TIME-RESOLVED NONLINEAR ABSORPTION

In initial studies, we have time-resolved the excitonic
saturation dynamics on picosecond time scales using a standard
pump-and-probe arrangement.   In these initial experiments,
electron-hole pairs were generated by band-to-band absorption of
an intense 42-ps pump pulse at 0.532 μm.   The energy of the pump
was adjusted by using continuously variable attenuators.   The
bleaching of the exciton was then probed at various time delays
by a weak broad-band ps optical continuum.   The observed
saturation behavior followed exactly that reported previously by
other workers in the field.   Figure 2 shows an example of the
absorption saturation spectra of a MQW consisting of 100 periods
of 150 Å barriers of $Al_{0.3}Ga_{0.7}As$ alternating with 50 Å GaAs
wells.   This figure illustrates the bleaching of the exciton with
increasing optically-created electron-hole density at a fixed
time delay (130ps) following excitation.   Detailed studies of
this type (together with the photoluminescence studies reported
below) will yield information not only on the excitonic bleaching
dynamics, but on the simultaneously occurring processes of
bandgap narrowing and nonlinear diffusion in these MQW's.
Moreover, the third-order susceptibility $\chi^{(3)}$ associated with the
saturation of the exciton and with bandgap narrowing will be
further investigated by using various degenerate-four-wave-mixing
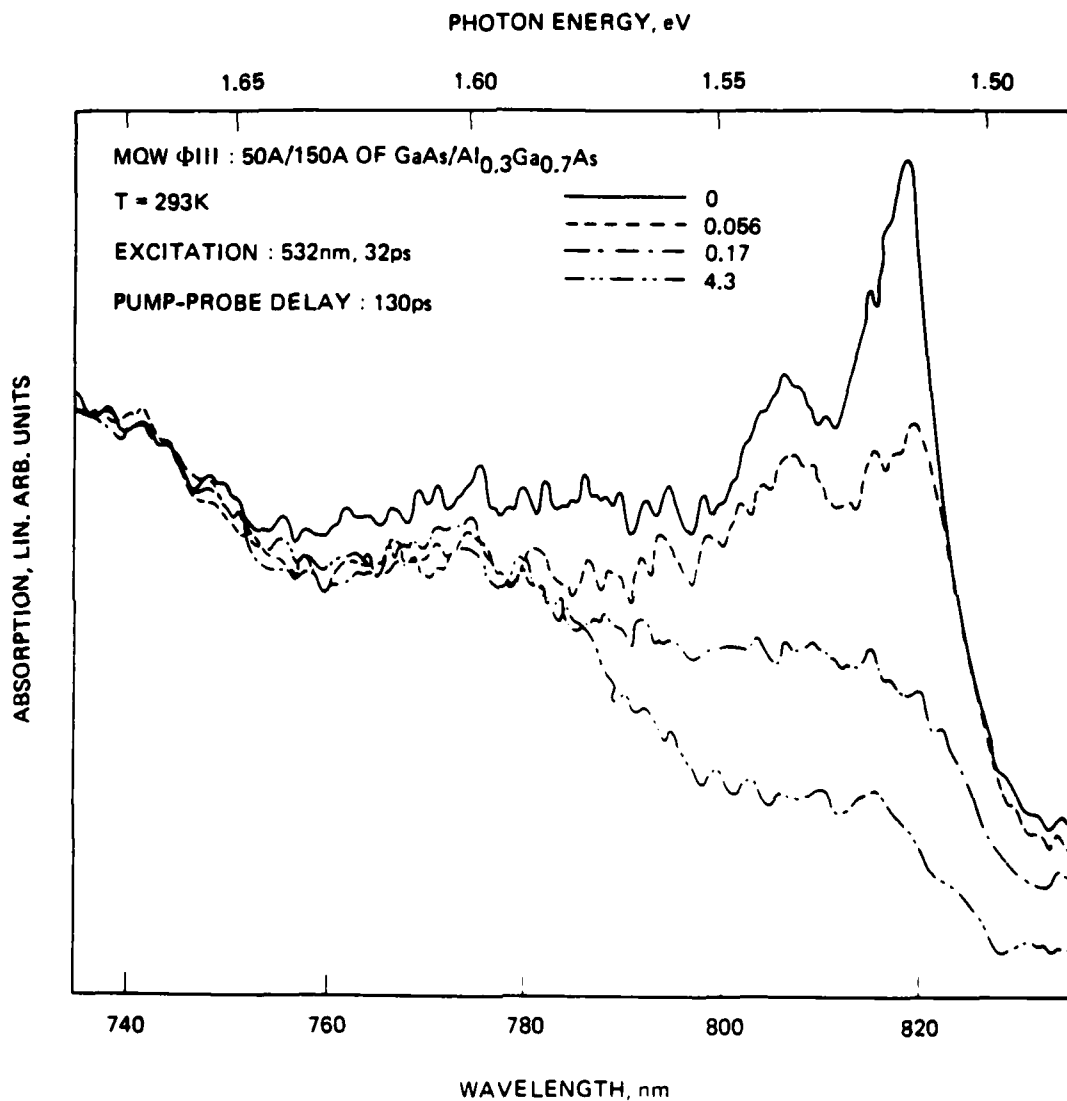geometries and techniques at a later date.

Figure 2: The bleaching of the exciton in a multiple quantum well consisting of 50Å layers of GaAs alternating with 150Å layers of AlGaAs (x=0.3) with increasing excitation fluence.

TASK 3: PICOSECOND TIME-RESOLVED PHOTOLUMINESCENCE

We have initiated (together with coworkers at North Texas State University) an extensive program to measure (i) the dynamics of hot carrier relaxation, (ii) nonlinear carrier diffusion, (iii) carrier bulk and surface recombination lifetimes and (iv) bandgap narrowing caused by high optically-created carrier densities in multiple quantum wells. One of several techniques that we are using to acquire this information is time-resolved photoluminescence. In these experiments, the sample is first excited by the absorption of an intense picosecond pump pulse whose photon energy is greater than the first quantum confined transition in the well. The recombination radiation from the sample is then collected following excitation and sent through a spectrometer. The spectrometer disperses the light horizontally according to wavelength. The spectrometer is then followed by a streak camera that disperses the light vertically in time. In this way, we obtain the complete recombination spectra as a function of time following excitation on a single record. Initial studies of this type have been performed on two MQW structures. The motivation here was to compare the recombination times, bandgap narrowing and nonlinear diffusion with that observed in bulk samples. The problem, as we discovered, is that these phenomena are not well understood in the bulk.

Consequently, we initiated an extensive program to measure these phenomena in bulk MBE layers (not MQW's) of the ternary alloy $Al_xGa_{1-x}As$. This compound is of special interest for a large variety of nonlinear optical and optoelectronic device applications and is also considered an attractive candidate for solar cell applications. These phenomena are being investigated on a picosecond timescale as a function of the alloy composition x, the lattice temperature, the initial density of excess optically-created carriers, and the excess energy of the excited carriers.

15

We are particularly interested in separating the correlation and exchange contributions to the bandgap renormalization in semiconductors by analyzing the picosecond time-resolved photoluminescence from these ternary alloys. The alloy AlGaAs is particularly well suited for these investigations because it exhibits a direct-to-indirect energy band crossover as the aluminum concentration x is increased above $x_c \sim 0.435$. Thus, for x values larger than x_c, the energy gap will be indirect, and most photoexcited electrons will reside in the indirect valleys. Consequently, both exchange and correlation effects should contribute to the renormalization of the indirect gap, while only correlation effects are expected to contribute to the narrowing of the direct gap. Conversely, for x values smaller than x_c, the gap will be direct, and most electrons will be found in the direct valley. In the latter case, exchange and correlation should determine the direct gap narrowing, but correlation alone should determine the indirect narrowing. We also wish to measure the bandgap for temperature regimes where the photoexcited carrier distributions are nondegenerate, and theoretical models are not currently available.

Initially, we investigated a single LPE-grown sample with an x-value ~ 0.23. The excitation source for these initial experiments was a frequency-doubled mode-locked Nd:YAG laser that produced pulses at 0.532 μm with a temporal width of 30 ps. The photoluminescence of the laser-excited sample was simultaneously spectrally and temporally resolved by using a combination of a spectrometer and a streak camera system. Such spectra were recorded for a full range of excitation levels up to the melting threshold. The long high energy tails of spectra obtained in this way indicated the presence of hot carrier distributions. The temporal decay of the recorded spectra reflected the dynamics of carrier cooling and recombination and provided evidence for a dynamic bandgap renormalization caused by the exchange and correlation effects associated with the dense carrier plasma.

Subsequently, we have extended these time-resolved photoluminescence measurements to include two additional samples

grown by MBE. One had an x-value of 0.38. For this alloy composition, the direct conduction valley is only approximately 60 meV below the indirect x-valleys. The other had an x-value of 0.52. For this composition, the lowest conduction band edge is indirect at the x-point and is approximately 100 meV below the direct valley. We also analyzed our data to extract the time-resolved carrier temperature, density, direct bandgap, and indirect bandgap from the initial photoluminescence spectra.

For the LPE-grown sample with x-value of 0.23 (well within the direct gap regime), plasma luminescence typical of a direct gap semiconductor was observed. The initial excess energy of the electrons was 630 meV. The peak temperature during the pulse was determined to be around 450 K. This indicates that the carriers have lost most of their initial excess energy on a time scale short compared to the pulsewidth. This was confirmed by the observation that the carrier temperature reached lattice temperature essentially as soon as the excitation ended. The carrier density (for this sample) showed essentially an exponential decay with a time constant of ~ 200 ps.

For an alloy composition of 0.38, two peaks were observed in the recombination spectra. The low energy peak was associated with recombination from the direct valley and the high energy peak was attributed to recombination from the indirect valleys. The decay times for the direct and indirect emission bands were found to be 105 ps and 60 ps, respectively. Emission from indirect valleys for alloy compositions near the direct-indirect crossover occurs predominantly without participation of phonons due to an electron scattering by random potential fluctuations. The relative intensity of the indirect emission band indicated a high efficiency for this recombination channel. The shorter decay time for the indirect emission is consistent with electron transitions from the indirect valleys to the lower Γ-valley which help to adjust an inter valley equilibrium distribution for the photo-excited electrons.

For the x=0.52 sample, again, two distinct emission bands were observed. The direct emission (high energy band) was

observed only during excitation, i.e., during the relaxation of the photo-excited electrons to the bottom of the bands. The decay time for the indirect emission increased to 640 ps. This is consistent with a decreasing probability for alloy scattering with increasing direct-indirect gap separation in the indirect gap regime.

An examination of band gap renormalization showed an enhanced renormalization of the Γ-gap for compositions below but close to x_c. This can be explained by an increase of the effective electron mass due to bandmixing effects associated with alloy scattering. The renormalization of gaps above the lowest gap appears to be reduced due to a reduced exchange contribution.

In summary, for alloy compositions near the direct-indirect gap crossover, emission from direct and indirect conduction band valleys is observed simultaneously. The relative intensity of the indirect (no-phonon) emission band indicates a high radiative recombination rate due to random potential fluctuations. Bandgap renormalization near x_c is influenced by disorder effects and by the distribution of the photo-excited electrons among several conduction band valleys.

Initial results on this project were presented at the International Quantum Electronics Conference in June 1986 in San Francisco and the Conference on Ultrafast Phenomena held in Aspen, also in June. A preprint of our contribution to the proceedings of the Conference on Ultrafast Phenomena is included as Appendix D.

There are two reasons for including these studies: First, they provide a data base for comparing these phenomena in the bulk with similar effects in MQW's, and second, these phenomena are, in themselves, of interest for nonlinear device applications. Specifically, we intend to demonstrate (during the next few months) that the nonlinear absorption changes experienced at wavelengths near the bandedge that accompany bandgap narrowing can be used to construct an absorptive biastable switch.

TASK 4: THEORY OF DRESSED-EXCITONS IN MULTIPLE QUANTUM WELLS

The understanding of the nonlinear optical responses of semiconductor multiple quantum wells (MQW) depends on the degree of laser-induced resonant excitation of the excitons. If the laser is tuned on resonance with the exciton line, then the phonon-assisted generation of electron-hole plasmas will induce screening effects on the exciton lineshape. On the other hand, if the laser is tuned below the spectral linewidth of the exciton, then plasma screening is unimportant and the excitonic features remain unaltered. It is in this latter regime that our calculation was performed.

We constructed an exact theory of the influence of a radiation field of arbitrary intensity on a MQW exciton. The calculation proceeded along the following steps. First, an effective mass approximation of the electron-hole Hamiltonian yielded two terms. One describes the center-of-mass motion of the exciton while the second term describes the relative motion of the exciton. Second, the three dimensional motion of the exciton can be separated into the motion along the z axis (defined to be the direction of the layered system) and motion along the xy plane provided that the effective mass along the z axis is large compared to that along the xy plane. We shall assume that this is the case for the GaAs-AlGaAs MQW system. Third, the confinement of the electron-hole system along the direction of the MQW gives rise to spatial quantization along the z axis. While, the motion of the exciton along the xy plane is described in terms of a two dimensional hydrogen atom having a charge z/ϵ; where ϵ is the effective static dielectric constant of the host lattice. Fourth, a basis set was chosen to represent the near resonant two-level model of the exciton. The basis set energies are determined by the quantized motion along the z axis, the free motion of the center-of-mass along the xy plane and the bound motion of the two dimensional hydrogen atom. And last, we solved the Schrodinger equation for the exciton in the presence of a near resonant radiation field.

The results of this calculation can be summarized as follows. First, the dressed-exciton energies were obtained by diagonalizing the infinite set of 2x2 Hamiltonian. Hence each unperturbed energy level is split into 2 symmetrically displaced dressed-exciton energies. The separation between the dressed states is given by the generalized Rabi flopping frequency. Second, the dressed-exciton states were obtained from the diagonalization procedure and they are given as linear coherent superposition of the basis (unperturbed) states. The solutions are valid for all intensity regimes provided that the laser detuning from resonance is outside of the exciton spectral linewidth. And last, we found that the emission process of the dressed-exciton showed that gain, in the absence of real population inversion, can be achieved for radiation which is downshifted from the pump by the generalized Rabi frequency. Hence in this regime, one can obtain broadband self-pumped phase conjugation in MQW.

TASK 5: DEVELOPMENT OF PICOSECOND AND FEMTOSECOND LASER SOURCES

The principal objective of this task is to develop reliable
sources of tunable picosecond and femtosecond optical pulses to
be used in support of the measurement tasks described in this
proposal and other internally funded IRD projects at NTSU and
HRL. We emphasize that this is not a project for which AFOSR was
to provide funding, and no AFOSR funds were expended on this
task. However, since our ability to perform measurement tasks
associated with this project are directly related to our ability
to develop ever more reliable and versatile sources of picosecond
and femtosecond pulses, a report of progress in this regard is in
order here. Again, we emphasize that support for the development
of these laser sources was provided by internal IRD funding at
HRL and by ONR at NTSU.

An Amplified Short-Cavity Dye Laser, Tunable in the Near
Infrared. One project on which we have made significant progress
over the past year is the development at North Texas State
University (with coworkers at NTSU) of a short cavity dye laser
system to extend the useful spectral range of our existing mode-
locked Nd:YAG laser system and to provide a tunable source of
picosecond pulses in the range of 800-850 nm (near the band edge
of GaAs). In this system, frequency doubled pulses from an
amplified actively-passively mode-locked YAG laser, operating at
10 Hz, are used to excite a short cavity dye laser and to pump a
three stage amplifier for pulses produced by the dye laser.
Typically, the doubled pulses from the YAG pump are 32 ps in
duration and have an energy of roughly 1 mJ (depending on
amplifier voltage settings). Once the amplifier flashlamp
voltages are chosen, however, more than 70% of the doubled pulses
are within ± 10% of the mean energy. A fraction of each doubled
pump pulse is used to excite a short cavity dye laser that
operates in a single axial mode and that can be tuned in
frequency by varying the cavity spacing using a piezoelectric
transducer. Typical cavity spacings are between 5 and 17 μm. An

21

opto-electronic feedback system is used to compensate for mechanical relaxation of the optical cavity by adjusting the voltage on the piezoelectric spacers and thereby correcting for any drift in the center frequency of the laser. The remainder of each doubled (green) pump pulse is divided into three parts, and each part is used to back-pump a dye amplifier stage. To characterize this system, we used a streak camera (with 2 ps resolution), and spectrometer, and an optical multichannel analyzer to simultaneously measure the pulsewidth, the spectrum and the spatial profile of single pulses from this frequency-stabilized system. In this way, we optimized laser performance by examining the influence of pump power, cavity lifetime (cavity spacing), and dye concentration on the pulsewidth and stability. The tuning range and overall energy conversion efficiencies were also determined. Typically, the amplified pulses had a spectral width of 3 to 3.5 A and a temporal width of 8±2 ps. The system proved to be tunable over the entire range 800-850 nm. The average pulse energy was roughly 5 μJ. More than 90% of the pulses had an energy within ±25% of the mean. We wish to emphasize that this is the first operation of a short cavity dye laser in the infrared. The system is now being used routinely in experiments on MQW structures and ALGaAs thin films. The system operation and design parameters are described in detail in a manuscript that has recently been accepted by the IEEE Journal of Quantum Electronics. A preprint of this work is included as Appendix E.

Amplified Femtosecond Dye Laser System. In a second project (again in collaboration with workers at North Texas State), we have made substantial progress in extending our ultrashort measurement capabilities into the femtosecond regime. A schematic of the overall system is shown in Fig. 3. As shown, the laser oscillator is synchronously pumped by the frequency-doubled, mode-locked output from a cw mode-locked YAG laser. In its initial configuration, the dye laser oscillator was a commercially-available linear cavity that contained a single dye
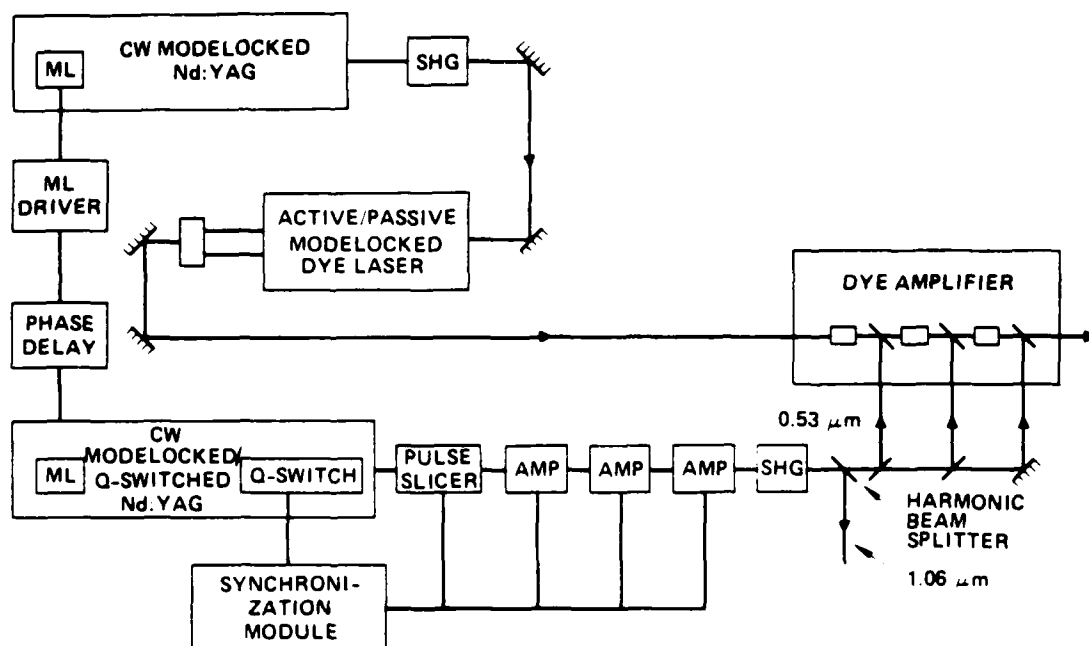
Figure 3: Schematic of Nd:YAG-based amplified femtosecond dye laser system.

23

jet and a birefringent tuning plate. When this oscillator was only synchronously pumped, it produced pulses a couple of ps in duration and could be tuned from 580-620 nm, when Rhodamine 6G was used as the active medium. When the mode-locking saturable-absorber DODCI was added to the mixture flowing through the dye jet, pulses as short as 300 fs were obtained, at the sacrifice of tunability. The pump source for the dye amplifier stages is a second amplified cw mode-locked YAG laser that is simultaneously Q-switched at a repetition rate of up to several kHz. The mode-locking crystal for this second YAG laser is driven from the same radio frequency synthesizer as the first to ensure less than 50 ps jitter between the two YAG output trains. An electro-optic pulse selector then slices a single pulse from the mode-locked, Q-switched train of the second YAG laser. This pulse is then amplified in three stages, frequency-doubled, and used to back-pump three dye-laser amplifier stages. We took great care in the YAG amplifier stages to avoid self-focusing and to ensure Gaussian spatial profiles. The frequency-doubled YAG pump pulses for the synchronous amplifier are typically 70 ps in duration and have an energy of roughly 20 mJ at a repetition rate of 10 Hz. The amplitude stability is ±10%. The synchronous dye amplifier system is similar in design to that used in the short cavity dye laser system described above. The overall amplifier gain was > 3×10^5, and typical output energies were 150 μJ in a 300 fs pulse.

More recently, our efforts have focused on designing and building (in-house at NTSU) a hybridly mode-locked cw dye laser oscillator capable of producing even shorter pulses. This laser oscillator consisted of a dual-jet linear cavity that incorporated two Brewster prisms to compensate for intracavity dispersion and chirp. Using several combinations of laser dyes and saturable absorbers, we successfully produced pulses well below 100 fs in duration at yellow, red and deep red wavelengths. Pulsewidths as short as 50 fs were observed. These are the shortest pulses ever produced by a synchronously pumped system. Moreover, we demonstrated that the laser spectral width could be adjusted and that the output pulsewidth could be tuned by more

than an order of magnitude by including a simple variable aperture between the second prism and the end mirror (a region of the cavity where the frequency components are spatially dispersed). Results of this development were reported as a post-deadline paper at the Fifth Conference on Ultrafast Phenomena in Aspen in June, 1986. More recent results will be presented at the Annual Meeting of the Optical Society of America in Seattle in October 1986. Three manuscripts have been prepared describing the development of the hybrid oscillator. The first, which describes the incorporation of the prism pair into the linear cavity, has been accepted by Optics Communications and is included as Appendix F. The second, which describes the production of variable width pulses by intracavity spectral filtering, has been accepted by Optics Letters and is included as Appendix G. Finally, the third, which describes the extension of laser operation to red and deep red spectral regions, has been submitted to IEEE Journal of Quantum Electronics.

TASK 6: ULTRAFAST PHOTOREFRACTIVE EFFECTS

The primary objective of this contract is to investigate nonlinear optical mechanisms in MQW structures. The expectation is that such basic studies will lead to a fundamental understanding of phenomena that have potential application in the development of nonlinear optical devices that operate on picosecond or subpicosecond time scales, at room temperature, and at low light levels. Such devices then could be eventually incorporated into optical data processing or communications systems. Under this task, we report the investigation of mechanisms in bulk GaAs that allows the switch-on speed of photorefractive devices to be improved from nanoseconds to picoseconds. Specifically, in these studies, we demonstrated weak beam gains of a few percent with a picosecond switch-on time using energy densities of only a few picojoules per squared micron.

Initially (again in collaboration with workers at North Texas State), we performed a detailed experimental investigation of two-beam coupling in GaAs on subnanosecond time scales. In these experiments, the energy transferred between two 43 ps, 1.06 μm pulses that were spatially and temporally coincident in a 3-mm-thick sample of undoped, semi-insulating GaAs was measured as a function of the ratio of energies in the two pulses, the total fluence, time delay between the two pulses, and crystal orientation. We found the direction of energy transfer between two equal beams to depend definitely on crystal orientation, an unambiguous signature of the photorefractive effect. This is the first observation of picosecond photorefractive beam coupling. However, for these pulsewidths, the accompanying contributions of two-photon absorption and free-carrier transient energy transfer (through the free carrier index) to the probe loss or gain were also evident.

More recently, our efforts have centered on the theoretical modeling of the voluminous and varied experimental data. For our

first stage of analysis, we attempted to isolate the photorefractive effects from those of two-photon absorption and free-carrier transient energy transfer. To do this, we essentially subtracted the measured net probe gain for the crystal oriented for photorefractive energy transfer from strong-to-weak beam from the data for the crystal oriented for energy transfer from weak-to-strong beams. For small energy transfer and no pump depletion, the difference for the two orientations should be twice the photorefractive transfer alone. Our theoretical calculations (based on charge transport and rate equations) are in good agreement with the measured photo-refractive transfer. Results show that the measured photo-refractive beam coupling gain of up to 4% in the fluence range 0.03 to 0.3 mj/cm^2 is caused by a charge separation between photoionized electrons and positively ionized EL2 donors. For fluences between 3 and 13 mj/cm^2, observed photorefractive gains of up to 12% can be attributed to charge separation between electron-hole pairs produced by two-photon ionization.

This work resulted in an invited presentation given at the Conference on Lasers and Electro-Optics (CLEO) in San Francisco in June, 1986 and a contributed talk at the Ultrafast Phenomena Conference held in Aspen, Also in June, 1986. In addition, a manuscript describing the initial bit of this work has been accepted for publication by Optics Letters. A preprint of that paper is included as Appendix I.

Appendix A: Observation of Symmetry
Forbidden Transitions in the Room
Temperature Photoreflectance Spectra of a
GaAs/GaAlAs Multiple Quantum Well.

A preprint of a paper accepted for
publication by Solid State Communications

Observation of Symmetry Forbidden
Transitions in the Room Temperature
Photoreflectance Spectra of a GaAs/GaAlAs Multiple Quantum Well

H. Shen[a], P. Parayanthal and Fred H. Pollak[a]
Physics Department
Brooklyn College of the City University of New York
Brooklyn, N.Y. 11210

and

Arthur L. Smirl, J.N. Schulman, R.A. McFarlane and Irnee D'Haenens
Hughes Research Laboratory
Malibu, CA 90265

[a] Also at Physics Department, Graduate School and University
Center, City University of New York, New York, N.Y. 10036

ABSTRACT

We have measured the room temperature photoreflectance spectra from a 100A/150A GaAs/GaAlAs multiple quantum well (MQW) ($x \gtrsim 0.17$). The entire spectrum from the MQW has been fit by a third-derivative functional form lineshape expression. In addition to all the allowed quantum transitions we have clearly observed features from several symmetry forbidden transitions. There also appears to be evidence for unconfined transitions, i.e. energies above the band gap of the GaAlAs barrier layer. There is good agreement between the experimentally determined energies of the various features and a theoretical calculation.

Electromodulation (electroreflectance and photoreflectance) is rapidly becoming an extremely powerful tool to study microstructural geometries [1-8] (superlattices, quantum wells and heterojunctions) in semiconductors. This method is useful since it yields sharp structure (related to the third-derivative of the optical constants) even at room temperature, has a well-defined lineshape[8] (Aspnes third-derivative functional form[9]) that can be used to accurately fit the spectra and is a function of surface (interfacial) electric fields.

The enhanced sensitivity and well-defined lineshape of electromodulation makes it a very important method to study weak features in the optical properties of these structures. For example, recent works indicate additional structure in the absorption coefficient due to the appearance of new critical points arising from a mixing of the light and heavy hole character of the valence subbands[10-13]. Photoreflectance (PR) is particularly useful since it is a contactless mode of electromodulation[1,5,9] In PR the optical constants of the material are modulated by the photo-injection of electron-hole pairs by a secondary (pump) light source. [1,5,9].

In this note we report a room temperature PR study of a GaAs/GaAlAs multiple quantum well (MQW) in which, for the first time, forbidden transitions have been clearly observed at 300K. We have detected three symmetry forbidden features from the MQW in addition to all the allowed quantum transitions. Also, there are features in the spectra which may be due to transitions involving unconfined states.[14] Glembocki et al. have recently reported the temperature dependence of PR in GaAs/GaAlAs multiple quantum wells[6]. Although they clearly observe forbidden features at low temperatures (149K and 125K) their

room temperature spectra reveals only two very weak structures which correspond to the forbidden transitions.

The sample used in this study was a 100A/150A GaAs/GaAlAs MQW ($x \approx 0.17$) grown by molecular beam epitaxy at the Hughes Research Laboratory. The PR technique has been described in the literature[1,5,9]. The pump beam was a 1 milliwatt He-Ne laser (6328A), the power density on the sample being about 100 microwatts/cm^2. For the probe beam we employed a Photon Technology International[15] 1/4 meter monochromater with f-matched Xenon arc source. All measurements were made in the "low-field" limit, i.e. the lineshape was independent of pump power density.

Shown by the dotted line of Fig. 1 is the experimental PR spectra. It has been demonstrated that the electromodulation spectra from superlattices and quantum wells[8] can be fit by the Aspnes third-derivative functional form (TDFF)[9]:

$$\frac{\Delta R}{R} = Re\left[\sum_{j=1}^{p} C_j e^{i\Theta_j}\left(E - E_{g,j} + i\Gamma_j\right)^{-m_j}\right] \tag{1}$$

where p is the number of spectral features to be fit, C_j , Θ_j, $E_{g,j}$, and Γ_j are the amplitudes, phases, energies and broadening parameters, respectively of the jth structure and m_j denotes critical point type.

The solid line in Fig. 1 shows a least-squares fit of Eq. (1) to the experimental data originating from the MQW (we have not fit E_{01} and will return to this point later) for $p = 10$ (i.e., ten spectral features). The energies of the various features are given by arrows at the top of the figure. The E_{01} structure at 1.415 ± 0.002 eV corresponds to the

lowest direct band of GaAs and originates from the GaAs substrate. Similar observations of E_{01} have been reported by other authors [2,5,8] on superlattice or quantum well systems.

The structure B is related to the direct band gap of the GaAlAs barrier layers. However, because of quantum effects it occurs at a somewhat higher energy, the energy difference being a function of the well and barrier parameters. The observation of this feature in electromodulation[3,5,8] is important since it is an indirect measure of the barrier height. The notation nmH or nmL for several of the peaks represents transitions between the nth conduction subband and the mth valence subband of heavy hole (H) or light hole (L) character. Allowed transitions have m=n while for symmetry forbidden transitions m≠n. The features A,B and C will be discussed in more detail below. The energies and broadening parameters of the various features from the MQW are listed in Table I. We find that the E_{01} structure could not be fit to Eq. (1) since it apparently exhibits Franz-Keldysh oscillations. However, an accurate value for the energy of E_{01} can be obtained from a three-point fit [9].

In order to demonstrate that the forbidden features 12H, 13H and 21L are indeed real we have attempted a fit of Eq.(1) to the experimental data by excluding these transitions (i.e., p=8). This is shown by the dashed line in Fig. 1. The fit which includes the forbidden transitions (solid line) is clearly better than the dashed line, particularly for the resolved peaks for 12H and 13H. By adding 21L, which is not clearly resolved from 22H, we have substantially improved the fit to the amplitude in the region of the allowed features 22H and 22L. This result demonstrates that there are features at the positions of these three forbidden transitions.

In order to verify the origins of the structures from the quantum wells in Fig. 1, we have performed a calculation based on the two-band tight-binding model.[16] We have employed the energy of E_{01} for the energy gap of the quantum well layers. The structure B cannot be interpreted as the energy gap of the barrier layers, however. Calculations show that the barrier gap is not directly observable as an optical transition. The quantum effect due to the finite layer widths raises the energy of the lowest allowed transition above the barrier transition to slightly higher than the barrier band gap. We find the 35H transition is the first unconfined to unconfined feature. The tight-binding model indicates it should be strong and easily observable. A good fit is achieved for the various transitions (including B) using a barrier height of 1.634 eV ($x \approx 0.17$) and a well width (W) of 99.1 A (35 layers of 2.83A per layer). This value of W is in good agreement with the growth conditions. The various theoretical energies and corresponding transitions also are listed in Table I. For several of the transitions we give a range of energies due to the dispersion along the direction of the minizone corresponding to the growth axis.

As can be seen from Table I, there is very good agreement between the experimentally determined energies of the various quantum transitions and the theoretical values, thus verifying the origins of the different allowed and forbidden features. The forbidden features 12H, 13H and 21L have recently been reported in the low temperature photo-luminescence excitation spectra [13] of quantum wells GaAs/GaAlAs ($x \approx 0.30$)quantum wells having dimensions similar to our sample. With respect to broadening parameters Ref. 14 finds the relation $\Gamma = C_o$hm meV, C_o being an adjustable parameter equal to the linewidth of the 11L

transitions. As can be seen from Table I our room temperature broadening parameters do not follow this relationship. The relative intensities of our observed transitions (except for A,B and C) appear to be in good agreement with those of Ref. 14. For example, we also find 21L and 22H to have about the same magnitude.

The origins of the A and C features are not clear at this point. The former could be due to either the forbidden 24H transition (1.598-1.595 eV from Table I) or possibly the 33H transition (1.610-1.624 eV). This latter transition is from a confined hole state to an unconfined conduction level. The C peak at 1.682 eV could be attributed to a 33L transition (both states being unbound), a 43H transition, or possibly a Franz-Keldysh oscillation of the B feature. These spectral features are under further investigation.

In conclusion we have investigated the room temperature PR spectra of a GaAs/GaAlAs superlattice. In addition to the allowed transitions we have clearly observed, for the first time at room temperature, three features corresponding to forbidden transitions. The fit to the Aspnes TDFF has allowed us to accurately determine the energies and broadening parameters for all the transitions. For the energies there is very good agreement between experiment and theory based on a two band tight-binding model. There are three features which may be related to transition involving unconfined states.

its Centers for Advanced Technology program and A.L. Smirl wishes to acknowledge the support of the Office of Naval Research and the Robert A. Welch Foundation.

REFERENCES

1. See, for example, F.H. Pollak in Proceedings of the Society of Photo-Optical Instrumentation Engineers (SPIE, Bellingham, 1981) 276, 142 (1981) and references therein.

2. E.E. Mendez, L.L. Chang, G. Landgren, R. Ludeke, L. Esaki and F.H. Pollak, Phys. Rev. Letts. 46, 1230 (1981).

3. M. Erman, J.B. Theeten, P. Frijlink, S. Gaillard, F.J. Hia and C. Alibert, J. Appl. Phys. 56, 3241 (1984).

4. C. Alibert, S. Gaillard, J.A. Brum, G. Bastard, P. Frijlink and M. Erman, Solid State Comm. 53, 457 (1985).

5. O.J. Glembocki, B.V. Shanabrook, N. Bottka, W.T. Beard and J. Comas, Appl. Phys. Letts. 46, 970 (1985); ibid, Proceedings of Society of Photo-Optical Instrumentation Engineers (SPIE, Bellingham, 1985) 524, 86 (1985).

6. O.J. Glembocki, B.V. Shanabrook and W.T. Beard, to be published in the Proceedings of the 2nd Int. Conf. (Yamada) on Modulated Semiconductor Structures, Kyoto, 1985.

7. T.P. Pearsall, F.H. Pollak, J.C. Bean and R. Hull, private communication.

8. H. Shen, P. Parayanthal, F.H. Pollak, M. Tomkiewicz, T.J. Drummond and J.N. Schulman, to be published in Appl. Phys. Letts.

9. See, for example, D.E. Aspnes in Handbook on Semiconductors, Vol. 2, ed. by T.S. Moss (North Holland, N.Y., 1980) p. 109 and references therein.

10. R.C. Miller, D.A. Kleinman, O. Munteanu and W.T. Tsang, Appl. Phys. Lett. 39, 1 (1981).

11. G.D. Sanders and Y.C. Chang, Phys. Rev. $\underline{B31}$, 6892 (1985).

12. Y.C. Chang and G.D. Sanders, Phys. Rev. $\underline{B32}$, 5521 (1985).

13. R.C. Miller, A.C. Gossard, G.D. Sanders, Y.C. Chang and J.N. Schulman, Phys. Rev. $\underline{B32}$, 8452 (1985).

14. J.N. Schulman and Y.C. Chang, Phys. Rev. $\underline{B31}$ 2056 (1985).

15. Photon Technology International, Princeton, N.J. 08542

16. J.N. Schulman and Y.C. Chang, Appl. Phys. Letts. $\underline{46}$, 571 (1985).

17. J.L. Aubel, U.K. Reddy, S. Sundaram, W.T. Beard and J. Comas, J. Appl. Phys. $\underline{58}$, 495 (1985).

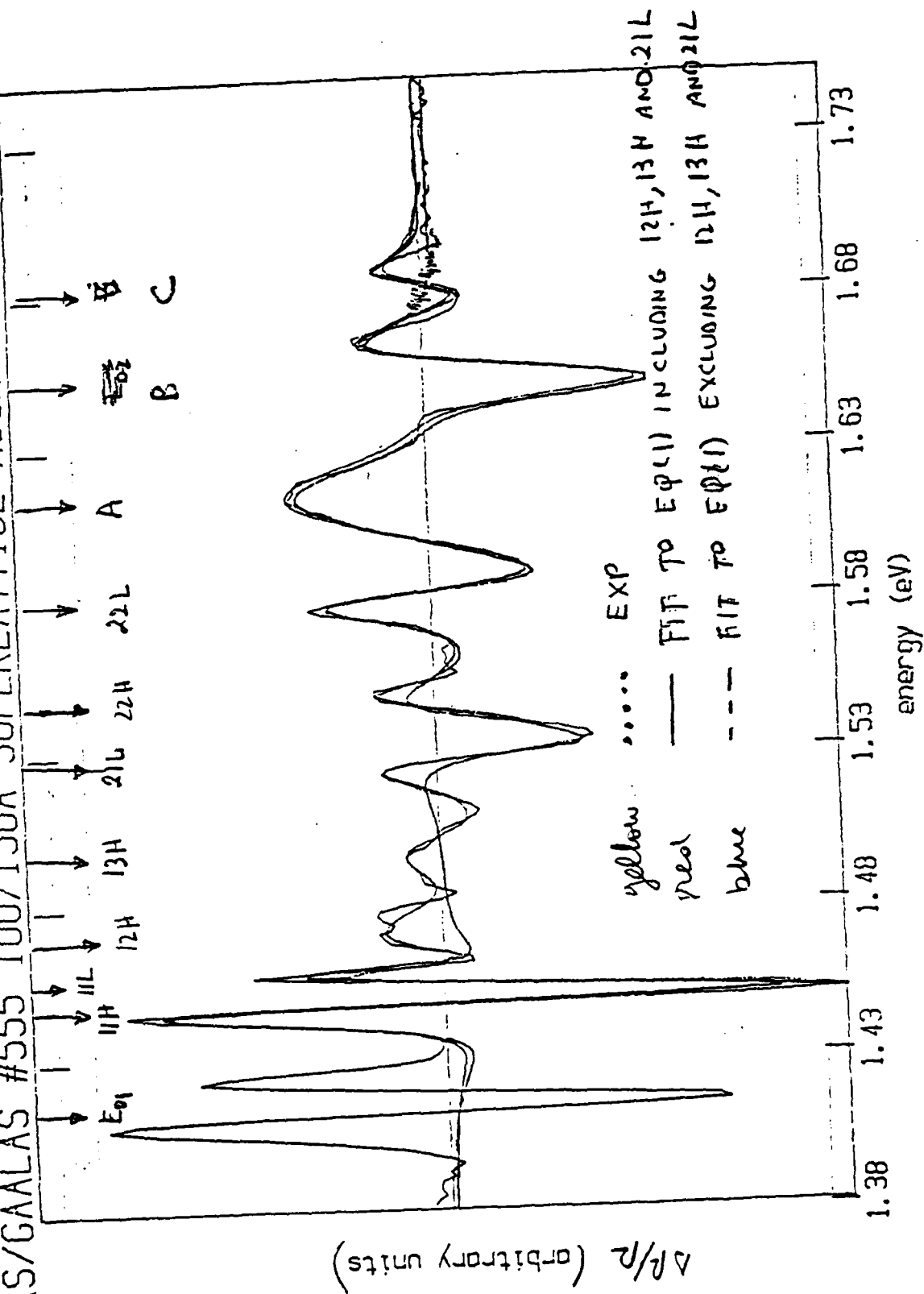18. R.C. Miller and D.A. Kleinman, J. Luminescence $\underline{30}$, 520 (1985).

Table I. Energies and broadening parameters (Γ) for the various quantum well transitions from a fit of Eq. (1) to the experimental data. Also listed are theoretical values for the various transitions using E_{01} (1.415$\pm$0.002 eV) as the energy gap of the quantum wells.

Spectral Features	Experiment		Theory [a,b]	
	Energy (eV)	Γ (meV)	Energy (eV)	Transition
11H	1.448$\pm$0.002	8$\pm$1	1.449	11H
11L	1.456$\pm$0.002	7$\pm$2	1.461	11L
12H	1.470$\pm$0.010	25$\pm$5	1.471	12H
13H	1.498$\pm$0.005	19$\pm$5	1.503	13H
21L	1.529$\pm$0.005	10$\pm$2	1.531	21L
22H	1.545$\pm$0.005	10$\pm$2	1.541	22H
22L	1.580$\pm$0.003	13$\pm$2	1.581	22L
A	1.614$\pm$0.005	30$\pm$5	1.602	24H
			1.618–1.632	33H
B	1.653$\pm$0.003	13$\pm$2	1.650–1.673	35H
C	1.682$\pm$0.003	11$\pm$2	1.654–1.680	33L
			1.673–1.640	43H

a) $m_e^* = 0.0665$, $m_{\ell h}^* = 0.094$, $m_{hh}^* = 0.34$ and $Q = 0.60$ from Ref. 18.

b) Using a well width of 99.1 A (35 layers of thickness 2.83 A per layer).

GAAS/GAALAS #555 100/150A SUPERLATTICE HUGHES SMALL SPOT 1

E_{01} 11H 11L 12H 13H 21L 22H 22L   A E_{02} B   C

A   B   C

yellow ..... EXP
real ——— FIT TO EQ(1) INCLUDING 12H,13H AND 21L
blue --- FIT TO EQ(1) EXCLUDING 12H,13H AND 21L

$\Delta R/R$ (arbitrary units)

energy (eV)

1.38   1.43   1.48   1.53   1.58   1.63   1.68   1.73

Appendix B: Observation of Symmetry
Forbidden Transitions in the
Photoreflectance Spectra of a GaAs/AlGaAs
Multiple Quantum Well

A preprint of the proceedings of the
International Conference on the Physics
of Semiconductors, Stockholm, Sweden,
August 11-15, 1986.

in the

OBSERVATION OF SYMMETRY FORBIDDEN TRANSITIONS ^PHOTOREFLECTANCE SPECTRA OF A GaAs/GaAlAs MULTIPLE QUANTUM WELL

H. Shen, P. Parayanthal and Fred H. Pollak

Physics Department, Brooklyn College, Brooklyn, N.Y. 11210

and

Arthur L. Smirl, J.N. Schulman, R.A. McFarlane and Irnee D'Haenens

Hughes Research Laboratory, Malibu, CA 90265

We have measured the photoreflectance spectra from a 100A/150A GaAs/GaAlAs ($x \approx 0.17$) multiple quantum well (MQW) at 300K and 77K. In addition to all the allowed quantum transitions we have clearly observed features from several symmetry forbidden transitions *even* at 300K. There also appears to be evidence for unconfined transitions. There is very good agreement between experiment and a theoretical calculation.

Electromodulation (electroreflectance and photoreflectance) is rapidly becoming an extremely powerful tool to study microstructural geometries (superlattices, quantum wells and heterojunctions) in semi-conductors.[1,2] This method is useful since it yields sharp structure that can be used to accurately fit the spectra and is a function of surface (interfacial) electric fields. The enhanced sensitivity and well-defined lineshape of electromodulation makes it a very important method to study weak features in the optical properties of these structures.

We have measured the photoreflectance (PR) spectra at 300K[3] and 77K from a 100A/150A GaAs/GaAlAs ($x \approx 0.17$) multiple quantum well (MQW). The entire spectra from the MQW have been fit by a third-derivative functional form lineshape expression.[2,4] In addition to all the allow-ed quantum transitions we have clearly observed features from several symmetry forbidden transitions (SFT). In addition there also appears to be strong evidence for unconfined transitions, i.e. energies above the band bap of the GaAlAs barrier layer. There is very good agree-

between the experimentally determined energies of the various features
and a theoretical calculation.

The sample used was a 100Å/150Å GaAs/GaAlAs MQW with a nominal Al
concentration of 17% grown by molecular beam expitaxy at the Hughes
Research Laboratory. The PR technique has been described in the liter-
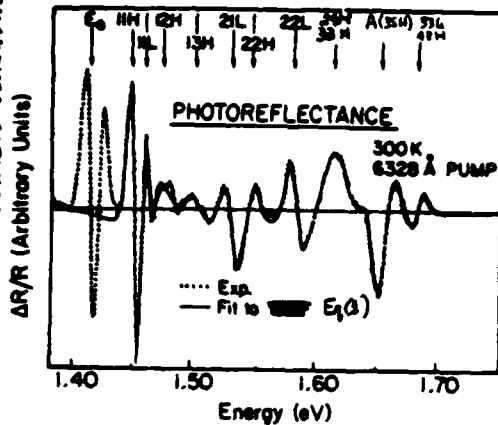ature.[1,2,4] The pump beam was the 6318Å line of a 1 mW He-Ne laser.
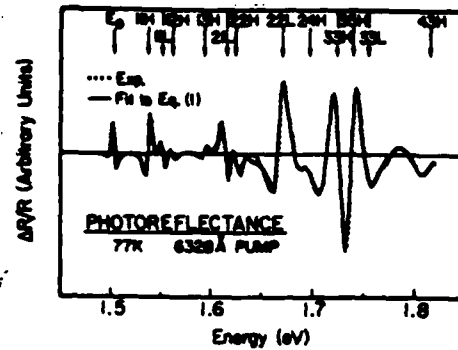

Fig. 1 Photoreflectance at 300K   Fig. 2 Photoreflectance spectrum
at 77K

Shown by the dotted lines in Figs. 1 and 2 are the experimental PR
spectra at 300K and 77K, respectively. The solid lines in these figures
is a least-squares fit of the experimental data from the MQW to the
Aspnes third-derivative functional form:[2,4]

$$\frac{\Delta R}{R} = Re\left[\sum_{j=1}^{p} C_j e^{i\theta_j}\left(E - E_{g,j} + i\Gamma_j\right)^{-M_j}\right]$$

(1)

where E is the photon energy, p is the number of spectral features to
be fit, C_j, θ_j, Eg_j, and Γ_j are the amplitudes, phases, energies and
broadening parameters of the jth structure and m_j denotes critical
point type. The energies of the various features are given by arrows
at the top of the figure.

The E_o structure at 1.415 eV for 300K and 1.503 eV for 77K cor-
responds to the lowest direct band gap of GaAs and originates from
the GaAs substrate. At 77K we have been able to fit this transition
by Eq. (1) (see Fig. 2) but at 300K this feature appears to exhibit

48

Franz-Keldysh oscillations and hence cannot be accounted for by Eq. (1)

In Figs. 1 and 2 the notation nmH (L) for the features from the MQW represents transitions between the nth conduction subband and the mth valence subband of heavy hole (H) or light hole (L) character. Allowed transitions have m=n while for SFT m≠n. The experimental energies and broadening parameters of the various features from the MQW at 300K and 77K are listed in Table I. The structure A is related to the direct band gap of the GaAlAs barrier layers. However, because of quantum effects it occurs at a somewhat higher energy, the energy difference being a function of the well and barrier parameters. We shall demonstrate below that this peak is caused by the 35H SFT. The observation of this feature in electromodulation is important since it is an indirect measure of the barrier height.

Comparison of Figs. 1 and 2 shows that while the SFT 12H, 13H and 35H are individual peaks at 300K other SFT (21L, 24H and 43H) become clearly resolved only at 77K. The presence of 21L at 300K was established on the basis of the detailed lineshape fit using Eq. (1). The fit to the amplitude was considerably improved in the region of the allowed feature 22H by including 21L.

In order to verify the origins of the structures from the quantum wells in Figs. 1 and 2 we have performed a calculation based on the two-band tight-binding model.[5] We have employed the energy of E_o for the energy gap of the quantum well layers at 300K and 77K. The mass parameters[6] were $m_e^* = 0.0665$, $m_{(e\eta)-lh}^* = 0.094$ and $m_{(NN)-hh}^* = 0.34$, the band offset[6] Q = 0.60 and the well width (W) employed was 99.1A (35 layers of thickness 2.83A per layer). The various theoretical energies and corresponding transitions also are listed in Table I. For several of of the transitions we give a range of energies due to the dispersion along the direction of the minizone corresponding to the growth axis. A good fit is achieved for the various transitions (including A) using a barrier height of 1.634 eV (x≃0.17)[7] at 300K and 1.722 eV at 77K. As can be seen from Table I, there is very good agreement between the experimentally determined energies of the various quantum transitions and the theoretical values, thus verifying the origins of the different allowed and forbidden features. The value of W is in good agreement with the growth condition.

49

The structure A cannot be interpreted as the energy gap of the barrier layers, however. Calculations show that the barrier gap is not directly observable as an optical transition. The quantum effect due to the finite layer widths raises the energy of the lowest allowed transition above the barrier transition to slightly higher than the barrier band gap. We find that A corresponds to the 35H transition, the first unconfined to unconfined feature. The tight-binding model indicates it should be strong and easily observable.

REFERENCES

1. See, for example, Glembocki, O.J., Shanabrook, B.V., Böttka, N., Beard, W.T., and Comas, J., Appl. Phys. Letts. 46, 970 (1985); ibid, Proceedings of Society of Photo-Optical Instrumentation Engineers (SPIE), Bellingham, 1985) 524, 86 (1985).

2. Parayanthal, P., Shen, H., Pollak, F.H., Glembocki, O.J., Shanabrook, B.V. and Beard, W.T., Appl. Phys. Lett. 48, 1261 (1986).

3. Shen, H., Parayanthal, P., Pollak, F.H., Smirl, A.L., Schulman, J.N., and D'Haenens, I., to be published in Solid State Comm.

4. See, for example, Aspnes, D.E. in Handbook on Semiconductors, Vol. 2, ed. by T.S. Moss (North Holland, N.Y., 1980) p. 109 and references therein.

6. Miller, R.C. and Kleinman, D.A., J. Luminescence 30, 520 (1985).

5. Schulman, J.N. and Chang, Y.C., Appl. Phys. Letts. 46, 571 (1985).

7. Aubel, J.L., Reddy, U.K., Sundaram, S., Beard, W.T., and Comas, J. J. Appl. Phys. 58, 495 (1985).

Table I. Experimental energies and broadening parameters (Γ) for the various quantum well transitions from a fit of Eq. (1) to the experimental data. Listed in parentheses are the theoretical values of the various transitions.

Spectral Features	300K		77K	
	Energy (eV)	Γ (meV)	Energy (eV)	Γ (meV)
11H	1.448±0.002 (1.449)	8±1	1.538±0.002 (1.537)	6±1
11L	1.456±0.002 (1.461	7±2	1.552±0.003 (1.549)	5±1
12H	1.470±0.010 (1.471)	25±5	1.561±0.003 (1.559)	6±1
13H	1.498±0.005 (1.503)	19±5	1.594±0.003 (1.591	6±1
21L	1.529±0.005 (1.531)	10±2	1.615±0.003 (1.618)	7±1
22H	1.545±0.005 (1.541)	10±2	1.624±0.005 (1.629)	10±2
22L	1.580±0.003 (1.581)	13±2	1.669±0.005 (1.669)	14±2
24H	1.614±0.005[a] (1.602)	30±5	1.696±0.005 (1.690)	10±2
33H	1.614±0.005[a] (1.618-1.632)	30±5	1.723±0.007 (1.703-1.723)	18±3
A(35H)	1.653±0.003 (1.650-1.673)	13±2	1.739±0.005 (1.738-1.761)	17±3
33L	1.682±0.003[a] (1.654-1.680)	11±2	1.752±10 (1.742-1.768)	50±5
43H	1.682±0.003[a] (1.678-1.640)	11±2	1.815±10 (1.766-1.825)	30±5

a) Unresolved at 300K

Appendix C: Photoreflectance of GaAs
Doping Superlattices

A preprint of a paper to be published in
the journal **Superlattices and
Microstructures**

PHOTOREFLECTANCE OF GaAs DOPING SUPERLATTICES

X.C. Shen,* H. Shen,** P. Parayanthal,* and F.H. Pollak**
Physics Department, Brooklyn College of CUNY
BROOKLYN, N.Y. 11210 USA

and

J.N. Schulman, Arthur L. Smirl, R.M. McFarlane, and Irnee D'Haenens
Hughes Research Laboratories
Malibu, CA 90265 USA

We have performed room-temperature photoreflectance measurements on two GaAs doping superlattices having considerably different built-in potentials (1.2 eV and 85 meV). The first sample exhibits Franz-Keldysh oscillations, the period of the oscillations corresponding to the large built-in dc field. A second dc pump beam has been used to change the electron-hole concentration and hence the built-in field. The spectrum of the second sample displays a number of features corresponding to quantized electron and hole states. There is qualitative agreement between experiment and theoretical calculation based on a two band tight binding model. In both samples the dependence of the amplitude of the photoreflectance signal on pump chopping frequency yields the minority carrier lifetime.

Semiconductors with a periodic doping profile of n- and p-doped layers, possibly separated by undoped (intrinsic, i) regions (n-i-p-i super-structures), exhibit interesting properties not found in either bulk crystals or compositional superlattices.[1,2] These n-i-p-i structures have an "indirect gap" in real-space, long electron-hole recombination lifetimes because of the spatial separation of the carriers, and a two-dimensional subband structure for the electrons and holes that can be tailored independently for each carrier type. Even though there have been considerable optical studies on these semiconductor structures, most of the investigations have dealt with the near band gap and below band gap regions.[1-3] Recently, work on the above band gap optical properties has also been reported.[4] The quantization of the electron states has been observed in resonance Raman scattering[5] and photoreflectance.[4] Investigators, however, have not reported on the quantization of the holes.

It has been demonstrated recently that electromodulation (electroreflectance and photo-reflectance) is a powerful method for studying quantum effects in compositional superlattices and quantum wells.[6,7] Electromodulation produces such sharp structures that, even at room temperatures, all the confined interband quantum transitions can be observed. The electromodulation spectra of these microstructural geometries can be fit by a derivative functional form (DFF),[4,7,8] thus making it possible to accurately determine the quantum energies, broadening parameters, etc. In addition, electromodulation yields information about the nature of the internal electric fields in these structures. Photoreflectance (PR), specifically, is a contactless mode of electromodulation in which the electric field is modulated by the photoinjection of electron-hole pairs via a chopped pump beam.[4,6,7]

In this paper we report room temperature measurements on two GaAs n-i-p-i superlattices having considerably different built-in potentials; i.e., 1.2 eV and 85 meV. In the 1.2-eV sample the spectrum is caused by Franz-Keldysh (FK) oscillations,[9] the period being related to the large built-in dc field.[10] We used a second dc pump beam to change the electron-hole concentration and hence the built-in field. This variation in turn resulted in a change in the FK oscillations, enabling us to gain information about the nature of the built-in field. In the second (85 meV) sample we

observed a number of features in the spectrum both below and above the band gap of GaAs. The spectrum was fit by a DFF procedure, and we performed a theoretical calculation of the energy levels and intensities using a two band tight-binding model[11] with material parameters deduced from the growth conditions.

There is general agreement between experiment and theory. In both samples the dependence of the amplitude of the PR signal on the pump chopping frequency (Ω_m) yields the minority carrier lifetime. In the former sample we observed a significant decrease in the minority carrier lifetime with increased dc pump power because of the change in spatial separation of the carriers. Thus, the PR investigation yielded important information about the doping superlattices.

The n-i-p-i superlattices used in this experiment were fabricated by molecular beam epitaxy at Hughes Research Laboratories. Sample n-i-p-i 498 consists of 21 n ($6.5 \times 10^{17} cm^{-3}$) and p ($2.5 \times 10^{17} cm^{-3}$) layers with n- and p-layer thicknesses of 800 Å (d_n) and 1400 Å (d_p). The second sample, n-i-p-i 497, has nominal n = $7 \times 10^7 cm^{-3}$ and p = $5 \times 10^{17} cm^{-3}$ with d_n = d_p = 233 Å. The values of the built-in potential, ($2V_n$), have been deduced from the growth parameters with n-i-p-i 498 having $2V_n$ = 1.2 eV, and n-i-p-i 497 having $2V_n$ = 85 meV, using Eq. (11) of Ref. 2. The PR technique has been described in the literature.[6,9,10] The probe beam was from a Photon Technology International[12] 1/4-meter monochromator. The ac pump beam was the 6328-Å line of a 1-mW He-Ne laser; the power density was about 1.5 mW/cm². The chopping frequency was in the 1.5 to 4000 Hz range. In addition, investigations were carried out on n-i-p-i 498 with a dc pump beam (5145-Å line of an Ar-ion laser).

Plotted in Fig. 1 are the 300K PR spectra of sample n-i-p-i 498, using 6328 Å as the ac pump, with dc pump (5145 Å) power densities of (a) 0.0, (b) 5.8 mW/cm² and (c) 37 mW/cm². For n-i-p-i 498 there is a very large built-in potential (1.2 eV) and hence the PR features are FK oscillations of the fundamental gap, E_o. The numbered peaks correspond to these electro-optical features. The structure denoted $E_o + \Delta_o$ corresponds to the spin-orbit split component of E_o. According to FK theory in the literature, the period of FK oscillations is related to the amplitude of the <u>modulating electric field</u>[9]. It should be pointed out that these theories are

based on modulation from flat-band and do not
take into account the presence of large built-in
dc fields. It can be shown that if the dc
built-in field is considerably larger than the
ac field, the period of the FK oscillations is a
measure of the former field, not the latter.[10]
This appears to be the case for n-i-p-i 498,
since it has such a large $2V_n$; i.e., built-in
potential. From the period of the oscillations
in Fig. 1(a) we deduce a field of 1.2×10^5 V/cm.
This value agrees quite well with the value of
the average built-in field:

$$2V_n/[(d_n + d_p)/2] = 1.1 \times 10^5 \text{ V/cm.}$$

The dc pump beam creates electron-hole pairs,
reducing the value of $2V_n$ and thus the built-in
field. This effect is evident in Figs. 1(b) and
1(c). From the FK oscillations in Fig. 1(c)
(37 mW/cm^2 at 5145 Å) we deduce a built-in field
of 0.5×10^5 V/cm, a significant decrease in
relation to the case of zero dc pump power.

The dotted line in Fig. 2 shows the 300K PR
spectrum of sample n-i-p-i 497 in the 1.30-to-
1.55-eV range using 6328 Å as the ac pump at
$\Omega_m = 150$ Hz. Experimental conditions were in
the "low-field regime"; i.e., lineshape indepen-
dent of ac pump beam intensity.

It has been proposed that electromodulation
spectra from superlattices and quantum wells can
be fit by a derivative functional form:[4,7,8,9]

$$\frac{\Delta R}{R} = \text{Re} \left[\sum_{j=1}^{p} C_j e^{i\theta_j} \left(E - E_{g,j} + i\Gamma_j \right)^{-k_j} \right] \quad (1)$$

where E is the photon energy, p is the number of
spectral features to be fit, and C_j, θ, $E_{g,j}$,
and Γ_j are the amplitude, phase, energy, and
broadening parameters of the jth structure. The
parameter k_j represents the type of critical
point and order of the derivative. For example,
$k_j = 1$ is the first derivative of a two-
dimensional critical point, $k_j = 3$ corresponds
to the third-derivative of a two-dimensional
critical point, etc.

The solid line in Fig. 2 is a least-squares
fit of the experimental data to Eq. (1) with
$p = 7$ and $k_j = 1$ (for $j = 1$ to 7). The energies
obtained are indicated by arrows at the top of
the figure and are listed in Table I, along with
the corresponding k_j. We find the fit for
$k_j = 3$ is indistinguishable from the former fit,
but that it yields somewhat different energies

58

and broadening parameters. These are also given in Table I. Thus, at present, we cannot make a definitive statement about the order of the derivative[4],[8] to fit the PR spectra of n-i-p-i structures.

We have performed a theoretical calculation of the quantized energy levels and transition intensities using a two-band tight-binding model[11] with material parameters cited above. Listed in Table I are the energies of the most intense transitions (based on matrix element and density of states) in the region of the various spectral features. The notation $nmH(0)$ or $nmH(\pi)$ denotes a transition from the nth conduction subband to the mth valence band of heavy-hole (H) character at the minizone center (0) or edge (π), respectively. We have found that transitions involving light-hole valence bands have considerably less amplitude than heavy-hole features and thus they have been neglected. Also we have neglected a number of weak heavy-hole transitions. For example, if we examine the energy region in the vicinity of the D feature there is a theoretical $33H(0)$ transition at 1.419 eV but it is weaker than $17H(0)$ or $25H(\pi)$ [see Table I] and therefore has not been included.

Unfortunately, theoretical calculation using the growth parameters does not give a unique assignment to the experimental data. We have also performed the calculation using other values of n, p, d_n, and d_p such that $2V_n$ is kept constant at 85 meV. It is also possible to make a correspondence between theory and experiment, but not necessarily with the same transitions. Thus, for other material parameters (keeping $2V_n$ constant) there are also fairly strong theoretical transitions in the energy range of the various experimental features, but they do not necessarily correspond to the same transitions. For example, in other calculations the theoretical energies around the D feature (1.420 eV) are not $17H(0)$ or $25H(\pi)$.

The PR of InP n-i-p-i structures at 300K and 80K has been reported in Ref. 4. The lineshapes have been fit by an expression based on a Lorentzian oscillator model originally developed for the electroreflectance of excitons. This corresponds to $k_i = 2$ in Eq. (1). In interpreting their data the above-referenced authors considered only the quantization of the electron subbands and not the valence (and spin-orbit split) states. We found that the valence band quantization is an important consideration for our case.

The optical transition selection rules between confined valence and conduction band states are similar to those for a Type II superlattice, in which the electrons and holes are spatially separated.[13] Thus $|n-m|$ must be even at the minizone center, while $|n-m|$ must be odd at the minizone edge. These selection rules do not hold for unconfined states. Since miniband dispersion was not considered in Ref. 4 these authors report contributions to the PR spectra from all miniband transitions.

We have also investigated the dependence of the amplitude of the PR signal on the chopping frequency, Ω_m. Shown in Fig. 3 are some experimental results (solid points) for samples n-i-p-i 497 and 498. Curve A is the frequency dependence of n-i-p-i 497 (no dc pump). From an exponential fit to the data points (solid line) we extract a time constant, τ, of 4.2 msec. For sample n-i-p-i 498 we have investigated the effects of the intensity of the dc pump on the lifetime. Curves B, C, and D correspond to power densities of 0, 60, and 600 mW/cm^2, respectively. The corresponding τ are listed in the figure. Increasing the dc pump power decreases the recombination lifetime, since the built-in potential is decreased and hence there is less separation of carriers.

In conclusion, we have measured the room temperature PR spectra from two GaAs doping superlattices with substantially different built-in potentials. The large-potential sample exhibits FK oscillations, the period being related to the dc built-in field rather than the ac modulation field. A second dc pump beam was used to reduce the built-in potential. In the second sample PR structures are observed which are caused by transitions between quantized electron and hole states. A correspondence between experiment and theory can be made, although not uniquely. The dependence of the PR on pump chopping frequency is a measure of the recombination lifetime.

References

*Permanent address: Shanghai Institute of
Technical Physics, Academia Sinica,
Shanghai, China
**Also at Physics Dept., Graduate School and
University Center, City University of New
York, New York, N.Y. 10036
*Present address: AT&T Bell Telephone
Laboratories, Murry Hill, N.J. 07974

[1] K. Ploog and G.H. Dohler, Advances in Physics
32, 285 (1983).
[2] H. Dohler, Superlattices and Microstructures
1, 279 (1985).
[3] G.H. Dohler, H. Kunzel, and K. Ploog, Physical
Review B 25, 2616 (1982); G.H. Dohler and
P. Ruden, Physcial Review B 33, 5932 (1984).
[4] M. Gal, J.S. Yuan, J.M. Viner, P.C. Taylor and
G.B. Stringfellow, Physical Review B 33, 4410
(1986).
[5] G. Fasol, P. Ruden, and K. Ploog, Journal of
Physics C 17, 1395 (1984) and references
therein
[6] O.J. Glenbocki, B.V. Shanabrook, N. Bottka,
W.T. Beard and J. Comas, Applied Physics
therein.
[7] P. Parayanthal, H. Shen, F.H. Pollak, O.J.
Glembocki, B.V. Shanabrook and W.T. Beard,
Applied Physics Letters 48, 1261 (1986).
[8] B.V. Shanabrook, O.J. Glembocki and W.T.
Beard, submitted to Physical Review; B.V.
Shanbrook and O.J. Glembocki, this
conference.
[9] D.E. Aspnes in Handbook on Semiconductors,
Vol. 2, ed. by T.S. Moss (North Holland, N.Y.,
1980) p. 109 and references therein.
[10] R. Bhattacharya, H. Shen, P. Parayanthal,
F.H. Pollak, T. Coutts and H. Aharoni, to be
published in Solar Cells.
[11] J.N. Schulman in Proceedings of the Symposium
on Layered Structures and Epitaxy, 1985 Fall
Meeting of the Materials Research Society,
Vol. 56 of Materials Research Society
Symposium Proceedings.
[12] Photon Technology International, Princeton,
N.J, 08542.
[13] P. Voisin, G. Bastard, and M. Voos, Physical
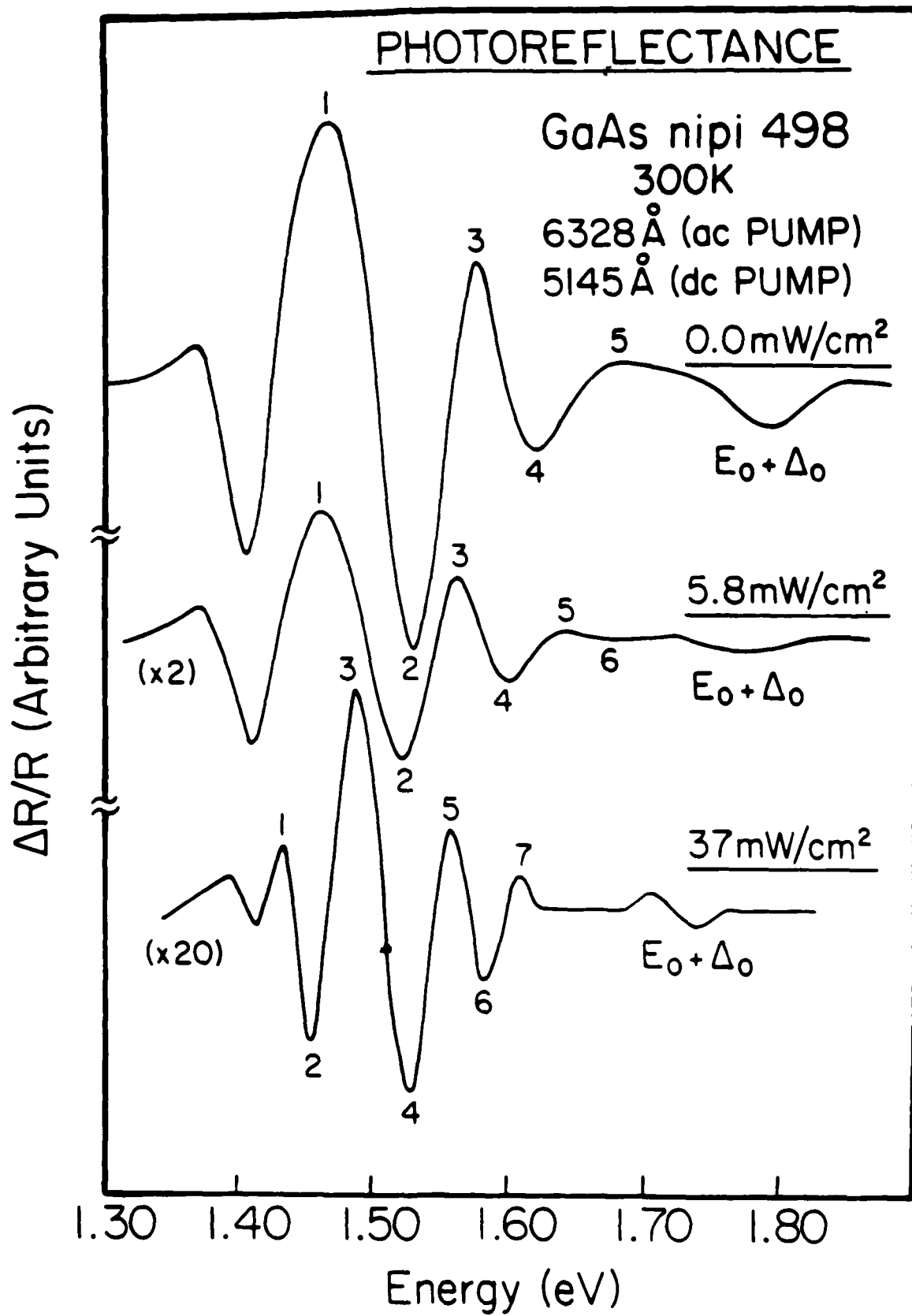Review B 29, 935 (1984).

Figure Captions

Fig. 1. Photoreflectance spectra at 300K of
GaAs n-i-p-i 498 for dc pump power
densities of 0, 5.8, and 37 mW/cm^2.

Fig. 2. Experimental photoreflectance spectrum
at 300K (dotted line) of GaAS n-i-p-i
497. The solid line is a least-
squares fit to Eq. (1) for $k_j = 1$.

Fig. 3. Photoreflectance intensity as a
function of ac pump chopping fre-
quency for GaAs n-i-p-i 497 (curve A)
and 498. For n-i-p-i 498 the depen-
dence on dc pump (5145 Å) power
densities of 0 (curve B), 60 mW/cm^2
(curve C), and 600 mW/cm^2 (curve D)
is shown. The respective time
constants, τ, are ilndicated.

Table 1. Experimental energies and broadening parameters (Γ) for the various photoreflectance features from a fit to Eq. (1) for k_j = 1 and 3. Also listed are the theoretical energies and corresponding transitions.
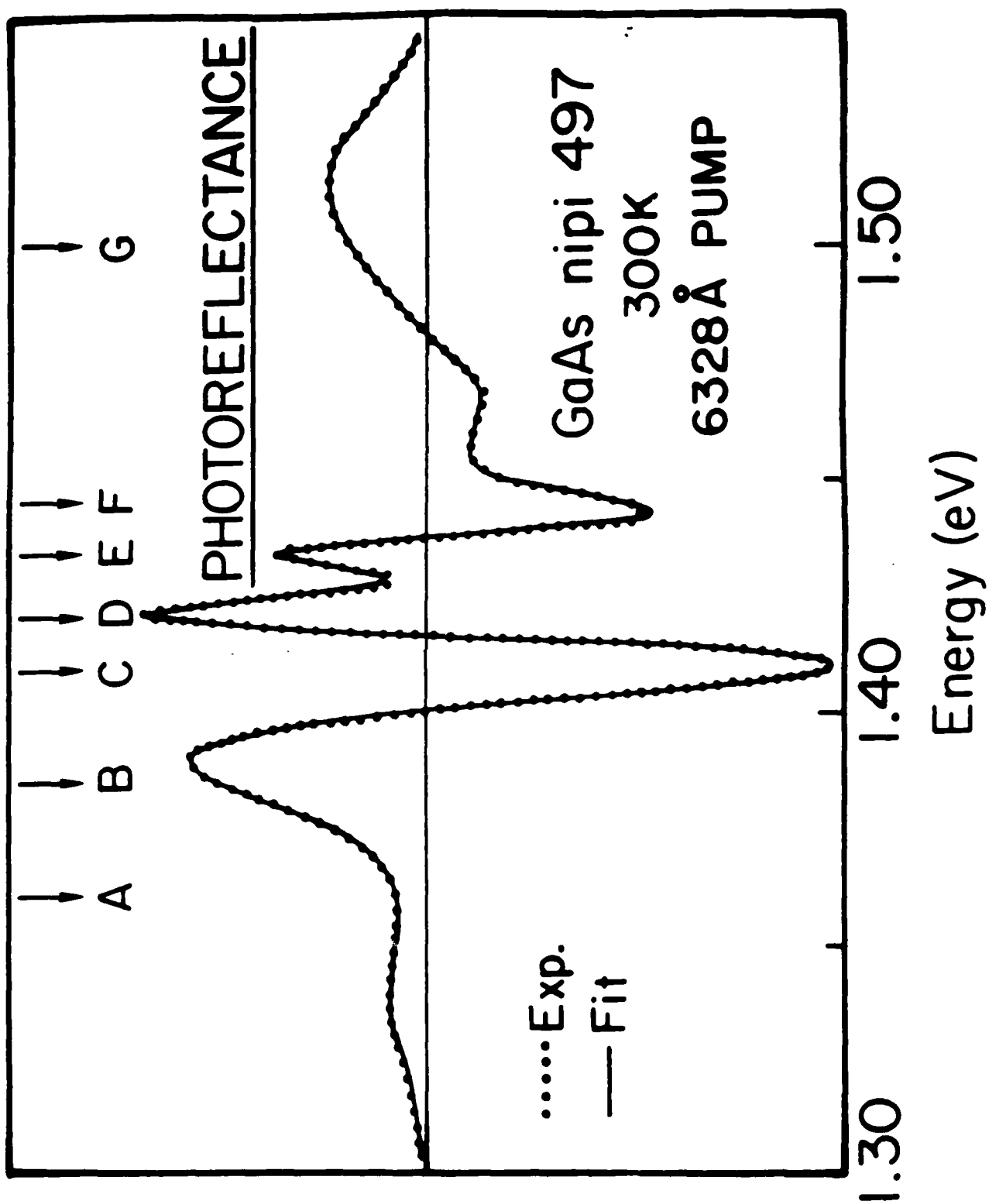
Spectral Feature	Experiment				Theory	
	Energy(a) (eV)	Γ(a) (meV)	Energy(b) (eV)	Γ(b) (meV)	Energy (eV)	Transition
A	1.360	21	1.350	74	1.369	13H(0)
B	1.385	20	1.386	27	1.381	22H(0)
C	1.408	12	1.414	23	1.408 / 1.408	16H(π) / 24H(0)
D	1.420	6	1.419	17	1.417 / 1.421	17H(0) / 25H(π)
E	1.434	4	1.432	13	1.433	26H(0)
F	1.444	5	1.443	16	1.445	35H(0)
G	1.500	20	1.507	54	1.491	55H(π)

(a) obtained with k_j = 1 in Eq. (1)

(b) obtained with k_j = 3 in Eq. (1)

63

PHOTOREFLECTANCE

ΔR/R (Arbitrary Units)

A B C D E F   G

GaAs nipi 497
300K
6328Å PUMP

····· Exp.
—— Fit

1.30   1.40   1.50

Energy (eV)

65

66
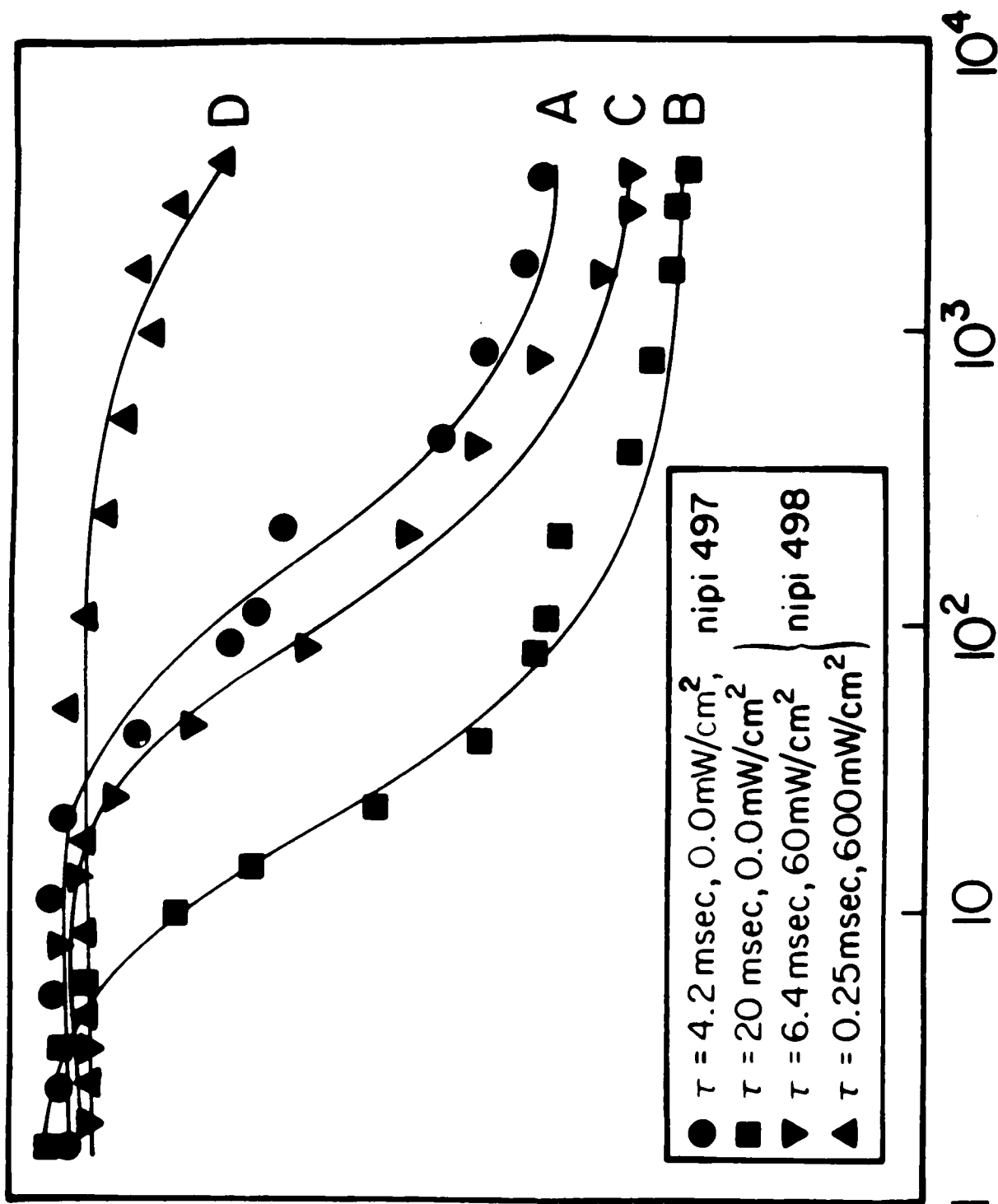
Appendix D: Time-Resolved
Photoluminescence Mesurements in
$Al_x Ga_{1-x}As$ Under Intense
Picosecond Excitation

A preprint of an article that is to
appear in the volume of Conference
Proceedings entitled **Ultrafast
Phenomena V, Springer Verlag**
(1986).

Time-resolved Photoluminescence Measurements in Al$_x$Ga$_{1-x}$As Under Intense Picosecond Excitation

K. Bohnert, H. Kalt, D. P. Norwood, and Thomas F. Boggess
Center for Applied Quantum Electronics
Department of Physics
North Texas State University
Denton, TX 76203

Arthur L. Smirl and R. Y. Loo
Hughes Research Laboratories
3011 Malibu Canyon Road
Malibu, CA 90265

The ternary semiconductor alloy Al$_x$Ga$_{1-x}$As exhibits a direct-indirect gap crossover with increasing aluminum concentration x at x_c=0.435 [1]. By varying the alloy composition, the relative energy separation between direct and indirect gaps in the vicinity of the crossover composition can be varied, and the distribution of photo-excited electrons among direct and indirect conduction band valleys can be externally controlled. In the following, we report preliminary results that illustrate the influence of the variation of the band structure with composition on the nature and dynamics of radiative carrier recombination following intense picosecond excitation. We further analyzed the photoluminescence with respect to bandgap renormalization which influences the spectral position of the emission bands. For appropriate energy separations between direct and indirect gaps (at compositions near x_c), the number of photo-excited electrons in the energetically higher lying conduction band valley(s) can be arranged to be significantly smaller than in the lower valley(s). The electron exchange contribution to the renormalization of the larger gap then is strongly reduced, whereas the lower gap is renormalized by full exchange and correlation effects. This, in principle, allows one to experimentally separate correlation and exchange contributions to band gap renormalization.

The investigated Al$_x$Ga$_{1-x}$As layers were grown on GaAs substrates by liquid phase or molecular beam epitaxy. Their thicknesses ranged between 2 and 10 μm. The samples were mounted in a closed-cycle refrigerator for temperature dependent measurements. The excitation source was a frequency doubled, actively/passively mode-locked Nd:YAG laser, providing single pulses with a temporal width of 32 ps (FWHM) at 532 nm. The photoluminescence from the center of the 700 μm (FWHM) excitation spot was dispersed in a 0.25 m spectrometer and time-resolved with a highly sensitive streak camera. The temporal resolution was determined by the width of the selected time window (typically between 30 and 70 ps).

Initially, an alloy composition well within the direct gap regime (x=0.23) was investigated where a significant interference by indirect band extrema was excluded. Plasma luminescence typical for a direct-gap semiconductor was observed. The temporal evolution of the spectrally-resolved emission was measured on a picosecond time scale, and carrier density and temperature were extracted as a function of time. The temporal evolution of the carrier temperature in room temperature Al$_{0.23}$Ga$_{0.77}$As is shown in Fig. 1a. The exciting fluence was 2 mJ/cm^2. The initial excess energy of the photo-excited electron-hole pairs was 630 meV. The temperature during the pulse maximum (t=0 ps) is around 450 K. This

indicates that the carriers lost most of their initial excess energy on a time scale short compared to the pulsewidth. The carrier temperature reaches lattice temperature essentially as soon as excitation ends. On time scales given by our temporal resolution, no definite evidence for a reduced carrier cooling rate due to screening of the carrier-phonon interaction [2] and/or the build-up of a nonequilibrium phonon distribution [3] at high densities of photo-excited carriers was found. The carrier density (Fig. 1b) shows essentially an exponential decay with a time constant of ~200 ps.

Figure 2a shows a low temperature photoluminescence spectrum for $Al_{0.38}Ga_{0.62}As$ at t=0 ps. For this alloy composition the direct conduction band valley is only approximately 60 meV below the indirect X-valleys. The nonrenormalized gaps are indicated by arrows. The low and high energy peaks in this spectrum are attributed to recombination from direct and indirect valleys, respectively. The decay times for the direct and indirect emission bands are 105 ps and 60 ps, respectively. Emission from indirect valleys for alloy compositions near the direct-indirect crossover occurs predominantly without participation of phonons due to an electron scattering by random potential fluctuations [4]. The relative intensity of the indirect emission band indicates a high efficiency for this recombination channel. The shorter decay time for the indirect emission is consistent with electron transitions from the indirect valleys to the lower Γ-valley which help to adjust an intervalley equilibrium distribution for the photo-excited electrons.

Figure 2b shows a luminescence spectrum at t=0 ps for x=0.52. For this composition, the lowest conduction band edge occurs at the X-point. It is separated from the direct Γ-minimum by approximately 100 meV. The non-renormalized band gaps are indicated by arrows. Again two distinct emission bands are observed. The direct emission (high energy band) is observed only during excitation, i.e., during the relaxation of the photo-excited electrons to the bottom of the bands. The decay time for the indirect emission now is increased to 640 ps. This is consistent with a decreasing probability for no-phonon transitions with increasing direct-indirect gap separation in the indirect gap regime [5].

An examination of band gap renormalization shows an enhanced renormalization of the Γ-gap for compositions below but close to x_c. This is explained by an increase of the effective electron mass due to multivalley effects [6]. The renormalization of gaps above the lowest gap appears to be reduced due to a reduced exchange contribution.

In conclusion, for alloy compositions near the direct-indirect gap crossover, emission from direct and indirect conduction band valleys is observed simultaneously. The relative intensity of the indirect (no-phonon) emission band indicates a high radiative recombination rate due to random potential fluctuations. Bandgap renormalization near x_c is influenced by disorder effects and by the distribution of the photo-excited electrons among several conduction band valleys.
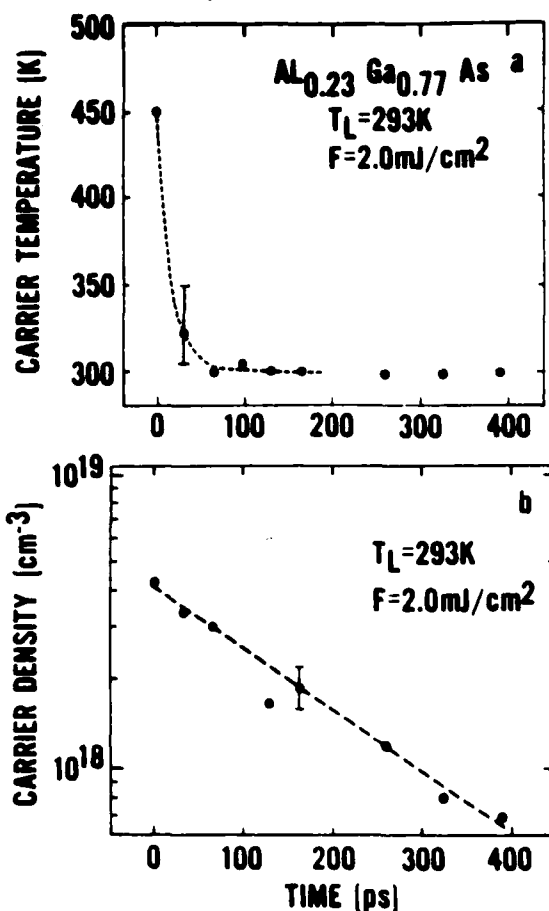
Figure 1. Temperature (a) and density (b) of the photoexcited carriers for room temperature $Al_{0.23}Ga_{0.77}As$ as a function of time
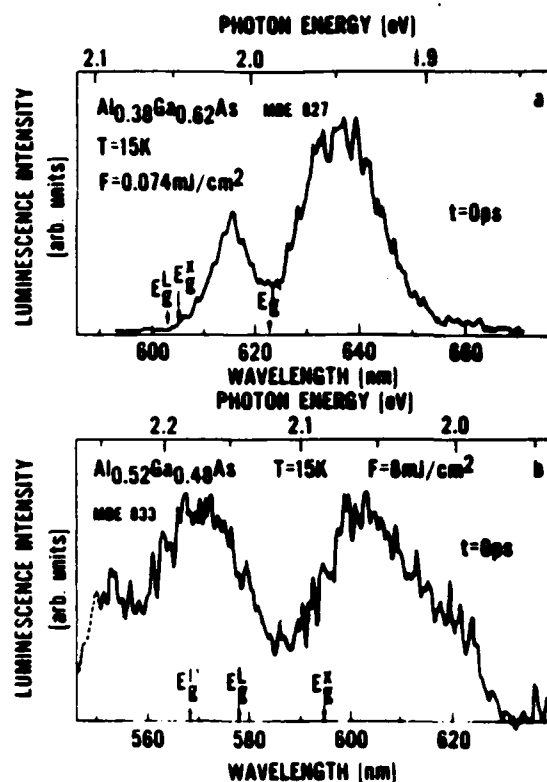
Figure 2. Low temperature photoluminescence spectra at t=0 ps for $Al_{0.38}Ga_{0.62}As$ (a) and $Al_{0.52}Ga_{0.48}As$ (b)

References

1. R. Dingle, R. A. Logan, and J. R. Arthur: In GaAs and Related Compounds, ed. by C. Hilsum (Institute of Physics, London, 1977), p. 210
2. H. J. Zarrabi and R. R. Alfano: Phys. Rev. B 32, 3947 (1985)
3. H. M. van Driel: Phys. Rev. B 19, 5928 (1979)
4. E. Cohen, M. D. Sturge, M. A. Olmstead, and R. A. Logan: Phys. Rev. B 22, 771 (1980)
5. A. W. Pikhtin: Fiz. Tekh. Poluprovodn. 11, 425 (1977) [Sov. Phys. Semicond. 11, 245 (1977)]
6. P. J. Pearah, W. T. Masselink, J. Klem, T. Henderson, H. Morkoc, C. W. Litton, D. C. Reynolds: Phys. Rev. B 32, 3857 (1985)

Appendix E: Tunable Near Infrared
Picosecond Pulses from a Short
Cavity Dye Laser

TUNABLE NEAR INFRARED PICOSECOND PULSES FROM A SHORT CAVITY DYE LASER

K. Bohnert, Thomas F. Boggess, Kamjou Mansour, and Dwight Maxson
Center for Applied Quantum Electronics
Department of Physics
North Texas State University
Denton, Texas 76203

and

Arthur L. Smirl
Hughes Research Laboratories
3011 Malibu Canyon Road
Malibu, CA 90265

Abstract

We report on the generation of tunable infrared picosecond pulses by a short cavity dye laser system consisting of a short cavity, a three stage amplifier, and a wavelength control unit. The laser emission is temporally, spectrally, and spatially resolved. The conditions for optimum performance are ascertained, and the output characteristics important to experimental applications are determined.

I. INTRODUCTION

Near infrared, tunable, picosecond pulses are of considerable interest for numerous applications in ultrafast spectroscopy. In particular, optical spectroscopy of novel semiconductor materials with band gaps in the near infrared spectral region has been a field of growing importance in recent years. A promising method for efficiently generating tunable, picosecond pulses within a wide spectral range is the short cavity dye laser (SCDL) [1-3].

In the past there have been various reports of the operation of short cavity dye lasers within the visible spectrum [1-11]. Early investigations were mainly concerned with the pulse shortening properties of these systems and were performed with lasers that produced a multi-mode spectral output [1,2,4,6,9]. Cox et al. [7,8] demonstrated that tunable, nearly Fourier transform limited, single-mode, picosecond pulses could be generated with a SCDL. Recently, Kortz et al. [10-11] have achieved total energy conversion efficiencies between 5 and 15 percent by amplifying such pulses.

In spite of these encouraging results, information concerning the reliable operation of short cavity dye lasers for experimental applications is scarce. Also, few experimental details have been published on the effects of the various system parameters such as cavity lifetime, dye concentration, or pump power on the laser emission, and to our knowledge, there have been no reports on the performance of short cavity dye lasers operating in the infrared.

In this paper, we report a detailed investigation of a SCDL system [12], primarily using the near infrared dye LDS 821. The laser system consisted of a short cavity, a longitudinally pumped three stage amplifier and a wavelength control unit. The laser emission was analyzed temporally, spectrally, and spatially as a function of the pump level, the cavity length (i.e., the cavity lifetime), and the dye concentration. Further experiments included the determination of the energy conversion efficiency and of the amplitude and wavelength

76

stabilities. From these measurements, the conditions for optimized performance were ascertained and the output parameters important to experimental applications were determined. In addition to LDS 821, the laser also was tested with Rhodamine 590 (RH 590) in order to examine its performance in a different spectral region and to demonstrate its spectral versatility.

II. EXPERIMENTAL CONFIGURATION AND PROCEDURE

The experimental apparatus (consisting of the pump source, the SCDL system and the characterization instrumentation) is shown in Fig. 1. The pump source was an actively and passively mode-locked Nd:YAG laser (Quantel YG 402). This system provided excellent energy stability (~5% shot-to-shot integrated over the entire pulse train), a key factor in stable SCDL operation. From the emitted pulse train, a single pulse was selected by a photodiode triggered pulse slicer. The selected pulse, after amplification and frequency doubling to 532 nm, had an energy of ~1 mJ and a temporal width of 32 = 4 ps (full width at half maximum, FWHM)[13]. The remaining, non-converted 1.064 μm pulse was rejected. The pulse repetition rate was chosen as either 1 or 5 Hz.

The heart of any single-mode short cavity dye laser system is a Fabry Perot resonator. The resonator mirror spacing is typically adjusted in a range (of a few microns) where only a single longitudinal mode is allowed to lase within the emission spectrum of the dye; the entire cavity volume is filled by an appropriate dye solution. The wavelength is then tuned by changing the cavity length. Since the resonator emission typically is only a few nanojoules most experimental applications require additional amplification. Also, to prevent a drift of the emission wavelength, a control circuit is necessary to stabilize the cavity length and to compensate for mechanical relaxations.

In our experiments, the cavity was formed by two identical broad band dielectric-coated mirrors with reflectivities greater than 90% over the emission

band of LDS 821 and reflectivities between 80% and 90% for the RH 590 emission band. The transmission at the pump beam wavelength was approximately 80%. The resonator length was coarsely adjusted with micrometer screws; the fine adjustment and wavelength tuning were achieved with a piezoelectric translator. The actual magnitudes of the resonator length were determined by interferometric methods. For our pulse repetition rates and small cavity volumes, only a small dye flow rate (typically a few milliliter per hour) was required. Consequently, a simple closed-cycle gravity pump was used for dye circulation; a single dye filling could be used for several days. The cavity was longitudinally pumped by a residual reflection of the incoming pump beam from an anti-reflection coated mirror substrate. Tne pump power was controlled further by neutral density filters. Finally, a lens focused the pump beam into the cavity; it was adjusted to maximize the SCDL output pulse energy.

Approximately 3%, 10%, and 87% of the incoming pump beam longitudinally pumped the first (A1), second (A2), and tnird (A3) cells, respectively, of a three stage amplifier. Tne amplifier system was designed to operate in the saturated regime in order to minimize amplified spontaneous emission (ASE). This required a good spatial overlap of pump and SCDL beams, as well as an appropriate choice of the size of the pumped dye volume. The proper temporal synchronization of pump and SCDL pulses was achieved by a movable prism in the path of tne cavity pump beam and/or by moving tne amplifier cells. The longitudinal pumping geometry chosen here yields better uniformity of the beam profile than side-pumping geometries while maintaining excellent efficiencies. The disadvantage is that dichroic mirrors are required, which make the system more expensive and cause losses for botn pump and amplified pulses. For details on the amplifier design see [11].

The cavity mirror spacing, i.e., tne emission wavelength, was stabilized by

an opto-electronic feedback loop similar to the one described in [10]. A small fraction of the emitted SCDL pulse was fed into a wavelength detector, which consisted of an 1800 grooves/mm grating and a silicon position sensor. The wavelength dependent signal from the position sensor was electronically compared to a reference voltage, i.e., a reference wavelength. A deviation of the laser wavelength, i.e., of the position sensor signal, from the reference value generated an appropriate corrector voltage. This voltage was applied to the piezo-electric translator to readjust the cavity length such that agreement of actual and reference wavelength were again achieved. The feedback loop was designed to keep the wavelength fluctuations small compared to the laser line width, which typically is on the order of 2-4 Å. This requires a stabilization of the cavity mirror spacing with a precision of roughly 1 to 2 nm.

A streak camera and a double 0.25-meter spectrometer were used to temporally and spectrally analyze the emitted pulses. In both cases, the signals were recorded by vidicons connected to multichannel analyzers. The overall temporal and spectral resolutions were 2.5 ps and 1.2 Å, respectively. In addition to the SCDL pulses, a small fraction of the 532 nm pump pulses was directed to the streak camera to serve as a reference for the determination of the expected pulse shortening properties of the SCDL. The relative time differences and the jitter between pump and SCDL pulses were also examined with this arrangement. The spatial beam profiles were determined by placing one of the vidicons directly into the beam path. The pulse energies were measured with a calibrated energy detector.

III. Results and Discussion

The amplified SCDL emission was analyzed as a function of the pump power, cavity length, and dye concentration. The spectral, temporal, and spatial pulse profiles, the energy conversion efficiency, the amplitude and wavelength stabil-

79

ities, as well as the width of the tuning range were investigated in detail. The majority of these experiments were performed using the near infrared dye LDS 821. In order to compare the infrared performance to the emission characteristics in the visible, the laser was operated with RH 590, as well. Since with the latter dye a wider range of dye concentrations could be obtained, it also was used to investigate the concentration dependence of the laser emission. In the following, we first describe the infrared performance of the SCDL.

In a first set of measurements, the SCDL pulses were analyzed temporally and resolved spectrally, while the cavity pump power was varied between the lasing threshold and 50 times this value. The LDS 821 concentrations were 3.5×10^{-2} mole/ℓ in the cavity and 4×10^{-4} mole/ℓ in the amplifier cells. The solvent was methanol. The cavity length was adjusted to 17 µm, and the laser line was tuned close to the emission maximum of the dye at 820 nm. Under these conditions, two additional modes were lasing at the edges of the tuning range. These modes, however, were between one and two orders of magnitude less in energy than the central mode.

At the highest pump levels, the time resolved SCDL pulses consisted of a main peak with a width of 13 ± 3 ps (FWHM) and a smaller trailing secondary feature. As the pump power was decreased, the tail first evolved into a single spike and, eventually, completely disappeared. Simultaneously, the main peak narrowed to a width of 7.5 ± 2.5 ps (FWHM). This value corresponds to a factor of four reduction compared to the pump pulses and is approximately one order of magnitude longer than the cavity lifetime. This behavior is illustrated in Fig. 2 for pump levels between 5 and 50 times threshold. Note that the pulsewidths shown were among the shortest observed for each corresponding pump level.

In contrast to the temporal envelope of the pulses, the spectra varied only weakly with pump power. Although the resolution of the spectrometer did not permit the detection of detailed structures within the laser line, the results

80

indicate a symmetric, Gaussian-like spectral profile at all pump powers above a few times the threshold value. With decreasing pump level the spectral width decreased slightly from 4 ± 0.5 Å at 50 times the lasing threshold to 3.4 ± 0.4 Å at five times threshold. The average time bandwidth product $\Delta t \Delta \nu$ was a factor of 2.5 above the Fourier transform limit. The latter pump level produced the most satisfying temporal and spectral pulse shapes and amplitude stability. Closer to threshold, stronger amplitude fluctuations were observed. The usable tuning range under these conditions extended from 805 nm to 840 nm as shown in Fig. 3.

The jitter between the pump and amplified SCDL pulses was determined by our streak camera measurements to be less than ~1.5 ps for a cavity spacing of 17 μm and a pump level 5 times threshold. Moreover, the experimentally measured time differences between pump and amplified SCDL pulses were nearly constant for pump powers between 15 and 50 times the lasing threshold. A reduction of the excitation level from 15 to 5 times threshold, however, introduced and additional relative time delay of 4 to 5 ps. The absolute time delays between pump and SCDL pulses were always considerably less than the pump pulse width. We emphasize that, for this reason, our results cannot be described by the giant pulse model originally developed to account for laser pulse evolution in Q-switched lasers [14] or by direct application of the theoretical analysis of picosecond SCDL developed by Duncanson and Struve [15], since these divide the temporal evolution of the laser pulse into four separate time periods: pumping, amplification, lasing, and decay. Our observations of secondary pulses and a decrease in the time delays between pump and SCDL pulses with increasing pump-level are in qualitative agreement with the simple rate equation approach presented by Scott et al. (See Fig. 4 of Ref. 8). The latter model, however, predicts much larger delay changes than those experimentally observed. Our

81

observations are, in this regard, similar to those reported by Scott et al. [8] for SCDL operation in the visible.

In a second set of experiments, the amplified SCDL emission was analyzed at various cavity lengths L. Results for $17 \mu m$ and $9.5 \mu m$ are compared in Fig. 4. In both cases the pump level was a few times the lasing threshold. The dye concentrations were identical. Decreasing the cavity length increased the lasing threshold as well as the temporal pulse width. The spectral width also increased slightly. The absolute pump power for $L = 9.5 \mu m$ was three times the value for $L = 17 \mu m$. The average temporal widths differed by roughly a factor of two. The relative magnitude of the broadband spontaneous emission from the cavity gradually increased as the cavity mirror spacing was reduced to values below $10 \mu m$. Simultaneously, the short cavity emission also became more divergent. An increase of the pump power and the introduction of a diaphragm into the beam path behind the cavity reduced the relative magnitude of the spontaneous emission and narrowed the spectral width of the laser line. At cavity lengths less than $5 \mu m$, lasing was no longer observed.

In a further step, we determined the gain in the individual amplifier stages and the overall energy conversion efficiency. The cavity length was $17 \mu m$. The dye concentrations were as given above. The cavity was pumped at 15 times the lasing threshold. For a total pump pulse energy of 1 mJ, we found preliminary amplification factors for the stages A1, A2, and A3, of 60, 20, and 5, respectively, yielding a total gain of 6×10^3. The decreasing gain values from stage 1 to stage 3 indicate an increasing gain saturation. The overall energy conversion efficiency under these conditions was 0.6%. The contribution of amplified spontaneous emission to the total output energy was on the order of a few percent. Although no serious efforts were made to optimize the amplifier dye concentrations for maximum amplification, we believe that this relatively small energy conversion efficiency can be mainly attributed to the lower effi-

82

ciency of infrared dyes compared to dyes for the visible.

Another favorable characteristic of the SCDL is its amplitude stability. When optimized to produce stable temporal and spectral pulse profiles we found that the energies of 40% (90%) of the pulses were within 10% (25%) of their average value. This has to be compared with the stability of the pump source. Approximately 70% of the pump pulses were within 10% of their average.

A determination of the wavelength stability showed that the opto-electronic feedback loop kept the laser line at the desired position with an accuracy of ± 1.5 Å. This value may be improved by optimizing the imaging optics of the stabilization unit. Within an observation period of 30 minutes, no detectable long term drift of the wavelength was observed. Such a drift could be produced, e.g., by mechanical or electronic instabilities of the feedback system itself.

Fig. 5 shows the spatially resolved SCDL beam in the near field as recorded on an optical multichannel analyzer. Fig. 5a is a horizontal scan with integration over the the vertical dimension. Fig. 5b shows a scan through the beam center with a 250 (75) μm resolution on the vertical (horizontal) dimension. The beam profile was found to be essentially Gaussian, although there were some small higher frequency (compared to the spot size) spatial fluctuations. The small energy associated with these fluctuations is diffracted well into the wings of the spatial profile in the far field and is easily filtered

Replacing LDS 821 by RH 590 did not introduce any significant changes in the system performance. In spite of the somewhat lower cavity finesse in the spectral region of RH 590, for comparable experimental conditions, similar temporal and spectral pulse profiles were observed. Temporally and spectrally resolved pulses of various RH590 concentrations are shown in Fig. 6. The pump levels were again a few times the lasing threshold. The cavity length was 10 μm. We found that the dye concentration could be varied over a relatively

83

wide range without dramatic effects on the SCDL output. The best results regarding pulsewidth, spectral width and amplitude stability were obtained at relatively low concentrations of 3×10^{-2} mole/ℓ. At concentrations above 10^{-1} mole/ℓ, the emission became less stable, and the spectra often exhibited two or more individual spikes. For cavity lengths shorter than $10\,\mu m$, dye concentrations closer to 10^{-1} mole/ℓ seemed to yield better results. Throughout the laser operation with RH 590, a Kiton Red solution (4×10^{-4} mole/ℓ) was used in the amplifier stages. An accurate measurement of the energy conversion efficiency for the RH590/Kiton Red combination could not be made, since the dichroic mirrors were not optimized for this dye. Based on the present results, we estimate that a finally attainable efficiency of about five percent can be expected for pump levels near threshold.

IV Conclusion

The measurements described above demonstrate that a SCDL system allows the generation of tunable, infrared, picosecond pulses with good stability. The significant performance characteristics are summarized in Table 1. For the given design and for operation in the infrared with the dye LDS 821, the best performance regarding temporal and spectral pulse shapes, output energy (per mode), and output stability was achieved for cavity lengths around 15 μm, dye concentrations of 3×10^{-2} mole/ℓ, and pump powers of roughly 5 times the threshold for lasing. Since under these conditions the mode spacing is slightly less than the width of the tuning range, additional spectral dispersion of the laser emission by a grating or prism (or the use of suitable spectral filters) may be necessary for some experimental applications. For true single mode operation in the near infrared, the cavity length must be reduced to 7-8 μm. These conditions still produced satisfying results. The pulses, however, were longer, less stable, and the relative magnitude of amplified spontaneous emis-

sion was enhanced. Improvements in this regard can be expected by optimizing the cavity mirror reflectivities and by selecting a more appropriate dye solvent that permits a wider solubility range for LDS 821. The energy conversion efficiency is, compared to operation in the visible, relatively low. Even so, the output energy is sufficient for experimental applications. Moreover, the pump power can be easily increased above the level used in the present experiments.

Our investigations also demonstrate that, with the same set of cavity mirrors, similar performance (at an improved energy conversion efficiency) can be obtained in the visible. The SCDL, thus, represents an effective and relatively simple method for the conversion of fixed-wavelength, single picosecond pulses into tunable picosecond pulses over an extended spectral range. Simultaneously, a considerable pulsewidth reduction can be achieved.

V. Acknowledgments

REFERENCES

1. B. Fan, T. K. Gustafson, "Narrow-band Picosecond Pulses from an Ultrashort-Cavity Dye Laser," Appl. Phys. Lett., Vol. 28, pp. 202-204, 1976.

2. H. Salzmann and H. Strohwald, "Single Picosecond Dye Laser Pulses by Resonator Transients," Phys. Lett., Vol. 57A, pp. 41-42, 1976.

3. A. J. Cox, G. W. Scott, and L. D. Talley, "Tunable Blue Picosecond Pulses from a Dye Laser," Appl. Phys. Lett., Vol. 31, 389-391, 1977.

4. J. A. Buck and Z. A. Yasa, "Dual Frequency Subnanosecond Pulses from a Millimeter-Cavity Dye Laser" IEEE J. Quantum Electron., Vol. QE 13, pp. 935 - 936, 1977.

5. A. J. Cox, D. E. Damshen, C. D. Merritt, G. W. Scott, and L. D. Talley, "Evidence for Nearly Transform-Limited Pulses from a Short Cavity Dye Laser," in Picosecond Phenomena, C. V. Shank, E. P. Ippen, and S. L. Shapiro, Eds, Springer-Verlag, Berlin, p. 63-66, 1978.

6. F. Aussenegg and A. Leitner, "A Short Resonator Dye Laser Pumped by a Traveling Wave N_2 - Laser, Opt. Comm., Vol. 32, pp. 121-122, 1980.

7. A. J. Cox, C. D. Merritt, and G. W. Scott, "Single Mode, Piezo-electrically Tuned, Picosecond Short-cavity Dye Laser," Appl. Phys. Lett., Vol. 40, pp. 664-666, 1982.

8. G. W. Scott, J. H. Clark, M. A. Tolbert, S. P. Webb, A. J. Cox, and G. Renz, "Simultaneous Determination of the Spectral and Temporal Properties of Tunable, Single, Picosecond Pulses from a Short-cavity Dye Laser," IEEE J. Quantum Electron., Vol. QE-19, pp. 544-550, 1983.

9. P. H. Chiu, S. Hsu, S. John, C. Box, and H.-S. Kwok, "A Cascade Pumped Picosecond Dye Laser System," IEEE J. Quantum Electron. Vol. QE-20, pp. 652-658, 1984.

10. H. P. Kortz, P. Pax, and R. Aubert, "Generation of High Energy Tunable Picosecond Pulses," Ultrashort Pulse Spectroscopy and Applications, M. J. Soileau, Ed., Proc. SPIE 533, pp. 32-37, 1985.

11. H. P. Kortz, A. J. Cox, G. W. Scott, D. M. Guthals, H. Nathel, S. W. Yeh, S. P. Webb, and J. H. Clark, "Amplification of Tunable Picosecond Pulses from a Single-Mode, Short Cavity Dye Laser," IEEE J. Quantum Electron. Vol. QE-21, pp. 1795-1798, 1985.

12. The experiments were performed with a Quantel prototype short cavity dye laser, which was improved by a home-made wavelength control unit.

13. Throughout this paper the ± error bars for the pulse durations and bandwidths represent the standard deviation for typically 10-20 laser shots.

14. W. G. Wagner and B. A. Lengyel, "Evolution of a Giant Pulse in a Laser," J. Appl. Phys., Vol. 34, pp. 2040-2046, 1963.

15. J. A. Duncanson and W. S. Struve, "The Picosecond Ultrashort Cavity Dye Laser: Giant Pulse Analogy and Active Etalon Model," IEEE J. Quantum Electron., Vol. QE-52, pp. 3800-3820, 1981.
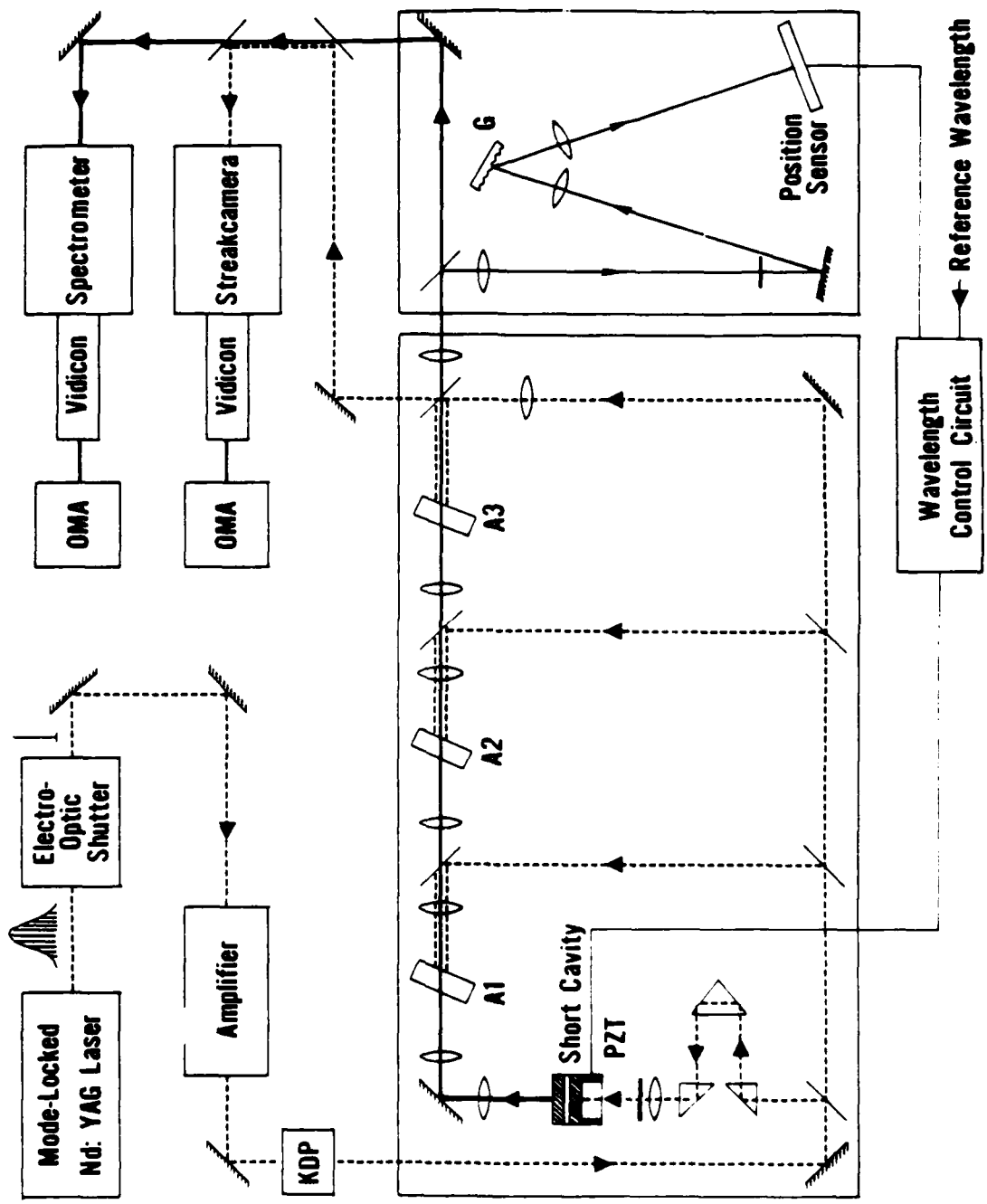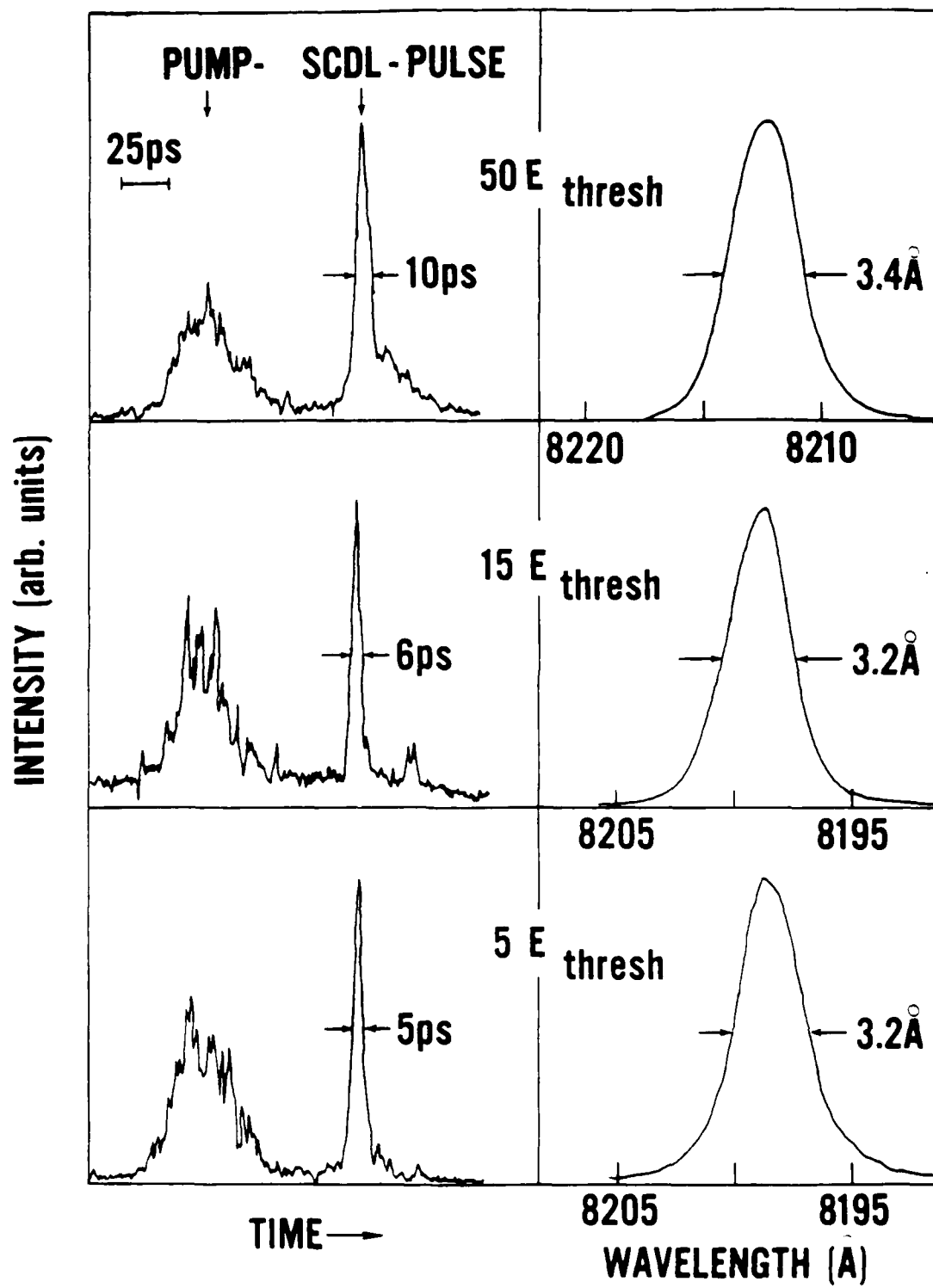
FIGURE CAPTIONS

Figure 1. Experimental set-up. PZT: piezoelectric translator, A1-A3: amplifier stages, G: reflection grating.

Figure 2. Temporally and spectrally resolved SCDL pulses and temporally resolved pump pulses for various pump powers (in units of the lasing threshold E_{thresh}).

Figure 3. Output energy per mode as a function of wavelength.

Figure 4. Temporally and spectrally resolved SCDL pulses for cavity lengths of 17 μm and 9.5 μm. The pump power was approximately five times the lasing threshold.

Figure 5. Vidicon recording of the spatial beam profile in the near field of slightly focused beam:
a) scan integrated in vertical direction
b) scan through beam center

Figure 6. Temporally and spectrally resolved SCDL pulses for various dye concentrations in the short cavity at pump levels a few times the lasing threshold.
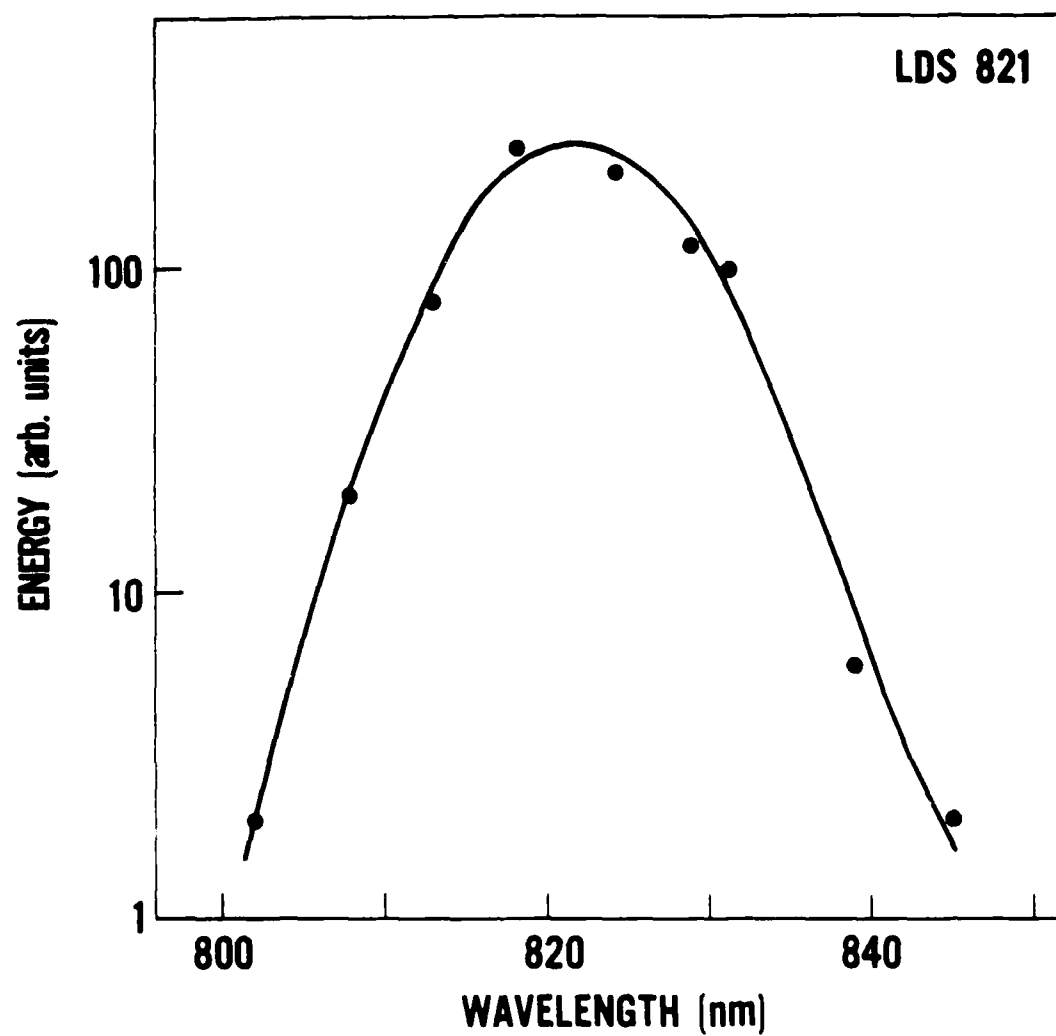
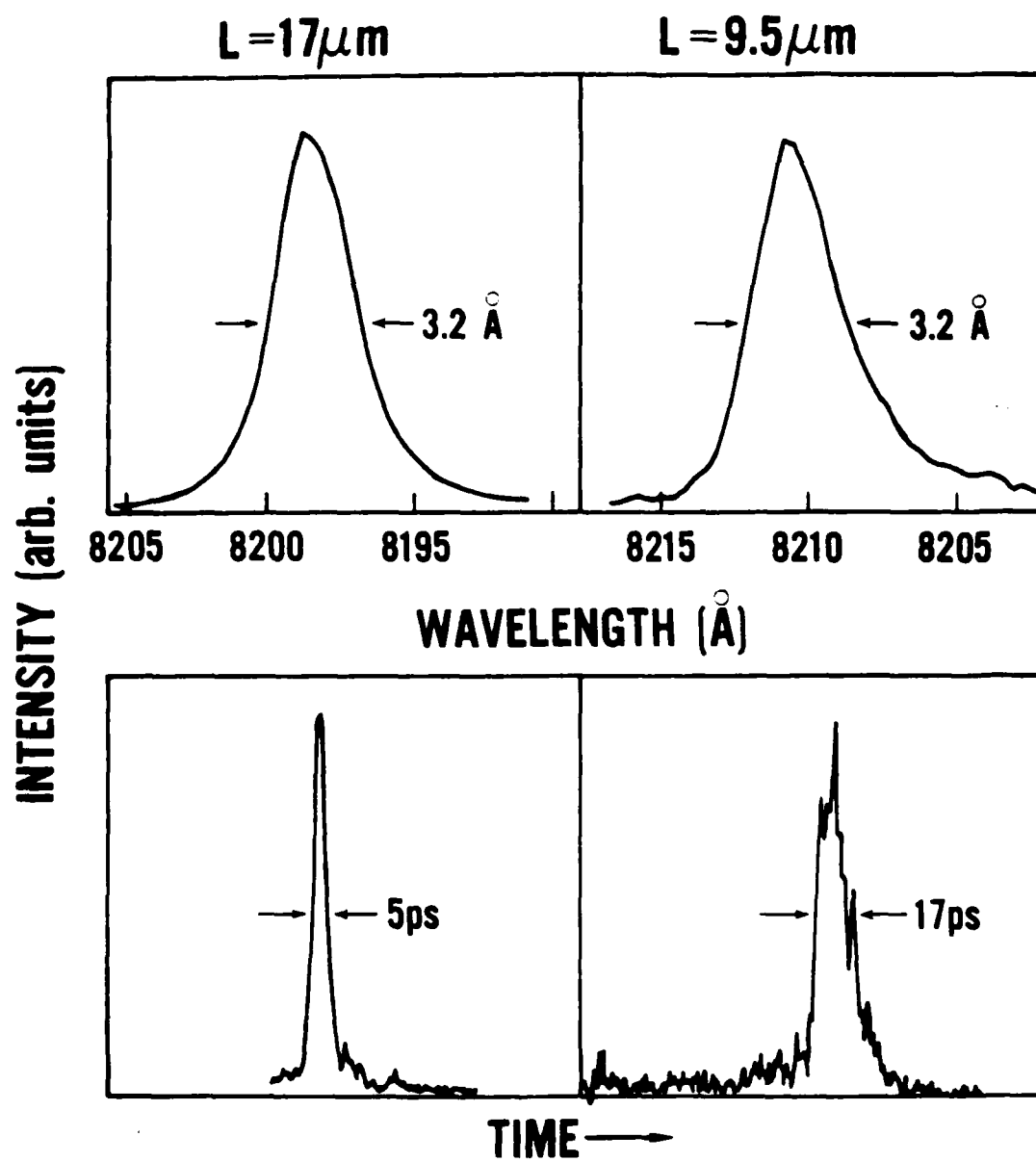
Table 1. SCDL Infrared Performance

Dye: LDS 821
Concentrations: 3.5 x 10^{-2} mole/ l (cavity)
                4 x 10^{-4} mole/ l (amplifier cells)
Solvent: methanol
Cavity lengths: 17μm, 9.5μm
Pump power: 5x threshold
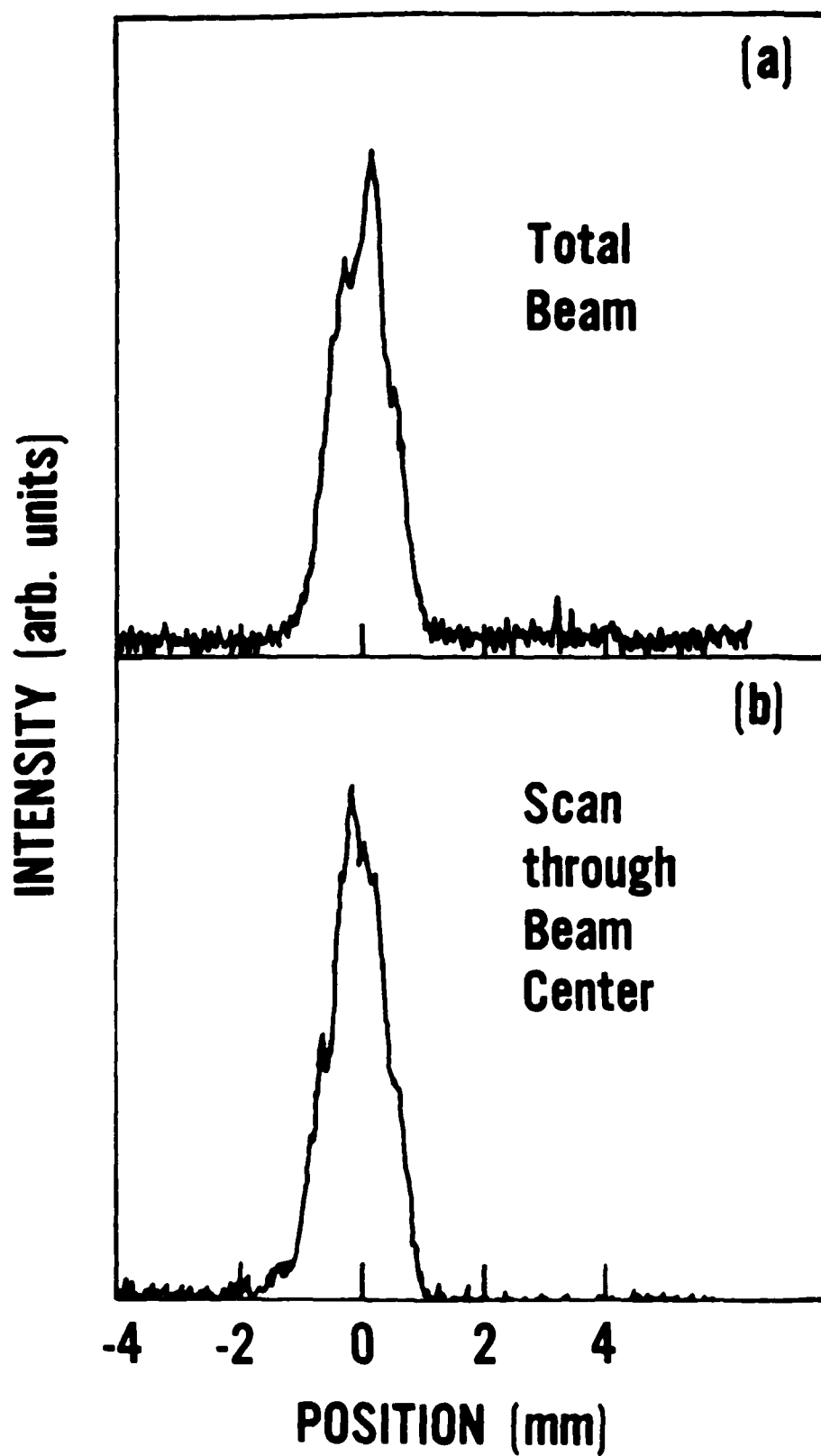
	Input	Output	
		L = 17μm	L = 9.5μm
Wavelength	532 nm	805 – 840 nm (tunable)	805 – 840 nm (tunable)
Temporal width (FWHM)	32 $\pm$ 4ps	7.5 $\pm$ 2.5ps	15 $\pm$ 4ps
Spectral width (FWHM)	0.6 Å	3.4 $\pm$ 0.4 Å	4.0 $\pm$ 1.0 Å
Energy/pulse	1 $\pm$ 0.15 mJ	5 $\pm$ 1.2μJ	~ 3μJ
ASE	—	< 10%	
Temporal jitter	—	$\pm$ 1.5ps	
Wavelength stability	—	$\pm$ 1.5 Å	$\pm$ 1.5 Å
Free spectral range	—	15 nm	27 nm

L=17μm   L=9.5μm

3.2 Å   3.2 Å

INTENSITY (arb. units)

WAVELENGTH (Å)

8205   8200   8195   8215   8210   8205

5ps   17ps

TIME →

Figure axis labels:
- Y-axis: INTENSITY (arb. units)
- X-axis: POSITION (mm)
- (a) Total Beam
- (b) Scan through Beam Center
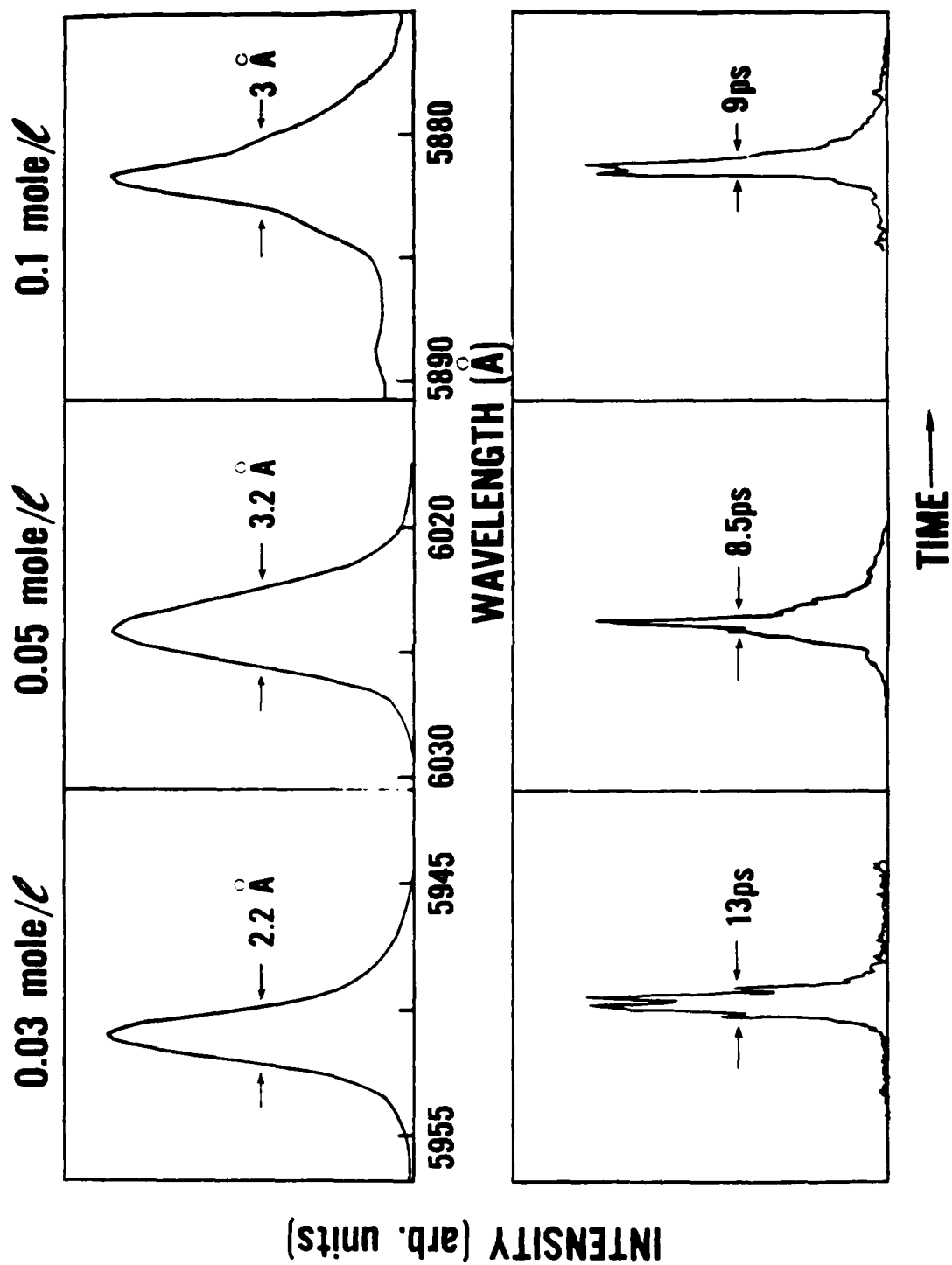- X-axis values: -4, -2, 0, 2, 4

INTENSITY (arb. units)

Appendix F: A Hybridly Mode-Locked
CW Dye Laser with Brewster Prisms

A preprint accepted for publication
by Optics Communications

A HYBRIDLY MODE-LOCKED CW DYE LASER WITH BREWSTER PRISMS

Martin D. Dawson, Thomas F. Boggess and Dennis W. Garvey
Center for Applied Quantum Electronics
North Texas State University
Denton, TX 76203 U.S.A.

and

Arthur L. Smirl
Hughes Research Laboratories
Malibu, CA 90265 U.S.A.

Abstract

Stable pulses as short as 69 fs duration have been generated by a linear-cavity, synchronously-pumped cw rhodamine 6G dye laser incorporating a pair of Brewster-angled quartz prisms and the saturable absorbers DQOCI and DODCI.

Classification: 8. Lasers

99

Direct generation of optical pulses having durations below 200 fs has most commonly been achieved with a cw-pumped, colliding-pulse, passively mode-locked (CPM), dye laser [1]. Recent recognition of the role played by self-phase modulation (SPM) and group velocity dispersion (GVD) in the pulse formation process [2,3] has culminated in the generation of 27 fs pulses from such a laser, where a sequence of four Brewster-angle cut quartz prisms was used to introduce adjustable GVD [4]. Synchronously mode-locked cw dye laser systems capable of producing pulses of 200 fs or less have been complicated by either the use of fiber-/grating pulse compressors [5-7] or, alternatively, conventional ring [8,9] or antiresonant ring [10,11] cavity arrangements which require either extremely critical positioning of a saturable absorber or external splitting of the pump beam [9] to achieve hybrid CPM. A four prism sequence has recently been incorporated into a synchronously pumped antiresonant ring laser to produce pulses as short as 70 fs [12].

With one published exception [13], simple linear-cavity, hybridly mode-locked, cw dye lasers have been limited to producing pulses longer than 200 fs, typically in the 300 - 800 fs range [14-17]. We report the generation of pulses with duration as short as 69 fs (full width at half maximum intensity,FWHM) from a linear-cavity hybridly mode-locked, cw dye laser incorporating a pair of Brewster-angle quartz prisms for dispersion compensation. Separate gain and absorber jet-streams helped to prolong the usable life of the absorber dyes (to weeks) and allowed independent focusing to adjust the relative saturation parameters of the active and passive dyes. The authors of [13] reported the generation of 70 fs pulses in a pellicle-tuned laser that had no deliberate means of dispersion compensation and incorporated a single jet-stream for both dyes. The low loss and high optical quality of the prisms compared to the uncoated pellicle used in [13] is an additional advantage of our system.

The cavity arrangement is shown in Fig. 1. A related cavity has produced

33 fs pulses by purely passive mode-locking [4]. The dye laser was pumped at a repetition rate of 82 MHz by frequency doubled pulses from a mode-locked cw Nd:YAG laser (Spectra-Physics Series 3000). The average pump power at 532 nm was 650 mW and the pulse duration was 70 ps as determined by a synchroscan streak camera. The pump beam was coupled into the gain medium (2×10^{-3}M rhodamine 6G in ethylene glycol) by a focusing mirror with a radius of curvature of 5 cm. The folded focusing section around the gain medium consisted of two mirrors, each with a radius of curvature of 7.5 cm, about a vertical jet-stream that was 200 μm thick. A 2.5×10^{-5}M solution of DQOCI, a 3.0×10^{-5}M solution of DODCI, and a mixed solution of 1.8×10^{-5}M DQOCI / 1.2×10^{-5}M DODCI in ethylene glycol were tried alternatively in the absorber section. A 100 μm absorber jet-stream was used with focusing mirrors of 3.75 cm radius of curvature. The dyes DQOCI and DODCI have been reported to have upper state lifetimes of 16 ps and 1.15 ns respectively [18]. All mirrors used were nominally 100% reflectively at 632.8 nm with a sufficient bandwidth to allow operation over the gain band of rhodamine 6G, except the output coupler which had a reflectivity of -90% at 590 nm. The two identical quartz prisms were arranged as shown in Fig. 1 and were aligned for minimum deviation and Brewster's- angle incidence at each surface. Each prism was mounted on a translation stage which allowed motion along a line normal to its base, and on tilt and rotation tables.

Fork et al. [19] have shown that terminating a linear-cavity laser with such a two-prism and flat mirror combination is equivalent to incorporating a four-prism sequence into a ring cavity. This configuration allows the introduction of variable GVD of either sign, adjustable through zero, without any net deviation of the beam after traversing the sequence. This geometry can compensate for frequency chirp in the pulses arising from the combined effects of SPM and GVD in the remainder of the cavity. The amount of negative dispersion,

101

which is proportional to the prism separation L, is adjusted to be large enough to compensate for the positive dispersion of the prism material (which may be varied by translating either prism normal to its base) combined with any additional chirp in the pulses. A length L = 250 mm has been calculated to be adequate to compensate for 6.6 mm of quartz at ~600 nm wavelength [19], and the prism sequence was initially set to operate close to these values.

Pulsewidth measurements were performed using non-collinear background - free autocorrelation in a 1 mm KDP crystal. The cross-over length due to the two converging beams has been estimated to be ~100 μm providing temporal resolution well below 100 fs. Spectral information was obtained with an optical multichannel analyzer and vidicon system coupled to a 1/4-meter spectrometer.

With a 2.5×10^{-5} M solution of DQOCI as saturable absorber, pulses as short as 114 fs (FWHM duration, hyperbolic secant squared profile assumed) were obtained when the dye laser cavity length was carefully matched to that of the pump laser. Such pulses were spectrally centered near 585 nm, a wavelength just below the 595 nm absorption peak of DQOCI. The spectral width of greater than 7 nm indicates operation above the Fourier transform limit for a hyperbolic secant squared pulse shape and may imply some residual frequency chirp that could be reduced by further optimization of the prism sequence.

Pulses of 96 fs duration (Fig. 2, hyperbolic secant squared profile assumed) of similar spectral width, centered at 581 nm, have been obtained using a 3×10^{-5}M solution of DODCI as the saturable absorber in the same cavity arrangement. The laser showed some tendency to be bistable in this case, with small (μm) adjustments of cavity length or slight realignment resulting in the wavelength jumping between 581 nm and 622 nm. However, insertion of an aperture between the second prism and the high reflectivity end mirror, a region of the cavity in which the frequency components are spatially dispersed, allowed suppression of oscillation in the red. The resulting high stability of the system

is evident from the autocorrelation of Fig. 2 which was obtained without a lock-in amplifier or other integrating device (other than the chart recorder itself) over a relatively long (minute) recording time.

Optimal operation of the laser was obtained using a mixed solution of the two saturable absorbers consisting of 1.8×10^{-5}M DQOCI and 1.2×10^{-5}M DODCI. Pulses of duration as short as 69 fs have been obtained with this combination (Fig. 3), with no tendency for dual wavelength operation. The time-bandwidth product of $\Delta\nu\Delta t = 0.42$ indicates operation close to the Fourier transform limit ($\Delta\nu\Delta t = 0.315$ for transform-limited hyperbolic secant squared pulses). Many such traces have been recorded on a day-to-day basis with pulsewidths consistently below 85 fs and average power of 55 mW for a 650 mW pump.

The effect of the passive dyes was investigated by switching off the absorber jet-stream. The resulting autocorrelation function consisted of a coherence spike on top of a broad base several picoseconds wide at the optimum cavity length. Such behavior is characteristic of synchronously mode-locked dye lasers with insufficient intracavity bandwidth restriction.

The performance of the laser with only a single prism in the cavity, but otherwise unchanged, was observed. At a DQOCI concentration of 2.5×10^{-5}M, a 520 fs pulse was obtained (again assuming a hyperbolic secant squared pulse shape). This duration is more characteristic of linear-cavity hybridly mode-locked cw dye lasers [14-17]. An autocorrelation of such a pulse is shown in Fig. 4.

In conclusion, we have demonstrated a linear-cavity, hybridly mode-locked, dye laser capable of producing pulses below 100 fs duration. Its advantages over other designs are principally its simplicity, ease of alignment and non-critical positioning of the saturable absorber jet, combined with its high efficiency and stability. The laser is well-suited for synchronous amplification

103

into the mJ pulse energy regime, and we are currently characterizing such a system.
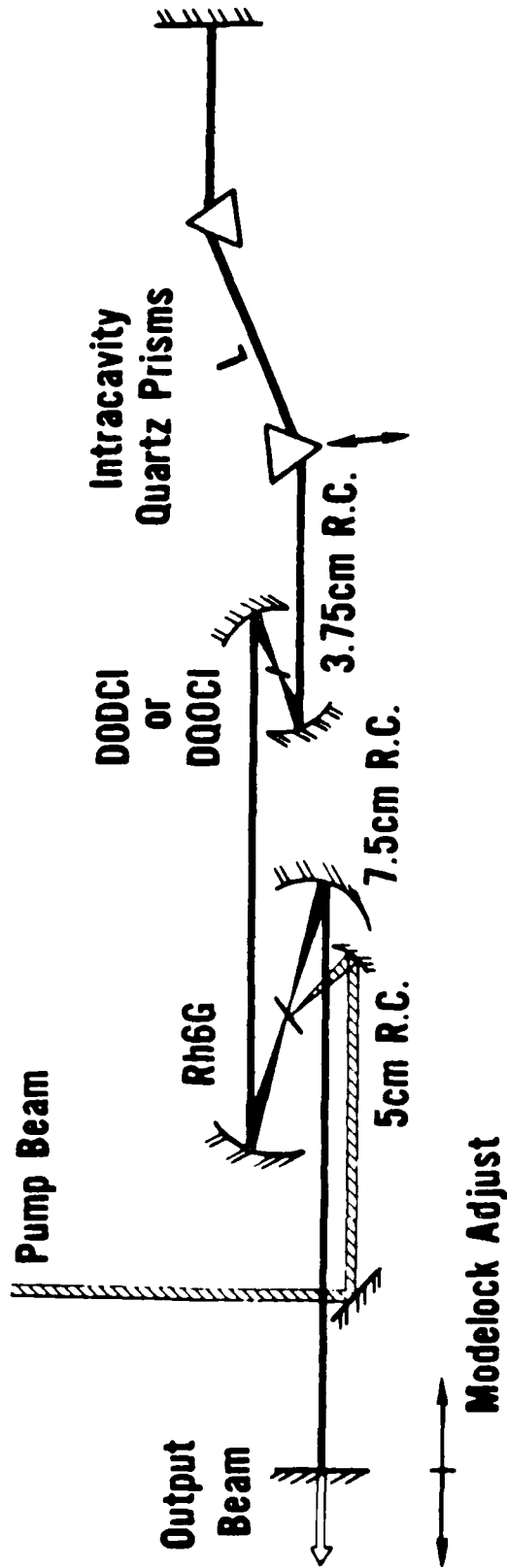
ACKNOWLEDGMENTS

''

REFERENCES

[1] R. L. Fork, B. I. Greene and C. V. Shank, Appl. Phys. Lett. 38 (1981) 671.

[2] J.-C. Diels, J. J. Fontaine, I. C. McMichael, B. Wilhelmi, W. Dietel and D. Kuhlke, Sov. J. Quantum Electron. 13 (1983) 1562.

[3] O. E. Martinez, J. P. Gordon, and R. L. Fork, Ultrafast Phenomena IV, D. H. Auston and K. B. Eisenthal, Eds., New York: Springer-Verlag, 1984, p. 7.

[4] J. A. Valdmanis, R. L. Fork and J. P. Gordon, Opt. Lett. 10 (1985) 131.

[5] A. M. Johnson and W. M. Simpson, IEEE J. Quantum Electron. 22 (1986) 133.

[6] S. L. Palfrey and D. Grischkowsky, Opt. Lett. 10 (1985) 562.

[7] J. D. Kafka and T. Baer, Proc. SPIE 533 (1985) 38.

[8] A. M. Johnson and W. M. Simpson, Opt. Lett. 8 (1983) 554.

[9] M. C. Nuss, R. Leonhardt and W. Zinth, Opt. Lett. 10 (1985) 16.

[10] H. Vanherzeele, R. Torti and J.-C. Diels, Appl. Opt. 23 (1984) 4182.

[11] T. Norris, T. Sizer II and G. Mourou, J. Opt. Soc. Am. B. 2 (1985) 613.

[12] T. Norris, I. N. Duling, M. Pessot, T. Sizer II, J. Dawes and G. Mourou Paper TuE4, Conference on Lasers and Electrooptics (May 1985), Technical Digest.

[13] G. Mourou and T. Sizer II, Opt. Commun. 41 (1982) 47.

[14] G. W. Fehrenbach, K. J. Gruntz and R. G. Ulbrich, Appl. Phys. Lett. 33 (1978) 159.

[15] D. Kuhlke, U. Herpers and D. von der Linde, Appl. Phys. B. 38 (1985) 233.

[16] Y. Ishida, K. Naganuma and T. Yajima, IEEE J. Quantum Electron. QE-21 (1985) 69.

[17] J. P. Ryan, L. S. Goldberg and D. J. Bradley, Opt. Commun. 27 (1978) 12F

[18] W. Sibbett, J. R. Taylor and D. Welford, IEEE J. Quantum Electron QE-14 (1981) 500.

[19] R. L. Fork, O. E. Martinez, and J. P. Gordon, Opt. Lett. 9 (1984) 150.

FIGURE CAPTIONS

Fig. 1. Laser Cavity Configuration

Fig. 2. Autocorrelation trace of 96 fs pulses obtained using DODCI.

Fig. 3. Autocorrelation trace of 69 fs mode-locked pulses (a) and corresponding integrated laser spectrum (b), obtained using mixed DQOCI/DODCI absorber.

Fig. 4. Autocorrelation trace of 520 fs pulse obtained with DQOCI at 605 nm with a single prism in the cavity.

"

Intracavity Quartz Prisms

DODCI or DQOCI

3.75cm R.C.

7.5cm R.C.

Rh6G

5cm R.C.

Pump Beam

Output Beam

Modelock Adjust

MICROCOPY RESOLUTION TEST CHART

NATIONAL BUREAU OF STANDARDS-1963-A

149fs
$t_p = 96fs$

TIME DELAY [fs]

SHG INTENSITY

108

(a)

1071s
$t_p = 69fs$

(b)

6.9nm

583nm

λ

TIME DELAY (fs)

SHG INTENSITY

-1700   -850   0   850   1700

808 fs
t_p = 520 fs
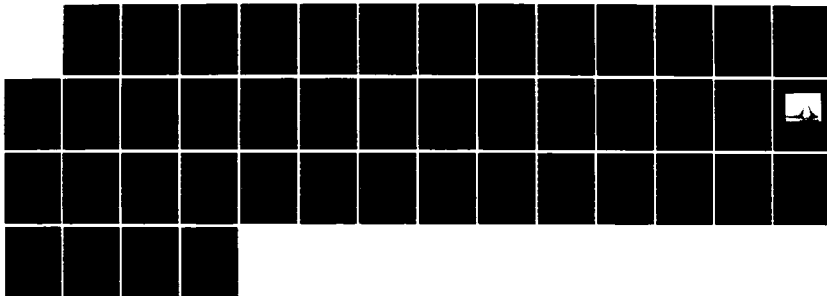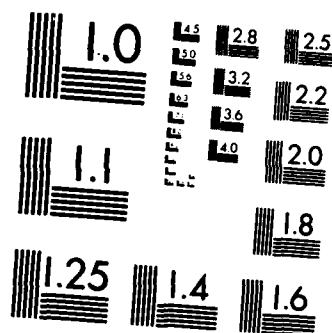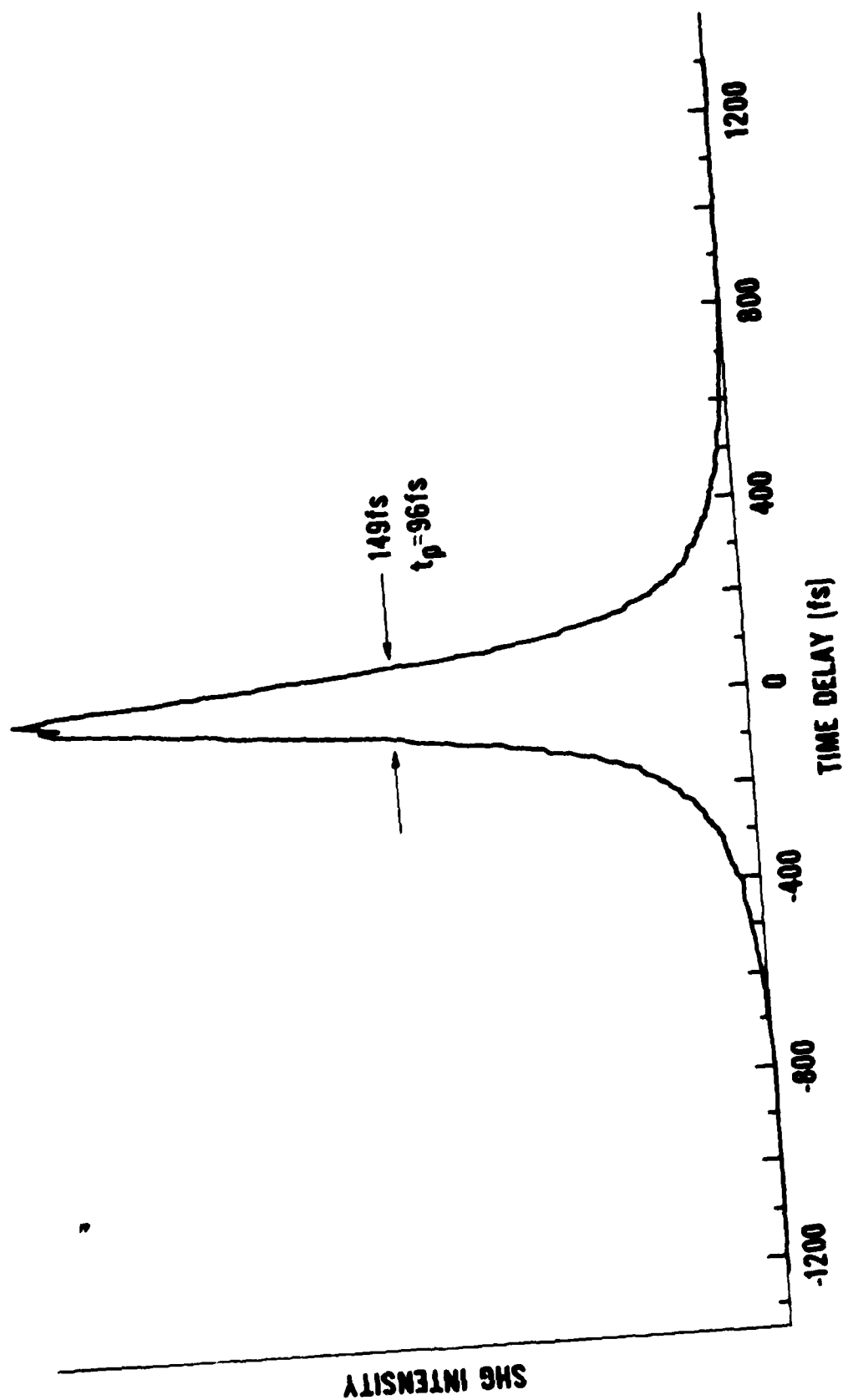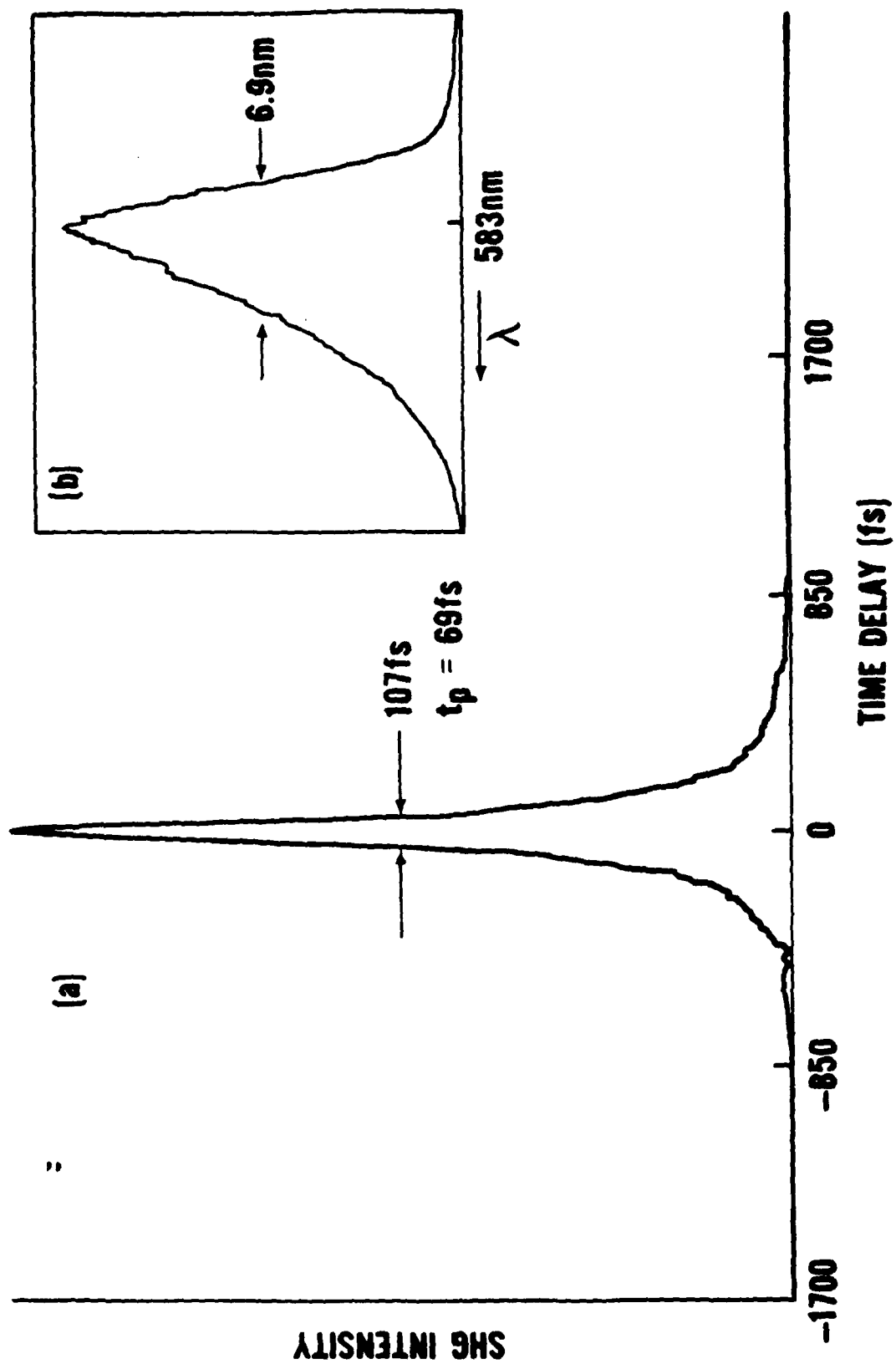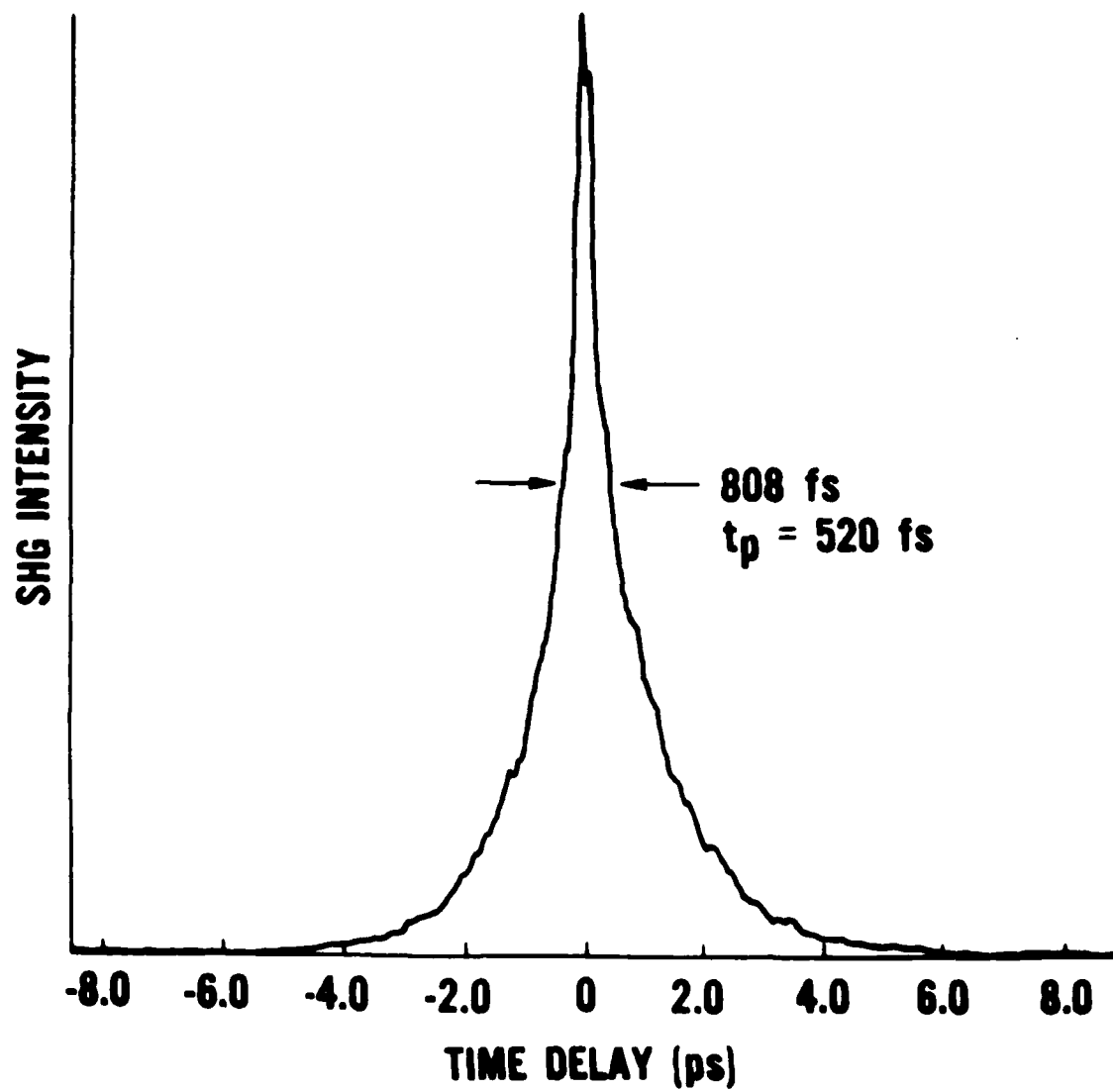
Appendix G: Variable Intracavity
Spectral Windowing in a
Synchronously-Pumped Hybridly Mode-
Locked CW Dye Laser

VARIABLE INTRACAVITY SPECTRAL WINDOWING IN A SYNCHRONOUSLY PUMPED

FEMTOSECOND CW DYE LASER

Martin D. Dawson, Thomas F. Boggess, and Dennis W. Garvey
Center for Applied Quantum Electronics
North Texas State University
Denton, Texas 76203 U.S.A.

and

Arthur L. Smirl
Hughes Research Laboratories
Malibu, CA 90265 U.S.A.

Abstract

An aperture of variable width has been placed within an intracavity prism sequence in a synchronously-pumped femtosecond dye laser. This is shown to allow direct control of the output pulsewidth in the range ~100-500 fs. Wavelength tunability is achieved by translating the aperture transversely.

In a fiber-and-grating pulse compressor,[1-5] pulses frequency-chirped by propagation in a single mode optical fiber are compressed using a grating pair dispersive delay line. Apodization of the amplitude and phase of the s₁ ially dispersed spectral components occurring within the grating pair compressor has recently allowed workers[6-9] to manipulate the temporal profile of the compressed picosecond and subpicosecond optical pulses. Using a variety of spectral masks, these authors have demonstrated nearly complete elimination of the energy in the wings of the compressed pulses,[6] synthesis of phase-coherent picosecond optical square pulses,[7] and generation of other temporal pulse shapes. The latter include pulse doublets and a burst of evenly spaced picosecond pulses.[8,9]

Transversely dispersed spectral components also occur within the Brewster prism sequence introduced to allow adjustment of intracavity group velocity dispersion (GVD) in femtosecond dye lasers.[10] In a four prism geometry,[10] typically used in ring cavities, the laser spectrum is angularly dispersed by the first prism in the sequence and is then collimated and transversely dispersed between the two central prisms. An equivalent arrangement can be achieved by terminating a linear cavity laser with two Brewster prisms near the high reflectivity end mirror.[10] In this case, the collimated dispersed spectral components occur between the second prism and the end mirror (Fig. 1). We have recently reported the generation of pulses as short as 69 fs duration from a dual-jet, synchronously pumped and passively mode-locked linear cw dye laser terminated by such a two-prism and plane mirror arrangement.[11] Here, we describe spectral windowing of the <u>intracavity</u> spatially dispersed laser spectrum occurring within the prism sequence in that linear cavity. A variable-width aperture allowed the oscillating laser bandwidth to be varied in a controllable manner, resulting in direct, continuous tunability of the pulsewidth from below 100 fs up to 500 fs. Translation of the aperture transversely to the beam direction provided wavelength tuning of the laser output.

114

The cavity arrangement used was described in detail in Ref. 11, and we present only an outline of its characteristics here. Briefly (Fig. 1), the laser was pumped by 650 mW average power, 70 ps pulses from a frequency-doubled mode-locked cw Nd:YAG laser. The pump pulses were coupled into the gain medium (2×10^{-3} M rhodamine 6G in ethylene glycol) by a 5 cm radius of curvature focusing mirror. The folded focusing section around the gain dye jet-stream consisted of two mirrors with a radius of curvature of 7.5 cm. The focusing mirrors around the saturable absorber jet-stream had radius of curvature 3.75 cm. The two identical quartz prisms were arranged as shown in Fig. 1 and were aligned for minimum deviation and Brewster's angle incidence at each surface. A mixed saturable absorber solution, consisting of 1.8×10^{-5} M DQOCI and 1.2×10^{-5} M DODCI in ethylene glycol, gave pulses as short as 69 fs spectrally centered at 583 nm. It had been previously determined[11] that, in this cavity arrangement, this absorber mixture resulted in the generation of shorter pulses than those achieved using either absorber separately. The time-averaged output power was ~60 mW when there was no windowing of the spectrum.

Pulsewidth measurements were performed by non-collinear background-free second harmonic generation in KDP using an autocorrelator that has a scanning display facility. Hyperbolic secant squared pulseshapes are assumed throughout in deriving the pulsewidth from the full width at half maxima (FWHM) of the autocorrelation functions. Spectral information was obtained with an optical multichannel analyzer (OMA) and vidicon system coupled to a 1/4 meter spectrometer. The overall spectral resolution of the OMA/vidicon system was 0.42 nm.

We first investigated the effect of a spectral aperture on the performance of the laser in purely synchronously mode-locked operation, i.e., with the saturable absorber jet-stream switched off. When no aperture is used, the two-

prism sequence shown in Fig. 1 provides an inadequate bandwidth restriction for complete mode-locking by synchronous pumping. At the optimum cavity length, the resulting autocorrelation consists of a coherence spike on a broad base that is 2.3 ps in duration [Fig. 2(a)]. The corresponding integrated spectral width of the laser output was 3.1 nm, giving a large time-bandwidth product, $\Delta v \Delta t$=6.4 (for transform limited sech^2 pulses $\Delta v \Delta t$=0.315). The output power of the laser was 90 mW, in this case.

When the aperture was inserted and closed to 0.7 mm, the output power was reduced to 20 mW and the oscillating bandwidth to 1.18 nm (deconvolved from the 1.25 nm measured bandwidth). As can be seen from Fig. 2(b), this cavity configuration then produced more completely mode-locked and considerably shorter (800 fs) pulses. In related early work on prism-tuned synchronously-pumped cw dye lasers, aperturing of the angularly dispersed spectrum was used, in a similar manner to that reported here, to improve the quality of the mode-locking.[13,14] By translating the aperture transversely to the laser beam direction in our laser, it was possible to tune the output between 572 and 600 nm. The corresponding time-bandwidth product of $\Delta v \Delta t$=0.84 for these pulses indicates some excess bandwidth. An attempt was made to reduce this by further closing of the aperture; however, the loss introduced by the aperture was such as to prevent laser oscillation when closed much below 0.7 mm.

With the saturable absorber jet-stream flowing in the cavity and the aperture fully opened, pulses of 100 fs duration were typically obtained in the manner described in Ref. 11. The autocorrelation of a typical pulse (with a duration of 103 fs) together with the corresponding integrated laser spectrum is shown in Fig. 3(a). The time-bandwidth product for this pulse is $\Delta v \Delta t$=0.57, indicative of reasonably well mode-locked operation. The aperture could be closed to 1.4 mm before any effect on the pulsewidth was observed. Under these conditions, the laser output could be tuned to well beyond 600 nm (~40 nm

tunability). An aperture within the four-prism sequence in a passively mode-locked colliding pulse laser has been used for wavelength tuning in this manner.[15] Figures 3(b) and (c) show the result of further reducing the aperture below 1.4 mm to 1.1 mm and 0.95 mm, respectively. It can be seen that the pulsewidth broadens from 100 to 500 fs as the oscillating laser bandwidth is reduced. The time-bandwidth product increases somewhat as the aperture is closed, most likely because the laser operates progressively nearer the threshold. (No readjustment of the prism sequence was performed between these measurements, and the reduction in power as the aperture is closed results in, among other effects, a changing of the frequency chirp imposed by the saturable absorber jet-stream.) The adjustable spectral aperture thus provides a direct means of varying the output pulsewidth and spectrum in a controllable manner. The output power for the 0.95 mm aperture width was 20 mW at 583 nm; the pulsewidth was 480 fs. Under these conditions, translation of the aperture across the beam resulted in some tunability of the laser in the wavelength range 578-586 nm. Further reduction of the aperture width below 0.95 mm resulted in increasingly unstable laser output, and laser oscillation ceased at an aperture width of 0.85 mm.

In conclusion, we have reported a demonstration of variable intracavity spectral windowing in a femtosecond mode-locked cw dye laser. Use of a simple variable aperture has allowed the lasing spectrum to be adjusted in a controllable manner, resulting in direct tunability of the output pulsewidth in the range 100-500 fs. In addition, translation of the aperture transversely to the beam direction provides some wavelength tunability. Variation of output pulsewidth from mode-locked lasers incorporating a prism sequence has previously been obtained[12] by increasing the negative dispersion introduced by the prism arrangement with respect to that giving optimal short pulse generation (excess

positive GVD leads to increasing instabilities in laser output). The advantage of variable aperturing for pulsewidth tunability in hybridly mode-locked systems is that no cavity length readjustment is required, which is not true for adjustments in the prism sequence. Such pulsewidth tunability can be readily applied, for example, to distinguish between intensity-dependent and fluence-dependent nonlinear optical processes.[16] It is also feasible that alternative low-loss masks could be used to produce additional intracavity pulse shaping, provided that the loss introduced is not sufficient as to prevent lasing. In addition, it may be possible to improve the spectral resolution in these intracavity windowing experiments by, for example, focusing the input beam through the prism sequence to decrease the spot size of any particular spectral component.[17]

Acknowledgements

118

References

1. C. V. Shank, R. L. Fork, R. Yen, R. H. Stolen, and W. J. Tomlinson, Appl. Phys. Lett. 40, 761 (1982).

2. B. Nikolaus and D. Grischkowsky, Appl. Phys. Lett. 43, 832 (1983).

3. A. M. Johnson, R. H. Stolen, and W. M. Simpson, Appl. Phys. Lett. 44, 729 (1984).

4. J. D. Kafka, B. H. Kolner, T. Baer, and D. M. Bloom, Opt. Lett. 9, 505 (1984).

5. A. S. L. Gomes, U. Osterberg, W. Sibbett, and J. R. Taylor, Opt. Commun. 54, 377 (1985).

6. J. P. Heritage, R. N. Thurston, W. J. Tomlinson, A. M. Weiner, and R. H. Stolen, Appl. Phys. Lett. 47, 87 (1985).

7. A. M. Weiner, J. P. Heritage, and R. N. Thurston, Opt. Lett. 11, 153 (1986).

8. J. P. Heritage, A. M. Weiner, and R. N. Thurston, Opt. Lett. 10, 609 (1985).

9. R. N. Thurston, J. P. Heritage, A. M. Weiner, and W. J. Tomlinson, IEEE J. Quantum Electron. QE-22, 682 (1986).

10. R. L. Fork, O. E. Martinez, and J. P. Gordon, Opt. Lett. 9, 150 (1984).

11. M. D. Dawson, T. F. Boggess, D. W. Garvey, and A. L. Smirl, Opt. Commun. (to be published).

12. J. A. Valdmanis and R. L. Fork, IEEE J. Quantum Electron. QE-22, 112 (1986).

13. R. K. Jain and J. P. Heritage, Appl. Phys. Lett. 32, 41 (1978).

14. J. P. Heritage and R. K. Jain, Appl. Phys. Lett. 32, 101 (1978).

15. R. L. Fork, private communication.

16. T. F. Boggess, K. Bohnert, K. Mansour, S. C. Moss, I. W. Boyd, and A. L. Smirl, IEEE J. Quantum Electron. QE-22, 360 (1986).
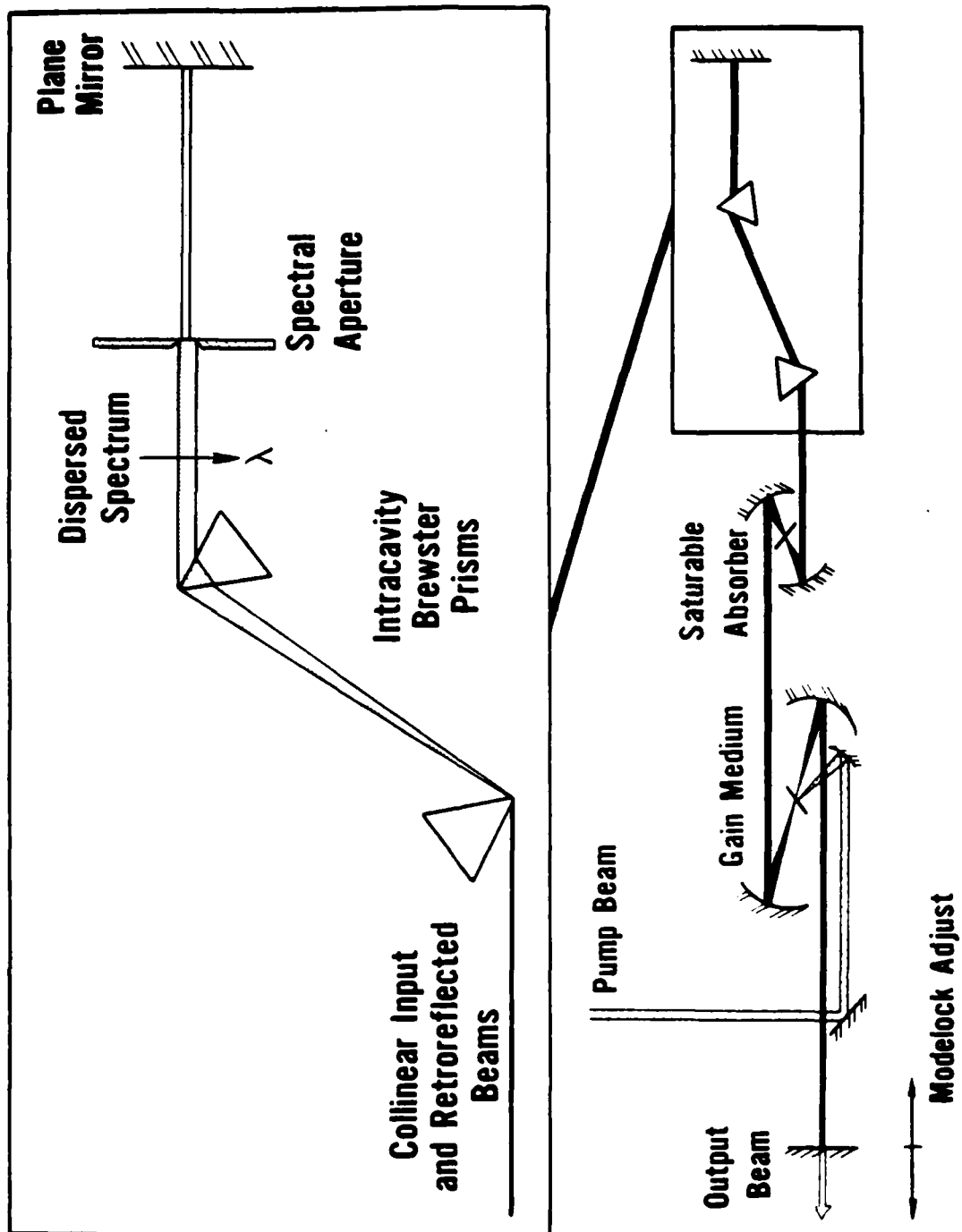
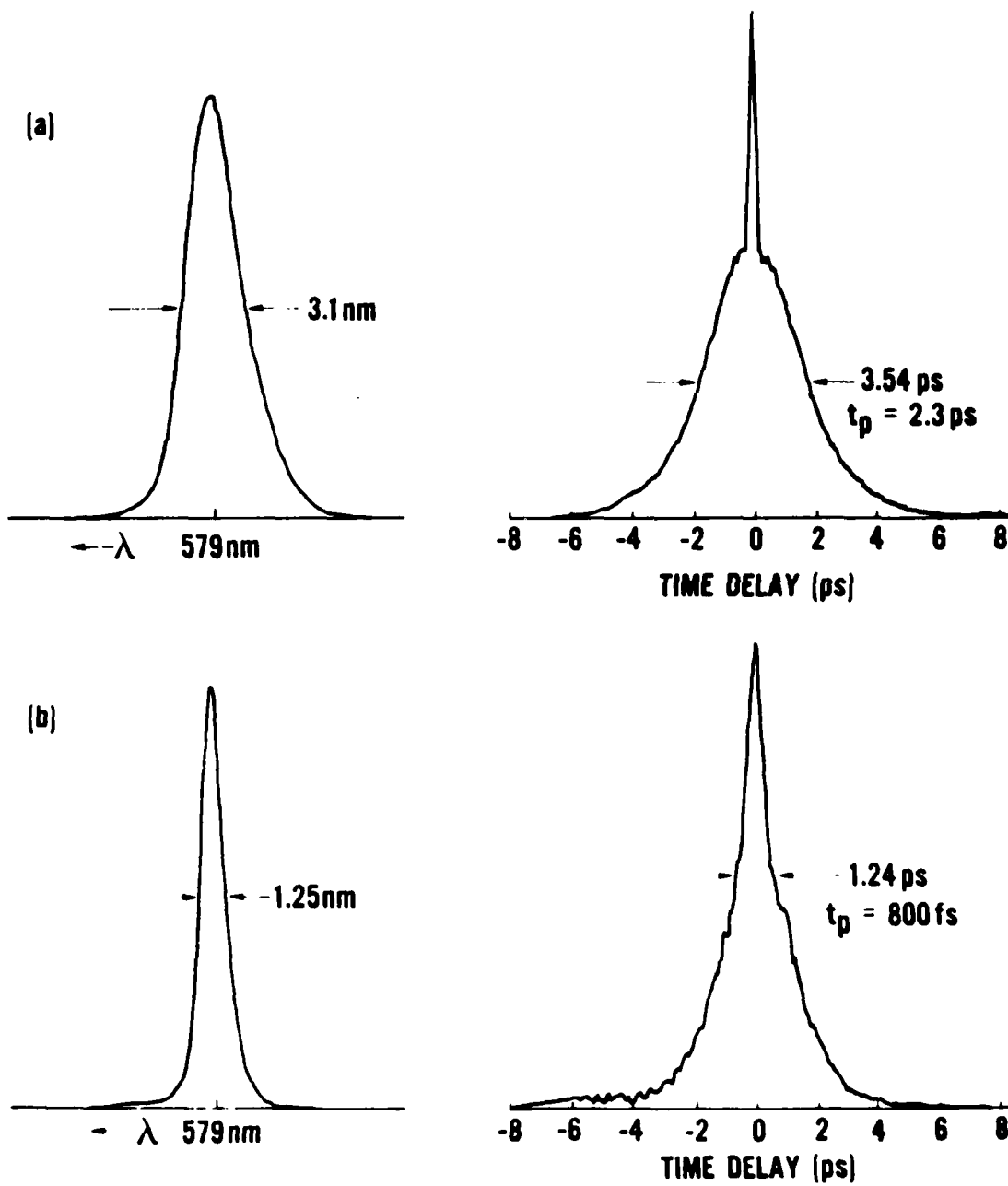17. J. P. Heritage, private communication.

Figure Captions

Figure 1. Laser cavity configuration with inset showing prism arrangement and position of spectral aperture.
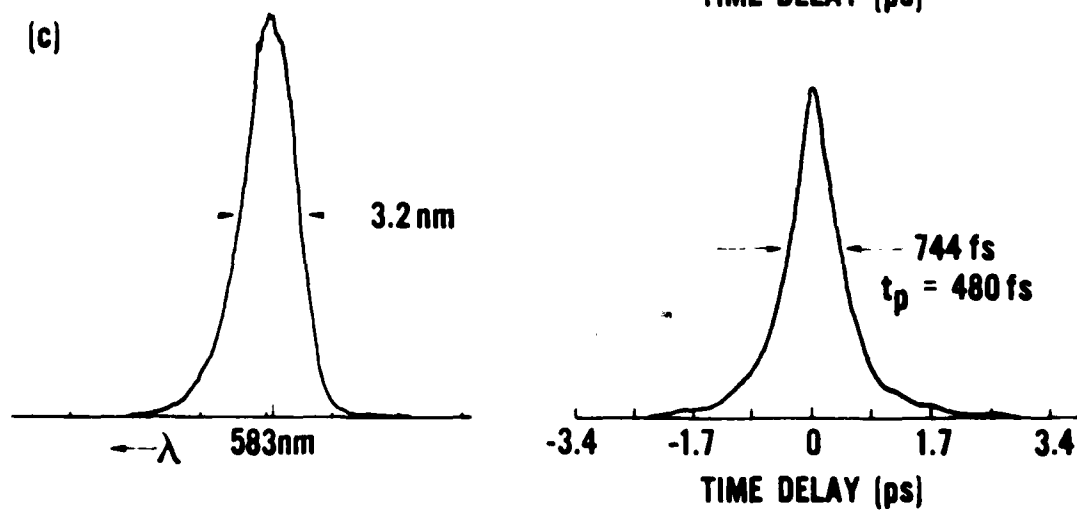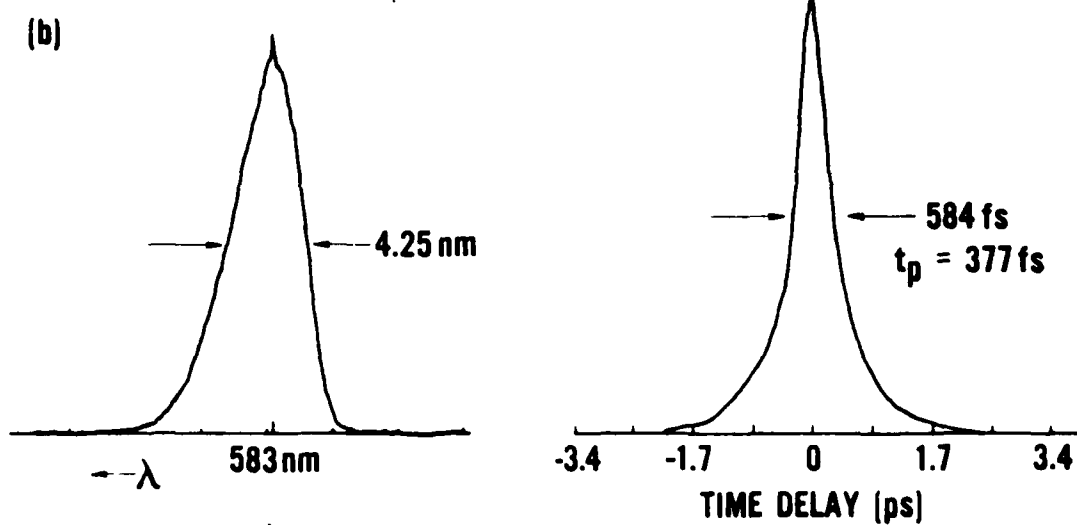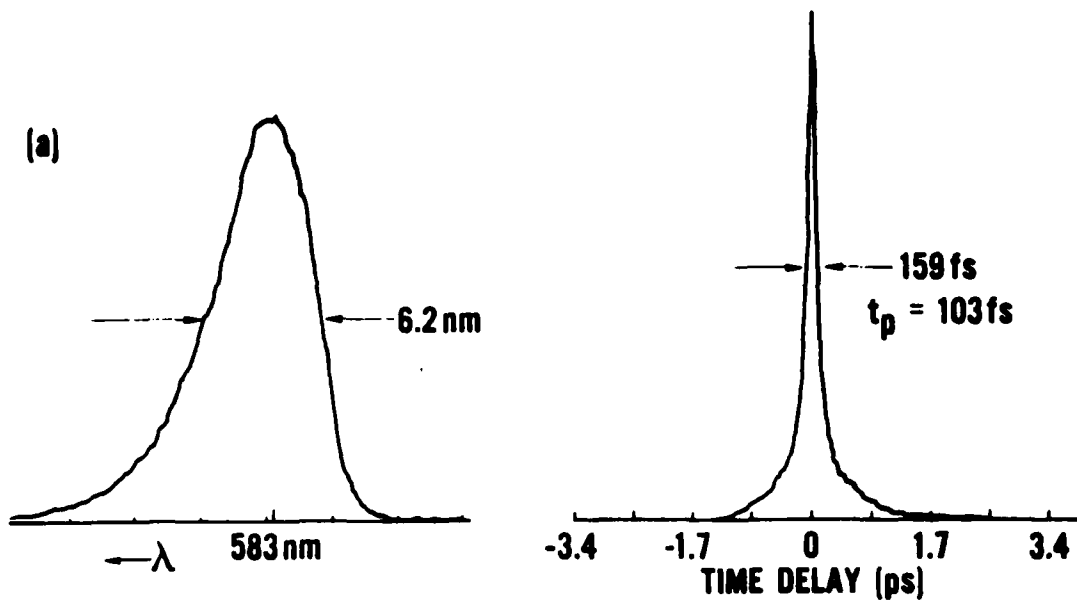
Figure 2. (a) Spectrum and autocorrelation from purely synchronously mode-locked laser without aperture and (b) spectrum and autocorrelation with aperture width=0.7 mm.

Figure 3. Spectrum and corresponding autocorrelation for synchronously pumped passively mode-locked dye laser (a) without aperture, (b) with aperture width 1.1 mm and (c) with aperture width 0.95 mm.

(a)

3.1 nm

3.54 ps
t_p = 2.3 ps

λ 579 nm

-8 -6 -4 -2 0 2 4 6 8
TIME DELAY (ps)

(b)

1.25 nm

1.24 ps
t_p = 800 fs

λ 579 nm

-8 -6 -4 -2 0 2 4 6 8
TIME DELAY (ps)

(a) — 6.2 nm — 583 nm — λ

159 fs, $t_p = 103$ fs — TIME DELAY (ps), -3.4, -1.7, 0, 1.7, 3.4

(b) — 4.25 nm — 583 nm — λ

584 fs, $t_p = 377$ fs — TIME DELAY (ps), -3.4, -1.7, 0, 1.7, 3.4

(c) — 3.2 nm — 583 nm — λ

744 fs, $t_p = 480$ fs — TIME DELAY (ps), -3.4, -1.7, 0, 1.7, 3.4

Appendix H: Femtosecond Pulse
Generation in the Red and Deep Red
Spectral Region

A preprint of a manuscript
submitted to **IEEE** Journal of
Quantum Electronics

FEMTOSECOND PULSE GENERATION IN THE RED/DEEP RED SPECTRAL REGION

Martin D. Dawson, Thomas F. Boggess and Dennis W. Garvey
Center for Applied Quantum Electronics
Department of Physics
North Texas State University
Denton, TX   76203 U.S.A.

and

Arthur L. Smirl
Hughes Research Laboratories
Malibu, CA   90265 U.S.A.

Abstract

Optical pulses as short as 55 fs in duration have been generated near 675 nm in a synchronously-pumped, hybridly mode-locked, Sulforhodamine 101 dye laser. Hybrid mode-locking of Rhodamine B in the same cavity arrangement yielded 187 fs pulses at 650 r.n.

Laser systems capable of generating femtosecond optical pulses include synchronously-pumped hybridly mode-locked [1,2] and, more commonly, passively mode-locked [3,4] cw dye lasers. Although a variety of novel gain/saturable absorber dye combinations have recently been identified for use in these systems [5-10], direct production of sub-100 fs pulses has thus far almost exclusively been limited to the spectral region around 615 nm, primarily using Rhodamine 6G and the saturable absorber DODCI [1-4]. Typically, the generation of pulses of this duration also requires the use of conventional ring [3] or antiresonant ring [1,2] cavity arrangements designed to utilize the colliding pulse mode-locking (CPM) effect, where counterpropagating pulses meet in the saturable absorber dye jet-stream.

We have lately reported obtaining 69 fs pulses centered at 583 nm from a linear cavity synchronously-pumped, hybridly mode-locked, Rhodamine 6G dye laser [11]. In addition, pulses down to 65 fs have been achieved near 850 nm [12] using the gain/saturable absorber dye combination of Styryl 9 and IR 140 , with which subpicosecond pulse generation had previously been demonstrated [10]. These are the only published reports of directly generated sub-100 fs pulses from dye lasers outside the "common" 605-630 nm wavelength range [13]. We describe here a further extension, producing 55 fs pulses around 675 nm by hybrid synchronous mode-locking of a Sulphorhodamine 101 (SR 101) dye laser that does not require the CPM technique. To our knowledge, these are the shortest pulses yet reported from a synchronously-pumped cw dye laser without the use of extracavity fiber-and-grating pulse compression. Hybrid mode-locking of Rhodamine B (RhB) in the same cavity arrangement yielded 187 fs pulses at 650 nm.

The laser cavity was described in detail previously and only an outline of its characteristics is presented here. Briefly, the laser was pumped at 82 MHz by 650 mW average power, 70 ps pulses from a frequency-doubled mode-locked cw

Nd:YAG laser (Spectra-Physics Series 3000). The pump beam was coupled into the gain medium (a 1.8×10^{-3} M solution of SR 101 or a 2×10^{-3} M solution of RhB in ethylene glycol) by a 5 cm radius of curvature focusing mirror. Except for the output coupler, single stack dielectric coatings, highly reflecting at 632.8 nm and having a bandwidth of greater than 100 nm, were used for all cavity mirrors. The mirror pair about the gain dye jet-stream had radius of curvature 7.5 cm, while those about the saturable absorber jet-stream had 3.75 cm radius of curvature. A plane output coupler was used that was 94% reflecting at 650 nm, 90% reflecting at 675 nm. The linear laser resonator was terminated by two Brewster prisms followed by a retroreflecting plane mirror, an arrangement that allows continuous adjustment of the intracavity dispersion [4]. Pulsewidth measurements were performed by both standard collinear type I and non-collinear background-free second harmonic generation autocorrelation in a 1 mm KDP crystal. Hyperbolic secant squared pulse shapes are assumed throughout in deriving the pulsewidths from the full width at half maxima of the autocorrelation functions. The autocorrelator had a scanning display facility that enabled straightforward optimization of dye laser performance. Spectral information was recorded using an optical multichannel analyzer and vidicon system coupled to a 1/4-meter spectrometer.

Optimal performance of the SR 101 laser was obtained using the dye 1,3' Diethyl 4,2' quinolylthiacarbocyanine iodide (DQTCI) as saturable absorber. This dye has a peak extinction coefficient of 11×10^4 mol^{-1} cm^{-1} at 628 nm in a 3:1 ethylene glycol:ethanol solution [7]. It has been identified as a versatile saturable absorber for use in flashlamp-pumped [14,15] and cw-pumped [7,8], passively mode-locked dye laser systems in the wavelength range 620-690 nm. Although the absorption maximum of the SR 101 gain dye (in ethanolic solution) occurs at 576 nm, typically requiring an energy transfer mixture with Rhodamine

129

6G for optimum power performance using cw Argon ion laser pumping [8,16], efficient direct excitation of the dye can readily be achieved using a frequency-doubled mode-locked Nd:YAG laser. Prior to addition of the saturable absorber dye, 95 mW average power output was obtained at 661 nm with ethylene glycol flowing in the passive section jet-stream.

Addition of DQTCI to form a 5×10^{-4} M solution, resulted in the generation of stable pulses having duration as short as 55 fs (Fig. 1) and time-averaged output power ~ 35mW. These pulses were spectrally centered near 675 nm, with a bandwidth of 9.5 nm, giving a time-bandwidth product of $\Delta v \Delta t = 0.34$ (note that $\Delta v \Delta t = 0.315$ for transform limited sech^2 pulses). With the autocorrelator aligned for collinear type I measurements, the scanning rate was reduced to 6 Hz, and the amplitude of the scan was decreased until interferometric auto-correlations [17] of the pulses were displayed (Fig. 2). These autocorrelations showed the necessary 8:1 peak-to-background ratio required for complete mode-locking and directly illustrate the highly coherent nature of the pulses.

Similar performance was achieved when the gain medium was replaced by the dye Rhodamine 101. Using a 2.1×10^{-3} M solution of this dye, 90 mW of time-averaged output power was measured, centered at 652 nm, prior to addition of the DQTCI saturable absorber. With the 5×10^{-4} M solution of DQTCI, 59 fs pulses were recorded with average power ~ 30 mW. These pulses were also spectrally centered near 675 nm, as in the case of SR 101, most likely because this wavelength is close to the long wavelength cut-off of the cavity mirrors.

Considerably longer pulses were obtained when DQTCI was used with RhB as the gain medium. Using a 2×10^{-3} M solution of RhB and a 10^{-4} M solution of DQTCI, the shortest pulses observed were of 320 fs duration, centered at 628 nm. The output power in this case was 25 mW. Improved performance was achieved, however, when DQTCI was replaced by Oxazine 720 (perchlorate) as the saturable absorber. This dye has a peak extinction coefficient that has been measured as

9.2×10^4 mol^1 cm^{-1} at 627 nm in ethanolic solution [18]. Pulses as short as 187 fs (Fig. 3) were obtained near 649 nm, using an absorber concentration of 3×10^{-5} M, with time-averaged output power ~ 30 mW.

In conclusion, femtosecond pulse generation has been obtained from synchronously pumped Sulforhodamine 101, Rhodamine 101 and Rhodamine B dye lasers, hybridly mode-locked with DQTCI and Oxazine 720 (perchlorate) saturable absorbers. With the Sulforhodamine 101/DQTCI combination, 55 fs pulses were recorded near 675 nm, achieving direct generation of sub-100 fs pulses in the deep red spectral region for the first time. The absence of colliding pulse mode-locking in this laser, and its linear cavity arrangement, allows ease of alignment, non-critical positioning of the saturable absorber jet, and high overall efficiency.

Acknowledgements

References

[1] T. Norris, T. Sizer II, and G. Mourou, "Generation of 85 fsec pulses by synchronous pumping of a colliding-pulse mode-locked dye laser," J. Opt. Soc. Am. B., vol. 2, pp. 613-614, Apr. 1985.

[2] H. Vanherzeele, R. Torti, and J.-C. Diels, "Synchronously pumped dye laser passively mode-locked with an antiresonant ring," Appl. Opt., vol. 23, pp. 4182-4184, Dec. 1984.

[3] R. L. Fork, B. I. Greene, and C. V. Shank, "Generation of pulses shorter than 0.1 psec by colliding pulse modelocking," Appl. Phys. Lett., vol. 38, pp. 671-672, May 1981.

[4] J. A. Valdmanis, R. L. Fork, and J. P. Gordon, "Generation of optical pulses as short as 27 femtoseconds directly from a laser balancing self-phase modulation, group velocity dispersion, saturable absorption, and saturable gain," Opt. Lett., vol. 10, pp. 131-133, Mar. 1985.

[5] P. M. W. French, M. D. Dawson and J. R. Taylor, "Passive modelocking of a cw dye laser in the yellow spectral region," Opt. Commun., vol. 56, pp. 430-432, Jan. 1986.

[6] P. M. W. French and J. R. Taylor, "Passively mode-locked continuous-wave Rhodamine 110 dye laser," Opt. Lett., vol. 11, pp. 279-299, May 1986.

[7] P. M. W. French and J. R. Taylor, "The passive modelocking of the continuous wave Rhodamine B dye laser," Opt. Commun., vol. 58, pp. 53-55, May 1986.

[8] P. M. W. French and J. R. Taylor, "Passive modelocking of an energy transfer continuous wave dye laser," IEEE J. Quantum Electron. To be published.

[9] K. Smith, N. Langford, W. Sibbett, and J. R. Taylor, "Passive modelocking of a continuous-wave dye laser in the red-near-infrared spectral region," Opt. Lett., vol. 10, pp. 559-561, Nov. 1985.

[10] K. Smith, W. Sibbett, and J. R. Taylor, "Subpicosecond generation via hybrid mode-locking of Styryl 9 in the near-infrared," Opt. Commun., vol. 49, pp. 359-361, Apr. 1984.

[11] M. D. Dawson, T. F. Boggess, D. W. Garvey, and A. L. Smirl, "A hybridly mode-locked cw dye laser with Brewster prims," Opt. Commun. To be published.

[12] J. Dobler, H. H. Shultz, and W. Zinth, "Generation of femtosecond light pulses in the near infrared around $\lambda = 850$ nm," Opt. Commun., vol. 57, pp. 407-409, Apr. 1986.

[13] A preliminary report of our measurements was presented as postdeadline paper WD8 at the Topical Meeting on Ultrafast Phenomena, Snowmass, CO. (June 1986): M. D. Dawson, T. F. Boggess, D. W. Garvey, and A. L. Smirl, "Generation of 55 fs pulses and variable spectral windowing in a linear cavity synchronously-pumped cw dye laser." A further dye combination for

femtosecond pulse generation was reported as postdeadline paper WD6 at the same meeting: W. H. Knox, "Generation of 70 fs pulses around 800 nm with the dye pair LDS 751: HITC-I in a synchronously pumped linear laser."

[14] E. G. Arthurs, D. J. Bradley, and A. G. Roddie, "Passive modelocking of flashlamp-pumped dye lasers tunable between 580 and 700 nm," Appl. Phys. Lett., vol. 20, pp. 125-127, Feb. 1972.

[15] J. R. Taylor, "Passive modelocking of DCM and Rhodamine 101 flashlamp-pumped dye laser systems," Opt. Commun., vol. 57, pp. 117-120.

[16] M. Yamashita, M. Kasamatsu, H. Kashiwagi, and K. Machida, " The selective excitation of lithium isotopes by intracavity nonlinear absorption in a cw dye laser," Opt. Commun., vol. 26, pp. 343-347, Sept. 1978.

[17] J.-C. Diels, J. J. Fontaine, I. C. McMichael, and F. Simoni, "Control and measurement of ultrashort pulse shapes (in amplitude and phase) with femtosecond accuracy," Appl. Opt., vol. 24, pp. 1270-1282, May 1985.

[18] W. Rudolph, private communication.

Figure Captions

Fig. 1   Collinear Type I autocorrelation (a) and corresponding integrated laser spectrum (b) of 55 fs pulses obtained using SR 101 and DQTCI.

Fig. 2   Interferometric autocorrelation of pulses from the SR 101 laser. Time scale is 30 fs/major division.

Fig. 3   Background-free autocorrelation (a) and corresponding integrated laser spectrum (b) of 187 fs pulses obtained using RhB and Oxazine 720.

(a)

290fs
tp=187fs

(b)

4.9nm

648.5nm

λ

TIME DELAY (fs)

SHG INTENSITY

-1700   -850   0   850   1700
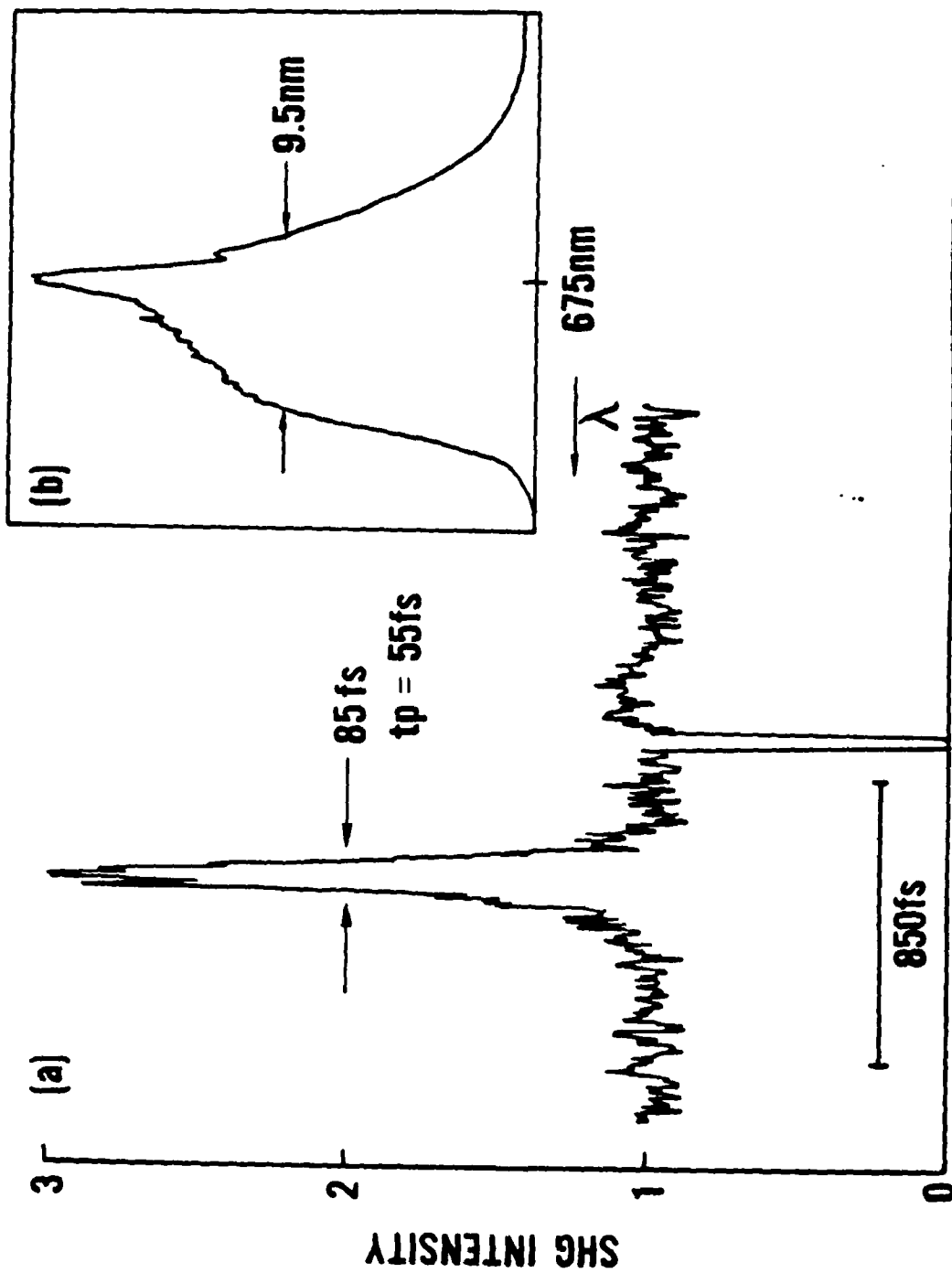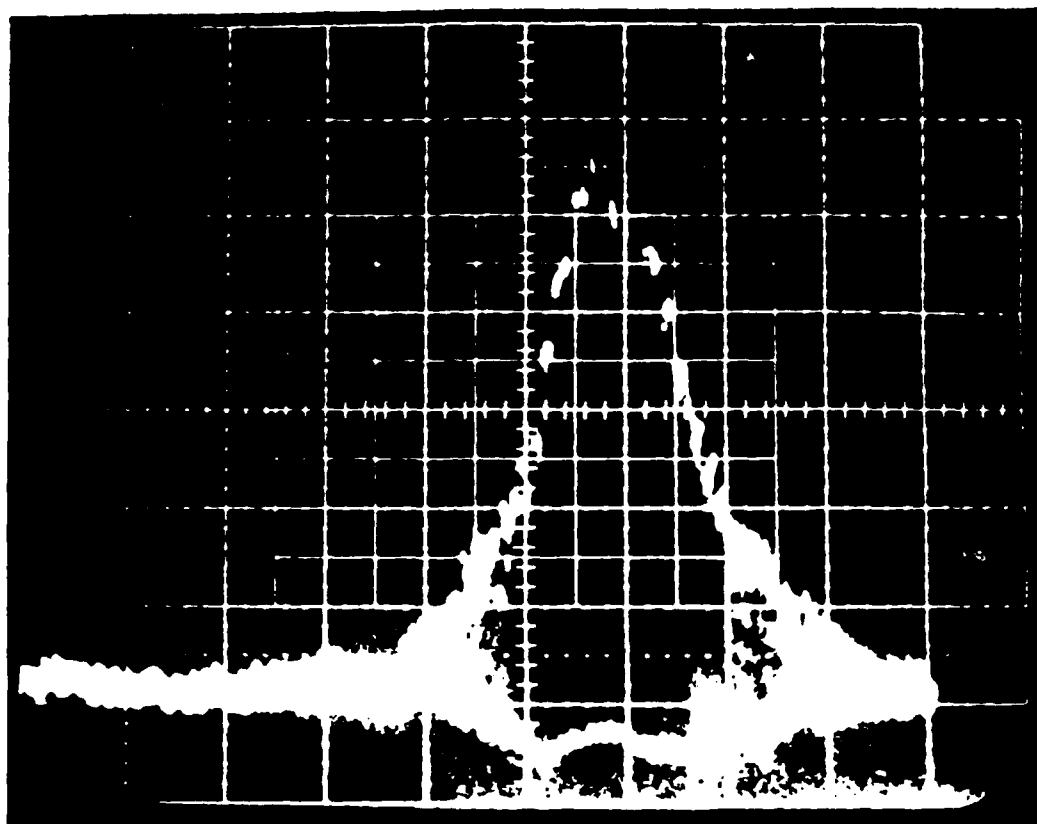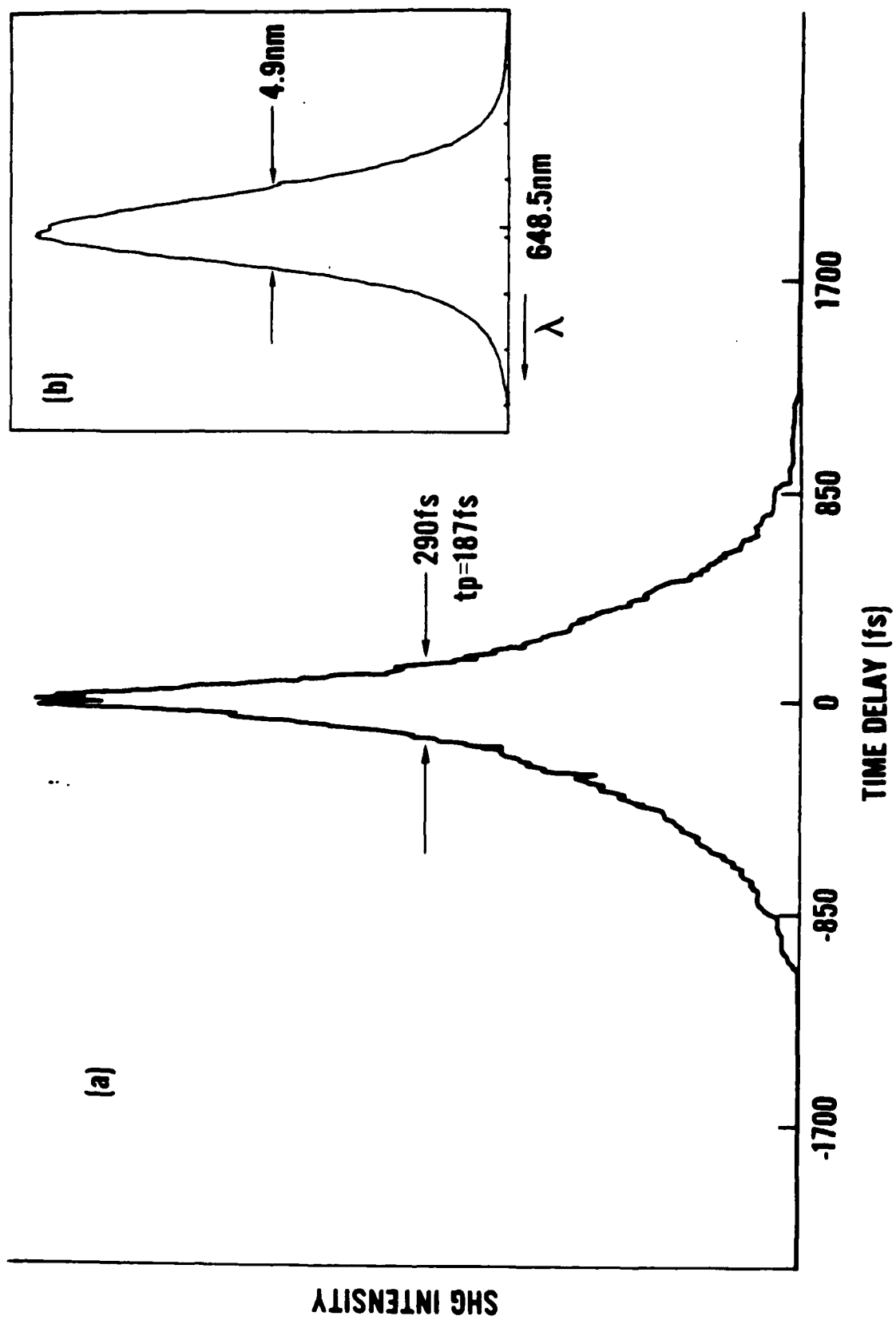
Appendix I: Picosecond
Photorefractive Beam Coupling
in GaAs

Picosecond photorefractive beam coupling in GaAs

George C. Valley, Arthur L. Smirl, M. B. Klein
Hughes Research Laboratories
Malibu, CA 90265

K. Bohnert and Thomas F. Boggess
Center for Applied Quantum Electronics
North Texas State University
Denton, TX 76203

Abstract   This paper reports the first observation of the photorefractive effect on picosecond time scales. Photorefractive beam coupling in GaAs with picosecond, 1.06 μm pulses is observed due to charge separation between electrons and the ionized defect EL2$^+$ at low fluences and by separation between free electrons and holes created by two-photon inter-band absorption for high fluences. The accompanying processes of linear absorption, two-photon absorption, and transient energy transfer are also observed.

Photorefractive materials such as $LiNbO_3$, $BaTiO_3$ and $Bi_{12}SiO_{20}$ have been widely investigated over the past 15 years for applications in holographic storage, optical data processing, and phase conjugation.[1] Recently, the photorefractive effect has been demonstrated in the semiconductors GaAs, InP and CdTe on time scales from 250 μs to steady state.[2-5] Here we report the observation of beam coupling in GaAs due to the photorefractive effect with single 43 ps pulses of 1.06μm radiation. Our results are attributed to the charge separation between photoionized, untrapped electrons and the ionized donor level EL2* at low fluences F (F < 0.3 mJ/cm^2) and to the separation between untrapped electrons and holes created by two-photon absorption for high fluences (F > 3 mJ/cm^2).

Previously, the photorefractive effect due to one-photon ionization and charges trapped at donor or acceptor sites has been observed with pulses as short as 10 ns in $LiNbO_3$, $BaTiO_3$, and $Bi_{12}SiO_{20}$.[6-8] Moreover, the photorefractive effect due to two-photon ionization of donors has been produced by trains of picosecond pulses in $LiNbO_3$[9,10] and by a single picosecond pulse and trains in potassium tantalate niobate (KTN)[11]. The minimum time needed to produce a grating was observed to be less than a few nanoseconds[7] to less than 2 ns[10], limited by the time resolution of the experiments. Our results in GaAs show

142

that it is possible to produce a photorefractive effect a factor of 100 to 1000 times faster than these time scales. In addition, our results show for the first time that a photorefractive effect can be produced by the charge separation between untrapped electrons and ionized donor levels (EL2$^+$) and also by the charge separation of electons and holes created by two-photon interband absorption.

Our experiments were performed using the same sample of semi-insulating, undoped GaAs and the same experimental configuration reported previously.[3] The sample is 5x5.5x3.3 mm^3 with the 3.3 mm length along the direction of propagation. Properties of our sample were reported in Ref. 3 or inferred from the literature as given in the Table. The deep level EL2,[17,18] which exists in both a neutral and a positively ionized state, was identified as the source of the steady-state photorefractive effect by the excellent agreement between the measurement of the ionized EL2 number density N$^+$ from conductivity as a function of temperature (N$^+$ = 1.4×10^{15}cm^{-3}) and from photorefractive beam coupling (N$^+$ = 1.3×10^{15}cm^{-3}).[3] In addition, the absorption spectrum of our sample is very similar to the EL2 absorption spectrum reported in ref. 18.

The laser source for our experiments was an actively and passively mode-locked Nd:YAG laser operating in the fundamental transverse mode. A single pulse was switched from the train of pulses and amplified. The average

pulsewidth, measured on a shot-by-shot basis, was 43 ps full width at 1/e of the peak irradiance. After amplification the pulse was divided into two parts and recombined at an angle to give a grating period of 1.7μm in the crystal. As in Ref. 3 both pump and probe were polarized along the (110) direction and the grating wave vector was along the (001) direction. The beam diameters at the sample were 5 mm (full width at e^{-1} of the maximum irradiance), as determined by pinhole scans performed in both the horizontal and vertical directions.

For fluences sufficient to observe significant energy transfer, investigation of the photorefractive effect is complicated by two-photon absorption and free-carrier refractive index changes. This is illustrated in Fig. 1, where the quantity $\Delta T/T$ is plotted as a function of peak pump fluence with the incident probe-to-pump energy ratio held constant at 4.4%. The quantity $\Delta T/T$ is defined as the probe energy transmission with the pump present minus the transmission without the pump all divided by the probe energy transmission T without the pump:

$$\frac{\Delta T}{T} = \frac{T(\text{with pump}) - T(\text{without pump})}{T(\text{without pump})} \tag{1}$$

Note that for small gain or loss the quantity $\Delta T/T$ is independent of linear absorption (e.g. if we could write the photorefractive gain as simply $\exp(\Gamma L)$ and the loss as $\exp(-\alpha L)$, $\Delta T/T$ would equal ΓL for small ΓL). The two curves

144

shown in Fig. 1 are for two orientations of the crystal. The top curve (open squares) represents data acquired with the crystal oriented such that protorefractive energy transfer is from pump beam to probe; the bottom curve (open triangles) represents data taken after the crystal was rotated by 180° about the surface normal that bisects the angle between the two beams. Fig. 1 shows that the energy transfer depends on crystal orientation, an unambiguous signature of the photorefractive effect. In the top curve the photorefractive gain competes with loss from two-photon absorption at fluences below 3 mJ/cm² with a zero-crossing at 1 mJ/cm², while in the lower curve both effects cause probe loss. At fluences above 3 mJ/cm² transient energy transfer[23] by the free carrier grating tranfers energy from the strong to weak beam in each orientation.

In order to isolate the photorefractive effect, we subtract the data for the two orientations given in Fig. 1. If the two-photon absorption and the free-carrier transient energy transfer are independent of the photorefractive effect (which is true for sufficiently small energy transfer and no pump depletion, conditions of our experiments), then the difference between $\Delta T/T$ for the two orientations should be twice the energy transfer due to the photorefractive effect alone. These data points are shown by the squares in Fig. 2.

We have performed detailed numerical calculations to determine if the data in Fig. 2 are consistent with the photorefractive effect due to production and transport of charge carriers, an internal space charge field due to charge separation, and a change in the refractive index through the electro-optic effect. Our calculations also include saturation of the EL2 absorption, the free carrier absorption and refractive index, and two-photon absorption, all of which contribute to $\Delta T/T$. The set of materials equations used for this modeling differs from that used previously[19,20] by the addition of the two-photon ionization and the neglect of recombination, which is not important in GaAs on time scales less than 100 ps[21]:

$$\partial N^*/\partial t = s_e I(N-N^*)/(h\nu) - s_h IN^*/(h\nu) \tag{2}$$

$$\partial p/\partial t = -(1/e)\partial j_p/\partial z + \beta I^2/(2h\nu) + s_h IN^*/(h\nu) \tag{3}$$

$$\partial n/\partial t = (1/e)\partial j_n/\partial z + \beta I^2/(2h\nu) + s_e I(N-N^*)/(h\nu) \tag{4}$$

$$j_p = e\mu_p Ep - \mu_p k_B T \,\partial p/\partial z \tag{5}$$

$$j_n = e\mu_n En + \mu_n k_B T \,\partial n/\partial z \tag{6}$$

$$\partial E/\partial z = (e/\epsilon)(p + N^* - n - N_A) \tag{7}$$

where z is the coordinate perpendicular to the direction of propagation, I is the irradiance, p, n, j_p, j_n are the hole and electron number and current densities, $h\nu$ is the photon energy, and $k_B T$ is Boltzmann's constant times temperature. N_A is the number density of negative ions that compensate for the charge of N^* in the dark, but that cannot be photoionized (these are thought to be carbon ions). The

remainder of the parameters are defined in the Table. These equations are combined with Maxwell's equations including the effects listed above and solved numerically.

Results of the numerical calculations for the two crystal orientations are shown by the dashed and dot-dashed curves in Fig. 1. These curves use one unknown parameter, the quantum efficiency of the EL2 donor, as a fitting parameter. The calculations shown in Fig. 1 use a quantum efficiency of .58, which is consistent with other photorefractive studies[24] and other studies of EL2[22]. In our calculations we have modeled the free carrier index with and without the interband correction factor.[25] The results shown in Fig. 1 are without the interband correction factor; results with the correction factor fit the data quite poorly. Excellent quantitative agreement between experiment and theory can be achieved easily by varying the other material parameters within physically reasonable limits, but without additional independent measurements there is no justification for such a forced fit. In particular, the high fluence region of the curve is very sensitive to the hole mobility, the two-photon absorption coefficient, and the interband correction factor.

The qualitative interpretation from comparison of the calculations to the data in Fig. 1 is quite clear. For the top curve, photorefractive gain initially competes with loss from two-photon absorption, and a net gain is observed.

Eventually, as the fluence is increased, all of the EL2 donors are ionized, and two-photon absorption begins to dominate, with a zero crossing near 1 mJ/cm^2. Finally, the electron and hole densities become sufficiently large that the free carrier grating (the real part of the Drude index) can transfer energy from the strong beam to the weak beam.[23] This results in probe gain for fluences larger than about 10mJ/cm^2, as shown. For the lower curve, the photorefractive energy transfer is from probe to pump, and this and two-photon absorption contribute to increasing probe loss with increasing fluence. Again, however, at the highest fluences, transient energy transfer begins to dominate and to reverse the sign of the slope of $\Delta T/T$ as a function of F.

Finally, we can isolate the photorefractive contributions from those of two-photon absorption and free-carrier transient energy transfer by recognizing that (in the small signal limit) only photorefractive energy transfer explicitly depends on crystal orientation. When the crystal is oriented for weak to strong beam transfer, the photorefractive grating contributes to probe loss; when the crystal is rotated 180° about the surface normal, the photorefracrtive energy transfer is reversed and is from strong to weak beam, while the other contribut ons maintain their sign. Consequently, twice the photorefractive part of $\Delta T/T$ is obtained by subtracting the two curves shown in Fig.

1.   Both the experimental data and the theoretical calculations are shown this way in Fig. 2.   At low fluences the space charge field leading to the photorefractive effect is primarily between one-photon-generated mobile electrons and immobile ionized EL2⁺ donors.   At higher fluences, the space charge field between two-photon-generated free electrons and holes also contributes.   At the highest fluences, transient energy transfer and the photorefractive effect appear to interact in a nonlinear way.

References

1. P.Günter, Phys. Repts. **93**, 200 (1983).
2. A.M.Glass, A.M.Johnson, D.H.Olson, W.Simpson and A.A.Ballman, Appl.Phys.Lett. **44**, 948 (1984).
3. M.B.Klein, Opt.Lett. **9**, 350 (1984).
4. J.Strait and A.M.Glass, J.Opt.Soc.Am.B **3**,342 (1986); A.M.Glass, M.B.Klein, and G.C.Valley, Electron. Lett. **21**, 220 (1985).
5. J.Strait and A.M.Glass, Appl.Opt. **25** 338 (1986).
6. C.-T.Chen, D.M.Kim, and D.von der Linde, Appl.Phys.Lett. **34**, 321 (1979).
7. L.K.Lam, T.Y.Chang, J.Feinberg, and R.W.Hellwarth, Opt.Lett. **6**, 475 (1981).
8. J.P.Hermann, J.P.Herriau, and J.P.Huignard, Appl.Opt. **20**, 2173 (1981).
9. D.von der Linde, A.M.Glass, and K.F.Rodgers, Appl.Phys.Lett. **25**, 155 (1974).
10. D.von der Linde, O.F.Schirmer, and H.Kurz, Appl.Phys. **15**, 167 (1978).
11. D.von der Linde, A.M.Glass, and K.F.Rodgers, Appl.Phys.Lett. **26**, 22 (1975).
12. D.T.F.Marple, J.Appl.Phys. **35**, 1241 (1964).
13. K.S.Champlin, R.J.Erlandson, G.H.Glover, P.S.Hauge, and T.Lu, Appl.Phys.Lett. **11**, 348 (1967).
14. M.Sugie and K.Tada, Japan.J.Appl.Phys. **15**, 421 (1976).
15. T.F.Boggess,Jr., A.L.Smirl, S.C.Moss, I.W.Boyd, and E.W.van Stryland, IEEE J.Quantum Electron. **QE-21**, 488 (1985).
16. J.S.Blakemore, J.Appl.Phys. **53**, R123 (1982).
17. W.Walukiewicz, J.Lagowski, and H.C.Gatos, Appl. Phys. Lett. **43**, 192 (1983).
18. G.M.Martin, Appl.Phys.Lett. **39**, 747 (1981).
19. N.V.Kukhtarev, Pis'ma Zh. Tekh. Fiz. **2**, 1114 (1976) [Sov.Tech.Phys.Lett.**2**, 438 (1976)]; G.C.Valley, IEEE J. Quantum Electron., **QE-19**, 1637 (1983).
20. G.C.Valley, J.Appl.Phys. **59**, 3363 (1986); F.P.Strohkendl, J.M.C.Jonathan, and R.W.Hellwarth, Opt.Lett., **11**, 312 (1986).
21. J.S.Weiner and P.Y.Yu, J.Appl.Phys. **55**, 3889 (1984).
22. M.Kaminska, M.Skowronski, J.Lagowski, J.M.Parsey, and H.C.Gatos, Appl.Phys.Lett. **43**, 302 (1983).
23. V.L.Vinetskii, N.V.Kukhtarev, and M.S.Soskin, Kvant. Elektron. **4**, 420 (1977) [Sov. J. Quantum Electron. **7**, 230 (1977)].
24. R.A.Mullen and R.W.Hellwarth, J.Appl.Phys. **58**, 40 (1985).
25. R.K.Jain and M.B.Klein, Optical Phase Conjugation, ed. by R.A.Fisher, New York: Academic Press, ch. 10, 307 (1983) .

Table Parameters of the GaAs crystal used for picosecond beam coupling.

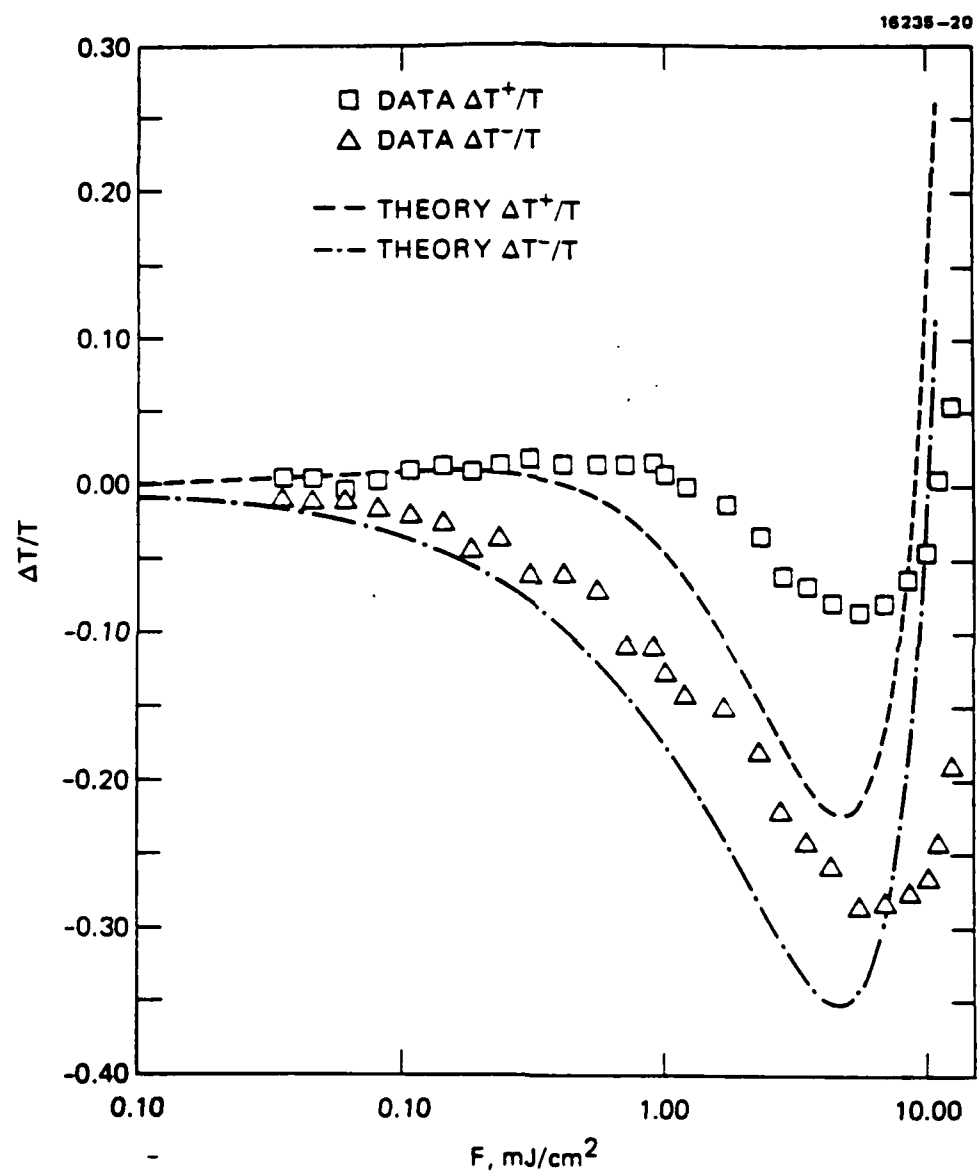| Parameter	Value	Reference
refractive index, n_b	3.48	12
dielectric constant, ϵ/ϵ_0	12.9	13
electro-optic coefficient, r_{41}	1.43 pm/V	14
absorption coefficient, α	1.2 cm^{-1}	3
two-photon absorption coefficient, β	26. cm/GW	15
free carrier cross section, s_{fc}	$3 \cdot 10^{-18}$	15
electron Hall mobility, μ_H	5800 cm^2/V s	3
electron drift mobility, μ_n	$\mu_H/\mu_n = 1.175$	16
hole drift mobility, μ_p	$\mu_n/\mu_p = 13$	17
Total EL2 density, N	$1.3 \cdot 10^{16}$ cm^{-3}	18[a]
ionized EL2 (EL2*) density, N*	$1.4 \cdot 10^{15}$ cm^{-3}	3
EL2 cross section, s_e	$< \alpha/(N-N^*)$	[b]
EL2* cross section, s_h	$s_e/4$	17

[a] This value is extrapolated from Fig. 2 of Ref. 18 using the absorption coefficient of 1.2 cm^{-1} measured in our sample.
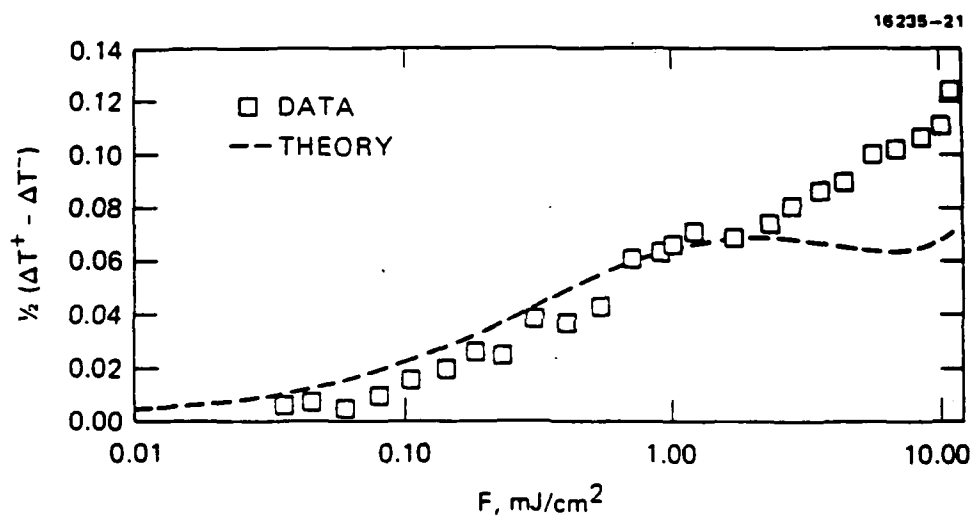
[b] $s_e = \alpha/(N-N^*)$ when the quantum efficiency for mobile electron generation from EL2 donors is one and there is no other absorption process in the material.

Figure Captions

Fig. 1. The normalized change in transmission of the probe beam $\Delta T/T$ as a function of the peak pump fluence for a grating spacing of $1.7\mu m$ and a constant pump-to-probe ratio 23:1. The sample was rotated 180° about the surface normal between measurements represented by the squares and triangles. The dashed and dot-dashed lines represent theoretical fits using the parameters of the Table.

Fig. 2. The normalized change in probe transmission for the sample oriented for energy transfer from the strong to weak beam $(\Delta T/T)^\cdot$ minus that for transfer from weak to strong $(\Delta T/T)^-$ as a function of peak pump fluence for a grating spacing of $1.7\mu m$ and a constant pump-to-probe ratio of 23:1. The dashed line indicates numerical calculations using rate and transport equations combined with Maxwell's equations.

16235-20

16235-21

155

END

12-86

DTIC